

Order number

People's Democratic Republic of Algeria

Ministry of Higher Education and Scientific Research

University Ain Temouchent Belhadj Bouchaib



Faculty of Science and Technology
Department of Mechanical Engineering
Smart Structures Laboratory



THESIS

Presented to obtain the **3rd cycle DOCTORAL diploma**

Faculty: Science and Technology

Department: Mechanical Engineering

Specialty: Energetic

By: Abdelfatah MARNI SANDID

Title of the thesis

Design of a seawater desalination unit working with solar energy

Supported publicly, the 22/06/2023, in front of the jury composed of:

Full Names	Grade	Quality	Establishment of attachment
BOUNIF Abdelhamid	Pr	President	University Ain Temouchent Belhadj Bouchaib
NEHARI Taieb	MCA	Supervisor	University Ain Temouchent Belhadj Bouchaib
NEHARI Driss	Pr	Co-Supervisor	University Ain Temouchent Belhadj Bouchaib
DEBAB Abdelkader	Pr	Examiner	University of Science and Technology of Oran
BOUAFIA Farida	Pr	Examiner	University Ain Temouchent Belhadj Bouchaib
SENOUCI Mohammed	Pr	Examiner	Higher School in Electrical and Energy Engineering of Oran

University Year: 2022/2023

Abstract

Solar thermal energy for membrane distillation desalination is a green and safe way for areas where water scarcity and solar irradiance are strongly correlated. In the desalination field, the membrane distillation (MD) is a new process of producing distilled water that has been developed and tested in recent years. In this thesis, the main studies include: (1) Effective study of operating parameters on the AGMD module for desalination. (2) Simulation and controlling study of the solar AGMD system small scale. (3) Development and optimization study of the solar AGMD system small scale. (4) Experimental, simulation and economic Study of the solar AGMD system large scale.

- The first study presents the effect of the operating temperatures and the flow rates on the distillate flux that can obtain from a hydrophobic membrane having the characteristics: pore size of 0.15 μm ; thickness of 130 μm ; and 85% porosity. The new approach in the present numerical modeling has allowed examining effects of the nature of materials (Polyvinylidene fluoride (PVDF) polymers, copolymers and blends) used on thermal properties. The obtained results found that, copolymer P(VDF-TrFE) (80/20) is more effective than the other materials of membrane distillation (MD). The mass flux and efficiency reach 193.5 ($\text{g}/\text{m}^2\text{s}$), and 83.29 % using turbulent flow and an effective area 3.1 m^2 , respectively.

- The second study presents the integrated single cassette AGMD module in the solar thermal desalination system which is validated and numerically simulated with the TRNSYS program. This model is studied to be ideal for obtaining a distilled water flow rate of 5.5 kg/h at different times under changing climatic conditions throughout the year in Ain-Temouchent weather, Algeria. Therefore, the energy needed is calculated for the auxiliary heater and is replaced by 10 photovoltaic panels, each one has an area of 1.6 m^2 using three of the energy storage batteries (12V, 100Ah) with 1.5 KW. It was found that when the inlet temperature of AGMD reaches 85 $^{\circ}\text{C}$, the distilled water flow from the distillation membrane reaches 5.5 kg /h and that remains stable on different days throughout the year by relying solely on solar energy.

- The third study presents a numerical study to investigate the solar AGMD system for seawater desalination. The solar MD system includes both flat plate collectors and photovoltaic panels with a total membrane area of AGMD: 0.2 m^2 . Therefore, the photovoltaic system with the energy storage batteries (12V, 100Ah) is used to power electrically the pumps and sensors. It was found that the solar AGMD system is used for the production of 3-5 L/h of distilled water flow. Besides, the brine that contains the high salt concentration is completely dispensed with this process. In addition, the energy efficiency of the AGMD module and the collector efficiency values reach 68 % and 74 % respectively.

- The fourth study presents an experimental study of the performance of a multi-channel spiral-wound AGMD module with an area 14.4 m^2 was carried out on a commercial scale. The lab-scale AGMD desalination pilot plant was driven by solar energy using the flat plate (FPC) and evacuated tube collectors (ETC) installed in Port-Said City, Egypt. The results showed that the permeate flux of AGMD with ETCs was 18.81%–30.44% higher than FPCs, and its cost was 22.48% lower. The STEC of the AGMD system ranged from 158.83 kWh/m^3 to 346.55 kWh/m^3 . The maximum GOR reaches 4.4 at 52 $^{\circ}\text{C}$, depending on the feed inlet temperature. The thermal efficiency of the air gap membrane distillation system is 72%. The proposed AGMD system produced 28.78 m^3/year of fresh drinking water at a cost of USD 14.73/ m^3 with remarkable reducing in carbon dioxide emissions by 7,274.45 kg/year.

Keywords: Solar Desalination, Air gap membrane distillation (AGMD), pilot scale analysis, solar collectors, Photovoltaic (PV) system, Temperature polarization, Thermal conductivity, Seawater, ANSYS-FLUENT, TRNSYS.

Résumé

Le dessalement thermique solaire pour la distillation membranaire est une méthode verte et sûre pour les régions où la rareté de l'eau et le rayonnement solaire sont étroitement liés. Dans le domaine du dessalement, la distillation membranaire (MD) est un nouveau procédé de production d'eau distillée qui a été développé et testé ces dernières années. Les principales études de cette thèse comprennent : (1) une étude effective des paramètres de fonctionnement sur une unité de dessalement AGMD. (2) Simulation à micro-échelle et étude de contrôle du système solaire AGMD. (3) Étude de développement et d'optimisation à petite échelle pour le système solaire AGMD. (4) Etude expérimentale, de simulation et économique d'un système solaire AGMD à grande échelle.

- La première étude présente l'effet des températures de fonctionnement et des débits sur l'écoulement des distillats pouvant être obtenus à partir d'une membrane hydrophobe ayant les caractéristiques : taille de pores de $0,15 \mu\text{m}$; épaisseur $130 \mu\text{m}$; et 85% de porosité. La nouvelle approche dans la modélisation numérique actuelle a permis d'examiner les effets de la nature des matériaux (polyfluorure de vinylidène (PVDF), copolymères et mélanges) utilisés sur les propriétés thermiques. Les résultats obtenus ont montré que le copolymère P(VDF-TrFE) (80/20) est plus efficace que les autres matériaux pour la distillation membranaire (MD). Le débit massique et l'efficacité étaient de $193,5 \text{ (g/m}^2\text{)}$ et de 83,29 % en utilisant un écoulement turbulent et une surface effective de $3,1 \text{ m}^2$, respectivement.

- La deuxième étude présente un module AGMD à cassette unique dans un système de dessalement d'eau solaire qui a été validé et simulé numériquement à l'aide du logiciel TRNSYS. Ce modèle a été étudié pour être idéal pour obtenir un débit d'eau distillée de $5,5 \text{ kg/h}$ à différents moments dans des conditions climatiques changeantes tout au long de l'année à Ain Temouchent, en Algérie. Par conséquent, la puissance nécessaire au chauffage supplémentaire est calculée et remplacée par 10 panneaux photovoltaïques de $1,6 \text{ m}^2$ chacun, utilisant trois batteries de stockage d'énergie (12 V , 100 Ah) de $1,5 \text{ kW}$. Il a été constaté que lorsque la température d'entrée de l'AGMD atteint $85 \text{ }^\circ\text{C}$, le débit d'eau distillée de la membrane de distillation atteint $5,5 \text{ kg/h}$ et reste constant à différents jours tout au long de l'année en s'appuyant uniquement sur l'énergie solaire.

- La troisième étude présente une étude numérique du système solaire AGMD pour le dessalement de l'eau de mer. Le système solaire MD comprend à la fois des capteurs plats et des panneaux photovoltaïques avec une surface totale de membrane d'AGMD : $0,2 \text{ m}^2$ carré. Par conséquent, un système photovoltaïque avec des batteries de stockage d'énergie (12V , 100Ah) est utilisé pour entraîner électriquement les pompes et les capteurs. Il a été constaté que le système solaire AGMD est utilisé pour produire $3 \text{ à } 5 \text{ L/h}$ de débit d'eau distillée. De plus, la saumure contenant une forte concentration de sel est complètement supprimée dans le processus. De plus, l'efficacité énergétique du module AGMD et les valeurs d'efficacité du collecteur atteignent respectivement 68% et 74%.

- Les quatrième étude présentent une étude empirique des performances d'une unité AGMD à bobine hélicoïdale multicanal de $14,4 \text{ m}^2$ réalisée à l'échelle commerciale. L'usine pilote de dessalement AGMD a été mise en service à l'échelle solaire à l'aide de capteurs à panneaux plats (FPC) et à tubes sous vide (ETC) installés à Port-Saïd, en Égypte. Les résultats ont montré que le débit de perméat de l'AGMD avec les ETC était de 18,81 % à 30,44 % supérieur à celui des FPC, et son coût était de 22,48 % inférieur. Le STEC pour le système AGMD variait de $158,83 \text{ kWh/m}^3$ à $346,55 \text{ kWh/m}^3$. Le GOR maximal atteint $4,4 \text{ à } 52 \text{ }^\circ\text{C}$, en fonction de la température de l'entrée d'alimentation. L'efficacité thermique du système de

distillation à membrane à entrefer est de 72 %. Le système AGMD proposé a produit 28,78 m³/an d'eau douce potable à un coût de 14,73 \$/m³ avec une réduction significative des émissions de CO₂ de 7 274,45 kg/an.

Mots clés: dessalement solaire de l'eau, distillation membranaire à entrefer (AGMD), analyse à l'échelle expérimentale, capteurs solaires, système photovoltaïque (PV), polarisation de la température, conductivité thermique, eau de mer, ANSYS-FLUENT, TRNSYS.

خلاصة

الطاقة الحرارية الشمسية لتحلية التقطير بالأغشية هي طريقة خضراء وآمنة للمناطق التي ترتبط فيها ندرة المياه عملية جديدة لإنتاج الماء المقطر تم (MD) والإشعاع الشمسي ارتباطاً وثيقاً. في مجال التحلية، يعتبر التقطير الغشائي تطويره واختباره في السنوات الأخيرة. تشمل الدراسات الرئيسية في هذه الرسالة ما يلي: (1) دراسة فعالة لمعايير التشغيل الشمسي. (3) دراسة AGMD لتحلية المياه. (2) دراسة المحاكاة والتحكم للمقياس الصغير لنظام AGMD على وحدة الشمسي AGMD الشمسي. (4) دراسة تجريبية ومحاكاة واقتصادية لنظام AGMD تطوير وتحسين النطاق الصغير لنظام على نطاق واسع.

تعرض الدراسة الأولى تأثير درجات حرارة التشغيل ومعدلات التدفق على تدفق نواتج التقطير التي يمكن الحصول عليها - من غشاء كاره للماء له الخصائص: حجم مسام 0.15 ميكرومتر؛ سمك 130 ميكرومتر؛ و 85٪ مسامية. سمح النهج الجديد والبوليمرات المشتركة (PVDF) في النمذجة العددية الحالية بفحص تأثيرات طبيعة المواد (بوليمرات البولي فينيلدين فلوريد (VDF)-P والخلانط) المستخدمة في الخصائص الحرارية. وجدت النتائج التي تم الحصول عليها أن البوليمر المشترك بلغ التدفق الشامل والكفاءة 193.5 (جم / م²) ، و (MD) أكثر فعالية من المواد الأخرى لتقطير الأغشية (80/20) (TrFE) 83.29٪ باستخدام التدفق المضطرب ومساحة فعالة 3.1 م² ، على التوالي.

ذات الكاسيت المفرد في نظام تحلية المياه بالطاقة الشمسية والتي تم التحقق من AGMD الدراسة الثانية تعرض وحدة - تمت دراسة هذا النموذج ليكون مثاليًا للحصول على معدل تدفق TRNSYS صحتها ومحاكاتها عددًا باستخدام برنامج للمياه المقطرة يبلغ 5.5 كجم / ساعة في أوقات مختلفة في ظل الظروف المناخية المتغيرة على مدار العام في طقس عين تموشنت ، الجزائر. لذلك ، يتم حساب الطاقة اللازمة للسخان الإضافي ويتم استبدالها بـ 10 ألواح كهروضوئية ، مساحة كل منها 1.6 متر مربع باستخدام ثلاث بطاريات تخزين الطاقة (12 فولت ، 100 أمبير) بقدرة 1.5 كيلو وات. وجد أنه عندما إلى 85 درجة مئوية ، فإن تدفق الماء المقطر من غشاء التقطير يصل إلى 5.5 كجم / AGMD تصل درجة حرارة مدخل ساعة ويظل ثابتاً في أيام مختلفة على مدار العام من خلال الاعتماد فقط على الطاقة الشمسية

الشمسية كلاً من MD الشمسي لتحلية مياه البحر. يشمل نظام AGMD تقدم الدراسة الثالثة دراسة عددية لبحث نظام - متر مربع. لذلك ، يتم استخدام AGMD: 0.2 مجمعات الألواح المسطحة والألواح الكهروضوئية بمساحة غشاء كلية تبلغ لتشغيل المضخات وأجهزة الاستشعار كهربائياً. وجد أن (100Ah ، V النظام الكهروضوئي مع بطاريات تخزين الطاقة (12) الشمسي يستخدم لإنتاج 3-5 لتر / ساعة من تدفق الماء المقطر. إلى جانب ذلك ، يتم الاستغناء عن المحلول AGMD نظام AGMD الملحي الذي يحتوي على تركيز عالٍ من الملح تمامًا في هذه العملية. بالإضافة إلى ذلك ، تصل كفاءة الطاقة لوحدة وقيم كفاءة المجمع إلى 68٪ و 74٪ على التوالي.

متعددة القنوات ذات اللفاف الحلزونية بمساحة 14.4 متر مربع AGMD تقدم الدراسة الأربعة دراسة تجريبية لأداء وحدة - على نطاق معمل بالطاقة الشمسية AGMD أجريت على نطاق تجاري. تم تشغيل المحطة التجريبية لتحلية المياه في المثبتة في مدينة بورسعيد ، مصر. أظهرت النتائج أن (ETC) ومجمعات الأنابيب المفرغة (FPC) باستخدام اللوح المسطح ، وكانت تكلفته أقل بنسبة 22.48٪. FPCs كان أعلى بنسبة 18.81٪ - 30.44٪ من ETCs مع AGMD التدفق المتخلل لـ 158.83 كيلو واط ساعة / متر مكعب إلى 346.55 كيلو واط ساعة / متر مكعب. AGMD لنظام STEC تراوحت إلى 4.4 عند 52 درجة مئوية ، اعتماداً على درجة حرارة مدخل التغذية. تبلغ الكفاءة الحرارية GOR يصل الحد الأقصى لـ المقترح 28.78 م³ / 3 سنة من مياه الشرب العذبة بتكلفة 14.73 AGMD لنظام التقطير بغشاء فجوة الهواء 72٪. أنتج نظام دولار أمريكي / م³ مع انخفاض ملحوظ في انبعاثات ثاني أكسيد الكربون بمقدار 7274.45 كجم / سنة

الكلمات المفتاحية: تحلية المياه بالطاقة الشمسية ، تقطير غشاء فجوة الهواء ، استقطاب درجة الحرارة ، التوصيل الحراري ، تحليل مقياس تجريبي ، مجمعات الطاقة الشمسية ، نظام الخلايا الضوئية مياه البحر ، ANSYS-FLUENT ، TRNSYS.

Preface

This doctoral thesis work has been performed at Smart Structure Laboratory and Department of Mechanical Engineering, University of Ain Temouchent, Algeria in collaboration with the Department of Chemical Engineering in Faculty of Engineering and Department of Mechanical Power Engineering, Port Said University, Port Said, Egypt.

Publications included in the thesis

The present thesis is based on a summary of the following publications:

Journal Papers:

A. Marni Sandid, M. Bassyouni, D. Nehari, Y. Elhenawy. Experimental and simulation study of multichannel air gap membrane distillation process with two types of solar collectors.

Energy Conversion and Management 243 (2021) 114-131

DOI: <https://doi.org/10.1016/j.enconman.2021.114431>

0196-8904/© 2021 Elsevier Ltd. All rights reserved.

A. Marni Sandid, D. Nehari, A. Elmeriah, A. Remlaoui. Dynamic simulation of an air-gap membrane distillation (AGMD) process using photovoltaic panels system and flat plate collectors. **Journal of Thermal Engineering** 7 (2021) 117-133

DOI: 10.18186/thermal.870383

A. Marni Sandid, T. Nehari, D. Nehari. Simulation study of an air-gap membrane distillation system for seawater desalination using solar energy. **Desalination and Water Treatment** 229 (2021) 40-51

DOI: 10.5004/dwt.2021.27394

A. Remlaoui, D. Nehari, M. Laissaoui, **A. Marni Sandid**. Performance evaluation of a hybrid solar thermal and photovoltaic systems powering a direct contact membrane distillation: TRNSYS simulation, **Desalination and Water Treatment** 194 (2020) 37–51

DOI: 10.5004/dwt.2020.25834

A. Marni Sandid, D. Nehari, T. Nehari. Effective study of operating parameters on the membrane distillation processes using various materials for seawater desalination. **Membrane and Water Treatment**. 13(5) (2022) 235-243

DOI: 10.12989/MWT.2022.13.5.235

T. Baki, **A. Marni Sandid**, D. Nehari. Sizing of an autonomous individual solar water heater based in Oran, Algeria. **Slovak Journal of Civil Engineering**. 30(3) (2022) 9-16

DOI: 10.2478/sjce-2022-0016

Summer University

A. Marni Sandid. Thermal system for membrane distillation using photovoltaic system panels in the weather Ain-Temouchent, **Algerian American Foundation (AAF'2019)** at Batna, Algeria. [28/07/2019 – 03/08/2019].

Conference papers:

A. Marni Sandid. 9th International Renewable and Sustainable Energy Conference (IRSEC'2021- EEE conference). Title: Investigation and simulation study of the various solar thermal systems for seawater desalination, at Tetouan, Morocco.

A. Marni Sandid, D. Nehari, I. Ait Yala, A. Remlaoui, H. Bekraoui. International Conference on Materials Science and Engineering and their Impact on the Environment ICMSE'2019. Title: Performance of the thermal system for membrane distillation using photovoltaic system panels and flat plate collector, at UDL Sidi-Bel-Abbes, Algeria.

A. Marni Sandid, D. Nehari, I. Ait Yala, H. Bekraoui, A. Remlaoui. International Conference on Renewable Energy and Energy Conversion ICREEC'2019. Title: Cooling system for membrane distillation using photovoltaic system panels in the weather Ain Temouchent, at USTO-MB Oran, Algeria.

A. Remlaoui, D. Nehari, H. Bekraoui, **A. Marni Sandid.** International Conference on Materials Science and Engineering and their Impact on the Environment ICMSE'2019. Title: Modeling a forced circulation solar water heater system (SWH) by TRNSYS Dynamic simulation, at UDL Sidi-Bel-Abbes, Algeria.

H. Bekraoui, D. Nehari, A. Remlaoui, **A. Marni Sandid.** International Conference on Renewable Energy and Energy Conversion ICREEC'2019. Title: Numerical simulation and theoretical investigation of direct contact membrane distillation, at USTO-MB Oran, Algeria.

A. Remlaoui, D. Nehari, I. Ait Yala, **A. Marni Sandid,** H. Bekraoui, A. Elmeriah. International Conference on Renewable Energy and Energy Conversion ICREEC'2019. Title: Solar Forced Circulation Water Heating Systems using Flat Plat Collector: A TRNSYS Dynamic simulation, at USTO-MB Oran, Algeria.

Other publications related to this research but not included in the thesis:**Journal Papers:**

T. Nehari, K. Bahram, D. Nehari, **A. Marni Sandid**. Numerical analysis of the influence of maximum residual thermal stresses on the intensity factor between the matrix and particle interfaces in metal matrix composite. **Frattura ed Integrità Strutturale** 54 (2020) 275-281
DOI: 10.3221/IGF-ESIS.54.19

Others:

A. Marni Sandid. 4th Cairo Water Week. Participation in the 4th African Young Water Professional's Forum (Af-YWPF), 25-27 October 2021 at Cairo, Egypt.

A. Marni Sandid. Participation in the day of support and assistance on: "Methodology of scientific research and the publication of a scientific article in an indexed journal", 08 January 2020, at « BENCHEHIDA Mohammed » University of Mostaganem, Algeria.

A. Marni Sandid. Participation in the 8th International Renewable and Sustainable Energy Conference IRSEC'21- EEE conference) 25-28 November, at Tetouan, Morocco.

A. Marni Sandid. Software training "ANSYS; Mechanical APDL" 09-12th December 2018, at University Belhadj Bouchaïb of Ain Temouchent, Algeria.

A. Elmeriah, D. Nehari, A. Remlaoui, I. Ait Yala, H. Bekraoui, **A. Marni Sandid**. The second day on structures and sustainable development JSDD April 11, 2019. Title: Numerical investigation of a flow inside a medium thermal energy storage density unit, at Tissemsilt, Algeria.

I. Ait Yala, D. Nehari, J. Ramos Garcia, F. Illan Gomez, **A. Marni Sandid**, A. Remlaoui. Celebration of world day for safety and health at work April 28, 2019. Title: CO2: Refrigerant of the future, at Ain Temouchent, Algeria.

Acknowledgments

First, before anything, thanks to "Allah" who the Almighty for having given me the courage, the will and the patience to complete this present work in the best conditions. I am indefinitely indebted to my parents and sisters whom devoted all her time for me during the preparation of this work, "Allah" bless them now and forever.

I would like to take this opportunity to express high emotion of benevolence and deepest gratitude to my supervisor Dr. Taieb NEHARI, Department of Mechanical Engineering, University of Ain Temouchent, Algeria who encouraged and provided me all necessary facilities throughout the course of my PhD studies. My sincere appreciations are also extended to my co-supervisor Prof. Driss NEHARI, Department of Mechanical Engineering, University of Ain Temouchent, Algeria for his extended support during the preparation of this thesis.

I would also like to deeply thank the PhD thesis defense committee members. The presidency of the jury: Prof. Abdelhamid BOUNIF from University of University of Ain Temouchent and all examiners members: Prof. Abdelkader DEBAB from "Université des Sciences et Technologie d'Oran", Prof. Farida BOUAFIA from University of Ain Temouchent and Prof. Mohammed SENOUCI from "Ecole Supérieure en Génie Electrique et Energétique d' Oran", for their valuable comments and suggestions for the insightful questions. I would like to express many thanks to Prof. Mohamed BASSYOUNI, Port Said University, Egypt for working with me during experimental investigation and appreciate support in publications. I cannot forget Prof. Yasser ELHINAWY, Port Said University, Egypt who worked in this project and helped me on several occasions. Words fail to express my gratitude to Prof. Yasser Elhinawy, who has been of great help.

I would like to extend my special thanks to all my friends for their moral support and encouragement during the course of study. I am also grateful to all the team of the Smart Structure Laboratory, University of Ain Temouchent and all my teachers from primary school to University whom helped me on this work and make it possible.

I don't have suitable words to acknowledge my family members for their patience and unconditional love especially my parents, whom have instilled in me the value of education, self-discipline, hard work and the importance of faith. It is very difficult to express my gratitude in words for their contribution. I am very much indebted to them. You are my encouragement and hope. I will keep on trusting you for my future.

At the end, I would like to thank all my friends who participated directly or indirectly in the realization of this modest work.

Although just a thank you is not enough, I sincerely thank you all so much.

ABDEL FATAH MARNI SANDID



Dedications

I DEDICATE THIS THESIS

TO MY PARENTS WHO HAVE PROVIDED ME WITH THEIR ENDLESS SUPPORT, LOVE AND THEIR SACRIFICES THAT MADE THIS THESIS POSSIBLE.

TO MY SISTERS FOR THEIR WHOLE-HEARTED SUPPORT.

TO ALL MY EXTENDED FAMILY.

TO ALL MY FRIENDS AND TEACHERS AT THE UNIVERSITY OF AIN TEMOUCHENT.

TO ALL WHO WERE THERE FOR ME, THANK YOU FOR YOUR HELP AND ENCOURAGEMENT.

TO ALL THOSE WHO HAVE BEEN SUPPORTIVE, CARING AND PATIENT.

I DEDICATE THIS WORK AND GIVE SPECIAL THANKS TO THOSE WHO LOVE ME FOR BEING THERE FOR ME THROUGHOUT THE ENTIRE DOCTORATE PROGRAM. ALL OF YOU HAVE BEEN MY BEST CHEERLEADERS.

"IN MY PHD, THEY WERE YEARS FULL OF DIFFICULTIES. I LOST A LOT, GRIEF A LOT, AND FACED MANY OBSTACLES, BUT I LEARNED TO THANK "ALLAH" SO MUCH FOR ALL OUR BLESSINGS, I LEARNED TO BE PATIENT, I LEARNED THAT NOT EVERYTHING THAT GLITTERS IS GOLD AND THE MOST INSIGNIFICANT THINGS ARE THE ONES THAT MAKE NOISE. AND THE BEST THING I'VE LEARNED IN THESE YEARS IS TO BE WITH "ALLAH" AND DON'T CARE."

THANK YOU ALL

ABDELFATAH MARNI SANDID

Table of Contents

Abstract
Preface
Acknowledgements
Dedication
Table of contents
Index of Figures
Index of Tables
Nomenclature and abbreviations

General Introduction

Research Objectives
 Structure of Thesis

CHAPTER I: Literature Review

- I. Introduction**
- I. 1. Drinking water problem**
- I. 2. Suggested solutions for desalination**
- I. 3. Desalination**
- I. 4. Properties of seawater**
- I. 5. History of seawater desalination**
- I. 6. The main water desalination technologies**
 - I. 6. 1. Thermal distillation processes**
 - I. 6. 1. 1. Multi-stage flash distillation (MSF)**
 - I. 6. 1. 2. Multi-effect distillation (MED)**
 - I. 6. 1. 3. Vapor compression (MVC, TVC)**
 - I. 6. 2. Desalination: membrane processes**
 - I. 6. 2. 1. Electrodialysis (ED)**
 - I. 6. 2. 2. Reverse osmosis (RO)**
 - I. 6. 2. 3. Membrane distillation (MD)**
- I. 7. Types of membrane distillation processes**
 - A. Direct Contact Membrane Distillation (DCMD)**
 - B. Air Gap Membrane Distillation (AGMD)**
 - C. Vacuum Membrane Distillation (VMD)**
 - D. Sweep Gas Membrane Distillation (SGMD)**
- I. 8. MD technology developers and promoters**
- I. 9. Advantages of AGMD**
- I. 10. Heat and mass transfer in AGMD**
 - I. 10. 1. Heat transfer**
 - I. 10. 2. Mass transfer**
- I. 11. Heat and mass transfer analysis in AGMD**
- I. 12. AGMD Configurations**
- I. 13. Renewable energy sources for desalination**

- I. 14. Definition and typology**
 - I. 14. 1. Solar energy**
 - I. 14. 2. Wind energy**
 - I. 14. 3. Geothermal energy**
- I. 15. Renewable energies in the world**
- I. 16. The development of renewable energies in Algeria**
- I. 17. Solar Desalination systems**
- I. 18. Solar Membrane Distillation (SMD)**
- I. 19. Solar AGMD systems**
- I. 20. Summary of literature review**
- References**

CHAPTER II:

Effects of operating parameters on the AGMD module for desalination

- II. Introduction**
 - II. 1. Presentation of "Fluent":**
 - II. 2. Procedure under "Fluent":**
 - II. 3. Turbulence models:**
 - II. 3. 1. k- ϵ model:**
 - II. 3. 1. 1. Standard k- ϵ model**
 - II. 3. 1. 2. RNG k- ϵ model:**
 - II. 3. 1. 3. Realizable model k- ϵ**
 - II. 4. Principle of the finite volume method**
 - II. 5. Reminder on the finite volume method**
 - II. 6. Mesh**
 - II. 7. Reynolds number**
 - II. 7. 1. Laminar flow**
 - II. 7. 2. Transient flow**
 - II. 7. 3. Turbulent flow**
 - II. 8. Equations and methodology**
 - II. 8. 1. Governing equations**
 - II. 8. 2. Mass flux**
 - II. 8. 3. Heat flux**
 - II. 8. 4. Thermal efficiency and temperature polarization coefficient**
 - II. 9. AGMD module**
 - II. 10. Grid Independent**
 - II. 11. Conclusion**
 - References**

CHAPTER III:

Simulation, controlling and optimization study of the solar AGMD system small scale

- III. Introduction**
 - III. 1. Description of the TRNSYS software**

- III. 1. 1. Advantages and disadvantages of the TRNSYS software
- III. 2. Equations and methods of the solar AGMD system small scale
 - III. 2. 1. AGMD module
 - III. 2. 2. Solar thermal system
 - III. 2. 3. Solar PV system
- III. 3. Main specifications of the solar thermal integrated MD system
- III. 4. Simulation and controlling of the solar AGMD system during the year “CASE 1”
 - III. 4. 1. System Description
 - III. 4. 1. 1. AGMD process
 - III. 4. 1. 2. Thermal system
 - III. 4. 1. 3. Photovoltaic (PV) system
 - III. 4. 1. 4. Weather data
 - III. 4. 1. 5. TRNSYS Model
 - III. 5. Development and optimization of solar AGMD system during the year “CASE 2”
 - III. 5. 1. Description of the AGMD system
 - III. 5. 1. 1. Solar-thermal system
 - III. 5. 1. 2. Solar photovoltaic (PV) system
 - III. 5. 1. 3. The AGMD module
 - III. 5. 2. The solar AGMD system in the TRNSYS simulation
- III. 6. Conclusion
- References

CHAPTER IV:
Experimental, simulation and economical Study of the solar AGMD system large scale

- IV. Introduction
- IV. 1. Methods
 - IV. 1. 1. Multi-channel spiral wound AGMD system
 - IV. 1. 2. Description of solar heating system
 - IV. 1. 2. 1. Description of solar FPC system
 - IV. 1. 2. 2. Description of solar ETC system
 - IV. 1. 3. Weather data
- IV. 2. Simulation
 - IV. 2. 1. Modeling of AGMD module
 - IV. 2. 2. Modeling of solar membrane distillation system
 - IV. 2. 2. 1. Spiral wound AGMD system using solar FPC system
 - IV. 2. 2. 2. Spiral wound AGMD system using solar ETC system
- IV. 3. Conclusion
- References

CHAPTER V: RESULTS AND DISCUSSION

V. 1. Effects of operating parameters on the AGMD module for desalination

V. 1. 1. Models validation

V. 1. 2. Temperature contours, velocity vectors, and total pressures of the AGMD module

V. 1. 3. Effect of operating temperatures

V. 1. 4. Effect of operating flow rates

V. 1. 5. Effects of different thermal properties on various materials of MD

V. 1. 6. Effects of different areas and flow regimes

V. 2. Simulation and controlling and optimization study of the solar AGMD system “SMALL SCALE”

V. 2. 1. Model validation

V. 2. 2. Temperatures inlet of AGMD and Distillate Flows without auxiliary heaters

V. 2. 3. Temperatures inlet of AGMD and Distillate Flows with auxiliary heaters

V. 2. 4. Auxiliary heating rate and power to load of the photovoltaic (PV) system

V. 3. Development and optimization study of the solar AGMD system small scale

V. 3. 1. Model validation

V. 3. 2. Weather data

V. 3. 3. Thermal capacity and permeate flux

V. 3. 4. Power to load of the Photovoltaic (PV) System

V. 3. 5. The flat plate thermal solar collector efficiency

V. 3. 6. The thermal energy efficiency of the AGMD system

V. 4. Experimental, simulation and economical Study of the solar AGMD system “LARGE SCALE”

V. 4. 1. Model validation

V. 4. 2. Thermal capacity and permeate flux

V. 4. 3. GOR and STEC of the AGMD system

V. 4. 4. The thermal energy efficiency of the AGMD system

V. 4. 5. Mitigation potential of CO₂ emissions

V. 4. 6. Economic analysis

References

GENERAL CONCLUSION

General conclusion and perspectives

Future work

APPENDIX

Appendix A: Compositions of drinking water quality

Appendix B: 3D Surface Plots

Index of figures

General Introduction

Figure 1: Outline of this thesis

Chapter I:

Figure I.1: Availability of fresh water in the world.

Figure I.2: Main water desalination processes.

Figure I.3: Multi-stage flash distillation.

Figure I.4: Multi-Effect distillation (MED).

Figure I.5: Mechanical Vapor compression (MVC).

Figure I.6: Electrodialysis (ED) process.

Figure I.7: Reverse osmosis process.

Figure I.8: Different configurations of MD process.

Figure I.9: Pilot plants of MD systems from different suppliers.

Figure I.10: Heat transfer process in AGMD.

Figure I.11: Mass transfer process in AGMD.

Figure I.12: Heat and mass transfer of AGMD.

Figure I.13: Membrane element configurations.

Figure I.14: Targeted renewable energy mix (2030).

Figure I.15: Representation of some possible combinations of renewable energy sources and desalination processes.

Figure I.16: The contribution of renewable energy resources in desalination.

Figure I.17: The experimental rig manufactured and used in the solar tubular MD module.

Figure I.18: A Pilot solar combined MD (SCMD) system installed at UAE.

Chapter II:

Figure II.1: Two-dimensional control volume.

Figure II.2: Diagram of the mesh.

Figure II.3: Schematic diagram of the AGMD module.

Figure II.4: Heat transfer coefficients (h) at various mesh sizes.

Figure II.5: The models discretization mesh of AGMD.

Chapter III:

- Figure III.1:** Bench-scale MD module and pictures of cassette fitted into module.
- Figure III.2:** Schematic showing an operation of solar domestic hot water (SDHW).
- Figure III.3:** Synoptic representation of the structure of a photovoltaic system with storage.
- Figure III.4:** (a) Ambient temperature, wind velocity and (b) irradiation in the weather of Ain Temouchent.
- Figure III.5:** Assembly diagram of the AGMD system in the TRNSYS simulation.
- Figure III.6:** The time value for operation of the AGMD system with ON / OFF control.
- Figure III.7:** Schematic of the solar AGMD System for seawater desalination.
- Figure III.8:** Pictures of cassette fitted into the module and bench-scale AGMD module.
- Figure III.9:** Diagram of the solar AGMD system in the TRNSYS program.

Chapter IV:

- Figure IV.1:** The experimental pilot plant.
- Figure IV.2:** Cross section of AGMD module.
- Figure IV.3:** Schematic of the solar system and the flow diagram.
- Figure IV.4:** (a) Ambient air temperature, wind speed and (b) Monthly irradiation.
- Figure IV.5:** Diagram of the AGMD system using FPC in the TRNSYS simulation.
- Figure IV.6:** Diagram of the AGMD system using ETC in the TRNSYS simulation.

Chapter V:

- Figure V.1:** Comparison between the experimental and simulation results of membrane and bulk surfaces temperatures in the AGMD module.
- Figure V.2:** Velocity vectors and Temperature contours of the AGMD module.
- Figure V.3:** Distribution of pressure along the membrane length permeate side of AGMD module.
- Figure V.4:** Effect of feed inlet temperature on mass flux.
- Figure V.5:** Effect of cold inlet temperature on mass flux.
- Figure V.6:** Effect of Reynolds number (Feed side) on mass flux.
- Figure V.7:** Effect of Reynolds number (Cold side) on mass flux.
- Figure V.8:** Efficiency, mass flux, and TPC on different materials of MD.
- Figure V.9:** Comparison of distillate flow between the simulation and the experimental data.
- Figure V.10:** Comparison of temperature outlet of the thermal system between the simulation and the experimental data.

- Figure V.11:** Feed AGMD inlet temperatures without auxiliary heaters ($^{\circ}\text{C}$).
- Figure V.12:** Distillate flows of AGMD module without auxiliary heaters (Kg/h).
- Figure V.13:** Feed AGMD inlet temperatures with auxiliary heaters ($^{\circ}\text{C}$).
- Figure V.14:** Distillate flows of AGMD module with auxiliary heaters (Kg/h).
- Figure V.15:** Power to load of the auxiliary heaters of the thermal system for AGMD.
- Figure V.16:** Power to load of the photovoltaic system for the auxiliary heaters for AGMD
- Figure V.17:** Effect of feed inlet temperature on flux.
- Figure V.18:** Comparison of temperature outlet of the thermal system between the simulation and the experimental data.
- Figure V.19:** Comparison of distillate flow between the simulation and the experimental data.
- Figure V.20:** Ambient temperature and wind velocity throughout the year in Ain-Temouchent weather.
- Figure V.21:** Irradiation throughout the year in Ain-Temouchent weather.
- Figure V.22:** Distribution of collector outlet temperature along the day during 4 seasons.
- Figure V.23:** Distribution feed inlet temperature of AGMD.
- Figure V.24:** Permeate flux of AGMD.
- Figure V.25:** Power to load of the PV System and pumps for the AGMD system.
- Figure V.26:** The flat plate thermal solar collector efficiency during 4 days.
- Figure V.27:** The thermal energy efficiency of the AGMD module during 4 days.
- Figure V.28:** The simulation and the experimental data of the permeate flux, hot and Cold feed outlet temperatures of the AGMD module with ($V_h=210\text{ L/h}$, $V_c=180\text{ L/h}$).
- Figure V.29:** The simulation and the experimental data of the permeate flux with ($J1: V_h=V_c= 600\text{ L/h}$, $J2: V_h=V_c= 360\text{ L/h}$ and $J3: V_h=V_c= 120\text{ L/h}$).
- Figure V.30:** Distribution of collector outlet temperature along the day during summer and winter season.
- Figure V.31:** Distribution feed inlet temperature of AGMD using FPC and ETC.
- Figure V.32:** Permeate flux of AGMD.
- Figure V.33:** Average temperatures on STEC (kWh/m^3) and GOR of the AGMD system ($V_f = V_c = 2, 3, 6$ and 10 L/min).
- Figure V.34:** Average temperatures on the thermal energy efficiency of the AGMD system ($V_f = V_c = 2, 3, 6$ and 10 L/min).
- Figure V.35:** The daily accumulated solar intensity: accumulated daily potable water productivity and saving of CO_2 against the solar collector configurations.

Appendix:

Figure 1: 3D Surface Plot of T_{ho} ($^{\circ}\text{C}$), T_{co} ($^{\circ}\text{C}$) and J (kg/h); $V_f = V_c = 600$ (kg/h).

Figure 2: 3D Surface Plot of T_{ho} ($^{\circ}\text{C}$), T_{co} ($^{\circ}\text{C}$) and J (kg/h); $V_f = V_c = 360$ (kg/h).

Figure 3: 3D Surface Plot of T_{ho} ($^{\circ}\text{C}$), T_{co} ($^{\circ}\text{C}$) and J (kg/h); $V_f = V_c = 180$ (kg/h).

Figure 4: 3D Surface Plot of T_{ho} ($^{\circ}\text{C}$), T_{co} ($^{\circ}\text{C}$) and J (kg/h); $V_f = V_c = 120$ (kg/h).

Figure 5: 3D Surface Plot of T_{ho} ($^{\circ}\text{C}$), T_{co} ($^{\circ}\text{C}$) and J (kg/h); $V_f = 210$ & $V_c = 180$ (kg/h).

Index of tables

Chapter I:

Table I.1: Major stocks of water on Earth.

Table I.2: Variation of drinking water resources per person in Algeria.

Table I.3: Composition of standard seawater.

Table I.4: Commercial MD technology developers and process utilized.

Table I.5: Membrane element configuration comparison.

Table I.6: Pilot scale solar driven AGMD systems.

Chapter II:

Table II.1: Values of the constants of the k- ϵ model.

Table II.2: Values of the constants of the RNG k- ϵ model.

Table II.3: Values of the constants of the realizable model k- ϵ .

Table II.4: Summary of PVDF, vapor, and total membrane thermo-physical properties.

Table II.5: Summary of boundary conditions for AGMD.

Chapter III:

Table III.1: Operational conditions of tested AGMD module.

Table III.2: Main specifications of the solar thermal integrated MD system.

Table III.3: Technical characteristics of the PV system.

Chapter IV:

Table IV.1: AGMD module properties and specifications.

Table IV.2: The spacer characteristics.

Table IV.3: FPC specifications.

Table IV.4: ETC specifications.

Table IV.5: Permeate fluxes from different feed and cooling water temperatures at different flow rates.

Table IV.6: Range of data.

Table IV.7: Operational conditions of tested AGMD module.

Table IV.8: Minitab results summary.

Chapter V:

Table V.1: Thermal properties of different materials of MD.

Table V.2: Comparison of different membrane parameters using different flow regimes.

Table V.3: Comparison between the present study and previous studies.

Table V.4: Cost breakdown of FPC case.

Table V.5: Cost breakdown of ETC case.

Table V.6: Cost breakdown of MD system.

Table V.7: Running cost estimation with LCOW of SMD system.

Table V.8: A leveled cost comparison with others.

Appendix:

Table 1: World Health Organization (WHO) guidelines for drinking water quality.

Nomenclature and abbreviations

Symbols:

C_{p_f}	Specific heat capacity of solar fluid, kJ.hr
V_f	Feed flow rate, kg / hr
J_d	Distillate flux, kg / hr
T	Temperature, °C
M_d	Mass of distillate water, kg
S	Effective membrane surface area of evaporation, m ²
Q_{md}	Thermal energy supplied, kWh
t	Time, hr
m_0	Solar fluid mass flow rate, kg / hr
UA	Overall loss coefficient between the heater and its surroundings during operation, kg / hr
C	Capacity rate, kJ / hr.K
Q	Heating rate of the heater, kg / hr
\bar{T}	Brackish water average temperature, K
T_{set}	Set temperature of heater internal thermostat, K
T_{env}	Temperature of heater surroundings for loss calculations, K
P_C	Power of the PV field,
D	Daily need, kWh / jour
F	Form factor,
N	Number of hour's equivalent,
$G_T(t)$	Solar radiation incident on the solar -PV array in the current time step, kW/m ²
$G_{T,STC}$	Incident radiation at standard test conditions, kW/m ²
N_j	Autonomy number of days without radiation,
P	Discharge.
C	Capacity rate, kJ / hr.K
I	Interest rate, %
m_0	Solar fluid mass flow rate, kg / hr
N	Economic lifetime (year)
Q_u	Useful heat gain, kW
Q_e	Thermal energy supply, kWh
U_b	Nominal voltage of the batteries,

V	Flow rate, kg / hr
SFF	Sinking Fund Factor
$STEC$	Specific thermal energy consumption (kWh/m ³)
$T_{cooling,out}$	Condenser outlet temperature (°C)
$T_{feed,out}$	Evaporator outlet temperature (°C)
$T_{feed,in}$	Evaporator inlet temperature (°C)
t_{life}	Economic lifespan
W_p	Annual running cost of the water pump (\$/year)
rc	Running costs

Greek symbols

ε	Heat exchanger counter flow effectiveness
η	Efficiency

Subscripts

in	Inlet
out	Outlet
h	Hot
c	Cold
p	Permeate
d	Depth
hr	Hour
$loss$	Losses
max	Maximum
min	Minimum
aux	Auxiliary
f	Feed
htr	Heater


Abbreviations

MD	Membrane Distillation
AGMD	Air-Gap Membrane Distillation
DCMD	Direct Contact Membrane Distillation
DMV	Vacuum Membrane Distillation

SGMD	Sweeping Gas Membrane Distillation
SDHW	Solar Domestic Hot Water
SCMD	Solar Combined Membrane Distillation
FPC	Flat Plate Collector
ETC	Evacuated tube collectors
CPC	Parabolic compound collectors
PV	Photovoltaic
PTFE	Polytetrafluoroethylene
PVDF	Polyvinylidene fluoride
PE	Polyethylene
PP	Polypropylene
GOR	Gain output ratio
LCOW	leveled cost of water



GENERAL INTRODUCTION



A. MARNI SANDID
DOCTORAL THESIS
2023

General Introduction

Population growth and the degradation of some freshwater resources are two problems that make us look for developing modern technologies for water desalination. In many countries and places across the world, seawater is used in desalination processes because it covers a large area of 70 percent of the land. The reverse osmosis technology has been used that provides a large flow of freshwater; however, it also consumes large electrical energy due to the use of huge pumps in this technology [1]. Therefore, the membrane distillation (MD) process has been used for seawater desalination. The MD processes are used at low temperatures and less than 100 °C. Therefore, more efficient methods have been used for the desalination process due to high salt rejection with low fouling and operating pressure in MD applications [2].

Membrane distillation is a thermal process in which water vapor is transported through a hydrophobic porous membrane. The liquid phase to be treated must be kept in contact with one face of the membrane without penetrating its pores unless the trans-membrane pressure is greater than the inlet pressure. The hydrophobicity of the membrane prevents liquid from entering the pores thanks to the surface tension. Thus, liquid/vapor interfaces are created near the pores. There are several types of membrane distillations. The differences only concern the permeate side and will condition the driving force of the separation. Until now, Polytetrafluoroethylene (PTFE), polyvinylidene fluoride (PVDF), polyethylene (PE), and polypropylene (PP) have been the most commonly used membranes for MD processes [3].

There are four main configurations of membrane distillation modules in the literatures: Direct Contact Membrane Distillation (DCMD) [4], Air Gap Membrane Distillation (AGMD) [5], Sweeping Gas Membrane Distillation (SGMD) [6], and Vacuum Membrane Distillation (VMD) [7]. This difference in the nature of the permeate treatment: the condensation of the vapor that has passed through the membrane takes place inside the module for DCMD and AGMD configurations and outside the module for VMD and SGMD configurations. DCMD is the most MD configuration technology studied due to the simplicity and ease of handling, where its energy efficiency, called the membrane thermal efficiency (MTE), is commonly related to the operating conditions [8]. In the MD process field, the DCMD process has a lower MTE against the AGMD procedure because of conduction heat losses. The mechanism functions of the AGMD systems are based on the stagnant air gap interposition between the membrane and condensation area, which leads to an inherently increase in the thermal energy efficiency of the process [9]. Consequently, the first patent to discuss the principle of AGMD

appeared with G. L. Hassler [10] and P. K. Weyl [11] for the basic knowledge, in which the concept and behavior of AGMD systems can be found in different literature studies [12, 13, 14].

According to the high-energy costs associated with existing desalination methods, there is a great demand for technologies that can use low-temperature sources like waste heat or solar energy. Although recent developments in AGMD configurations, the first flat plate AGMD system was developed by the Swedish Svenska Utvecklings AB in 2016 [15], while such modules today are manufactured and commercialized by Scarab Development. Each module is made up of 10 planar cassettes with an overall membrane surface of 2.3 m² and a global capacity of 1–2 m³/d of distillate water [16]. The single-stage consists of injection-molded plastic frames containing two parallel membranes, feed and exit channels for warm water, and two condensing walls [17].

On the other hand, Khan et al [18] conducted experimental analysis from arsenic removal using single cassette AGMD with an effective membrane area of 0.2 m² and reported fluxes of 20 L/m²h at a temperature difference of 50°C between hot and cold inlet temperatures. He et al [19] applied factorial design and RSM to analyze the relationships between operating parameters (hot and cold inlet temperatures, feed flow rate) on performance indicators including distillate flux and gained output index of a hollow fiber AGMD module.

In Kumar's work et al [20], a single cassette air-gap membrane distillation (AGMD) module is characterized to identify the effect of process parameters on distillate flux and thermal efficiency. Favorable conditions to obtain a distillate flow rate of 3–5 kg/h determined on a bench-scale experimental setup. The developed RSM regression model was tested by analysis of variance (ANOVA) and studied using experimental results of Asim et al [21]. Parametric optimization was carried out as well to identify suitable conditions for operating MD with constant or dynamic energy supply (e.g. solar thermal energy). Then, experiments on a solar MD system were carried out in October during which maximum radiation would be incident on solar collectors installed in the United Arab Emirates (UAE).

Dynamic simulation of the combined system using tools such as TRNSYS and parametric analysis enables to design of a functional system and then optimizes it. In this study of Kumar et al [22], the application of the cogeneration system for residential households in the UAE is considered for per capita production of 4l/day of pure water and 50l/day of domestic hot water. The optimized cogeneration system utilizes more than 80% of the available solar energy gain and operates at 45% and 60% collector efficiencies for FPC and ETC systems respectively. The cogeneration operation reduces 6–16% of thermal energy demand and also enables 25% savings in electrical energy demand. In Gowtham's paper et al [23], a novel solar thermal polygeneration (STP) system for the production of cooling, clean water, and domestic

hot water is modeled and analyzed for the weather conditions of the UAE using TRNSYS software. The system comprises solar collectors for the production of thermal energy. Economic benefits are analyzed for different collectors and fuel costs savings. The lowest payback period of 6.75 years is achieved by STP with evacuated tube collector field having a gross area of 216 m².

For seawater desalination, the configuration studied in this thesis is AGMD. In the thermal membrane process AGMD, the driving force behind the transfer being a partial pressure difference on either side of the membrane created by a temperature difference. Compared to other membrane distillation techniques, AGMD seems interesting for its aspects of low membrane wetting and the fact that there is no additional energy consumption linked to the use of an additional pump. In recent years, AGMD has experienced more sustained development, mainly in research, thanks to developments in membrane manufacturing techniques. Seawater desalination is one of the most promising fields for the application of solar thermal energy due to the coincidence, in many places of the world, of water scarcity, seawater availability, and good levels of solar radiation (like Algeria). The Solar Membrane Distillation (SMD) is recently an under-investigation desalination process suitable for developing self-sufficient small-scale applications. The use of solar energy considerably reduces operating costs.

Research Objectives

The main objective of this doctoral work is to analyze and optimize renewable driven AGMD systems small and large scales. This objective can contribute to ensuring the availability of the distillate water using the solar desalination process. All objectives of this thesis are focused on:

- ➔ Effective study of the operating temperatures and the flow rates on the distillate flux of the hydrophobic membrane for seawater desalination.
- ➔ Effects of the nature of materials (Polyvinylidene fluoride (PVDF) polymers, copolymers and blends) used on the thermal properties of AGMD process.
- ➔ Investigation study of the mass and heat transfer of the PVDF membrane AGMD application using the commercial CFD code ANSYS-FLUENT.
- ➔ Performance study of the integrated single cassette AGMD module in the

solar thermal desalination system in different weathers throughout the year.

- ➔ Modeling, controlling and optimization study of the solar AGMD system using photovoltaic panels system and flat plate collectors for supply energy demand.
- ➔ Experimental study of the lab-scale AGMD desalination pilot plant using solar energy.
- ➔ Experimental and comparison study of flat plate and evacuated tube collectors for the solar AGMD system using the commercial TRNSYS program.
- ➔ Finally, the techno-economic study of solar AGMD systems for dynamic simulation and parametric optimization to analyze annual performances.

Structure of Thesis

Fig. 1 the roadmap of this thesis:

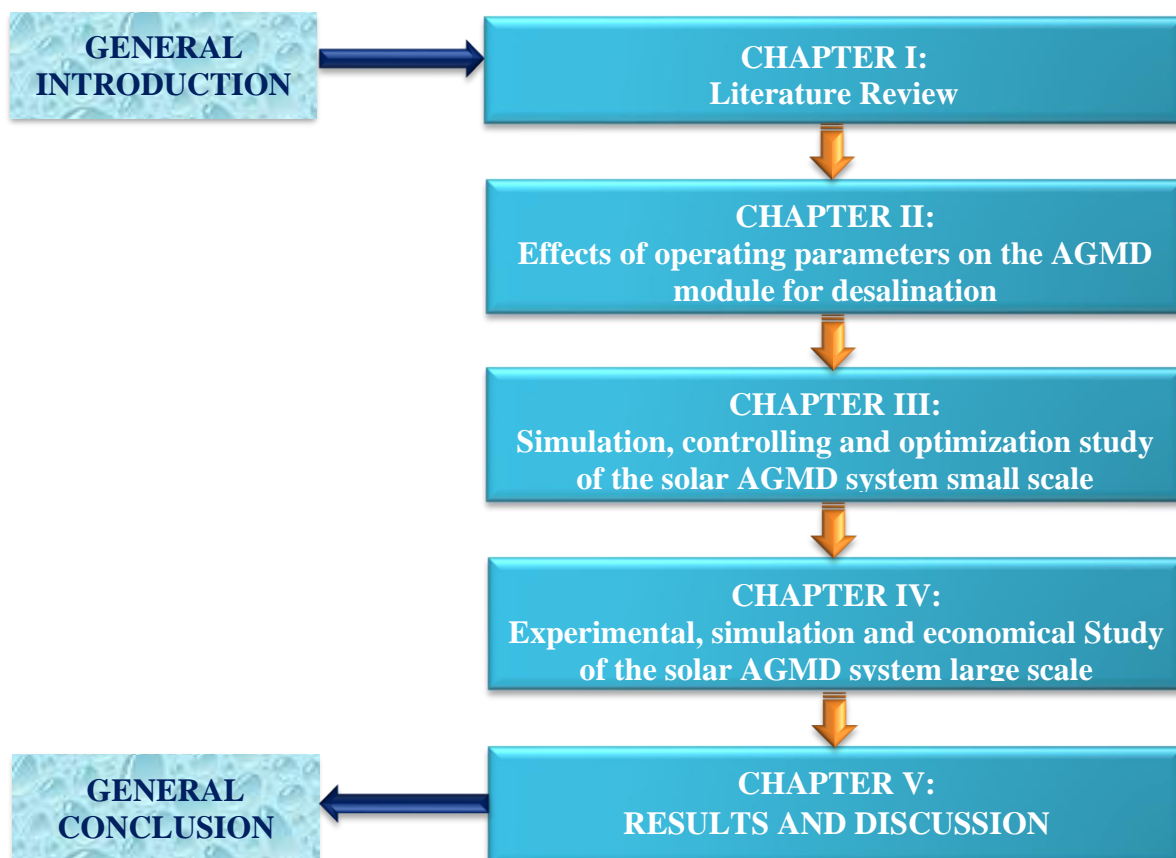


Figure 1: Outline of this thesis

This thesis is divided into following chapters:

- ✚ Chapter I presents the literature review and background for this research work. This chapter includes the drinking water problem in the world with suggested solutions, the main water desalination technologies with the advantages of the AGMD process. In addition, it also describes the heat and mass transfer in AGMD, renewable energy sources for desalination in the world with the development of renewable energies in Algeria and the solar AGMD systems.

- ✚ Chapter II describes effects of membrane physical properties and operating parameters (Temperatures and velocities) on the various materials of the AGMD module using the commercial CFD code ANSYS-FLUENT.

- ✚ Chapter III shows how to control the solar AGMD system small scale. Additionally, a new approach using a single cassette AGMD module integrated in the solar thermal desalination system is developed. The dynamic simulation of the solar AGMD process with photovoltaic panels and flat plate collectors uses the TRNSYS software during the year.

- ✚ Chapter IV contains experimental, simulation and techno-economic study of the solar AGMD system large scale using two types of solar collectors. In addition, this chapter contains a comparison of different renewable energy systems integrating a multi-channel spiral-wound AGMD module.

- ✚ Chapter V presents conclusions and discussions of thesis work. Moreover, the perspectives for future developments are also presented in this chapter.

Remarque:

General introduction includes our Article:

- **A. Marni Sandid, T. Nehari, D. Nehari. Simulation study of an air-gap membrane distillation system for seawater desalination using solar energy. *Desalination and Water Treatment* 229 (2021) 40-51
DOI: 10.5004/dwt.2021.27394**

References

- [1] M.T. Ali, H.E.S. Fath and P.R. Armstrong, A comprehensive techno-economical review of indirect solar desalination, *Renewable Sust. Energy Rev.*, 15 (2011) 4187–4199.
- [2] J. Phattaranawik, R. Jiratananon and A. Fane, Heat transport and membrane distillation coefficients in direct contact membrane distillation, *J. Membr. Sci.*, 212 (2003) 177–193.
- [3] M. Teoh and T. Chung, Membrane distillation with hydrophobic macrovoid-free PVDF-PTFE hollow fiber membranes, *Sep. Purif. Technol.*, 66 (2009) 229–236.
- [4] R.W. Schofield, A.G. Fane and C.J. Fell, Heat and mass transfer in membrane distillation, *J. Membr. Sci.*, 33 (1987) 299–313.
- [5] A. Boubakri, A. Hafiane and S.A.T. Bouguecha, Direct contact membrane distillation: Capability to desalt raw water, *Arab. J. Chemistry.*, 10 (2017) 75–81.
- [6] A.K. Thakur, I.M. Hsieh, M.R. Islam, B. Lin, C.C. Chen and M. Malmali, Performance of sweeping gas membrane distillation for treating produced water: Modeling and experiments, *Desal.*, 492 (2020) 554–597.
- [7] A. Alkudhiri, N. Darwish and N. Hilal, Membrane distillation: A comprehensive review, *Desal.*, 287 (2012) 2–18.
- [8] R. Ullah, M. Khraisheh, R.J. Esteves, J.T. McLeskey, A. Mohammad, G. Mohamed and H.V. Tafreshi, Energy efficiency of direct contact membrane distillation, *Desal.*, 433 (2018) 56–67.
- [9] M. Qtaishata, T. Matsuura, B. Kruczek and M. Khayet, Heat and mass transfer analysis in direct contact membrane distillation, *Desal.*, 219 (2008) 272–292.
- [10] Hassler G L. U.S. patent US3129146A (14 April 1964).
- [11] Weyl P K. U.S. patent US3340186A (5 September 1967).
- [12] A.S. Jonsson, R. Wimmerstedt and A.C. Harrysson, Membrane Distillation – A Theoretical Study of Evaporation Through Microporous Membranes, *Desal.*, 56 (1985) 237.
- [13] C. Gostoli, G.C. Sarti and S. Matulli, Low Temperature Distillation Through Hydrophobic Membranes. *Separation and Purification Technology.*, 22 (1987) 855.
- [14] F.A. Banat, F.A. Al-Rub, R. Jumah and M. Shannag, Theoretical investigation of membrane distillation role in breaking the formic acid-water azeotropic point: Comparison between Fickian and Stefan-Maxwell-based models, *Inter. Commu. Heat and Mass Transf.*, 26 (1999) 879–888.
- [15] J. Swaminathana, H.W. Chunga, D.M. Warsingera, F.A. AlMarzooqib and H.A. Arafatb, Energy efficiency of permeate gap and novel conductive gap membrane distillation, *J. Membr. Sci.*, 502 (2016) 171–178.

- [16] A.M. Alklaibi and N. Lior, Membrane-distillation desalination: Status and potential, *Desal.*, 171 (2005) 111–131.
- [17] L. Camacho, L. Dumée, J. Zhang, J.d. Li, Duke, J. Gomez and S. Gray, Advances in Membrane Distillation for Water Desalination and Purification Applications, *Water.*, 5 (2013) 94–196.
- [18] E.U. Khan and A.R. Martin, Water purification of arsenic-contaminated drinking water via air gap membrane distillation (AGMD), *Period. Poly. Mech. Eng.*, 58 (2014) 47–53.
- [19] Q. He, P. Li, H. Geng, C. Zhang, J. Wang and H. Chang, Modeling and optimization of air gap membrane distillation system for desalination, *Desal.*, 354 (2014) 68–75.
- [20] N.T. Uday Kumar and A. Martin, Experimental modeling of an air-gap membrane distillation module and simulation of a solar thermal integrated system for water purification. *Desal. Water Treat.*, 84 (2017) 123–134.
- [21] M. Asim, N.T. Uday Kumar, A. Martin, Feasibility analysis of solar combi-system for simultaneous production of pure drinking water via membrane distillation and domestic hot water for single-family villa: pilot plant setup in Dubai, *Desal. Water Treat.*, 57 (2015) 21674–21684.
- [22] N.T. Uday Kumar and A. Martin, Techno-economic optimization of solar thermal integrated membrane distillation for co-generation of heat and pure water, *Desal. Water Treat.*, 98 (2017) 16–30.
- [23] M. Gowtham, N.T. Uday Kumar, P. K Manoj and A. Martin, A novel solar thermal polygeneration system for sustainable production of cooling, clean water and domestic hot water in United Arab Emirates: Dynamic simulation and economic evaluation, *Appl. Energy.*, 167 (2016) 173–188.



CHAPTER I: LITERATURE REVIEW

A. MARNI SANDID

DOCTORAL THESIS

2023



I. Introduction

Nowadays, the demand for drinking water is increasing rapidly on the world level. Therefore, people face this problem in water demand in the industrial and irrigation fields, as well as in the incompressible needs of the population in large agglomerations across the world. Researchers are focusing on water desalination to face water scarcity in different countries where water resources are insufficient to population and agriculture [1].

Seawater represents an unlimited resource, but it contains more salt concentration than allowed by the World Health Organization (WHO). The maximum salt concentration is 500 mg/l for human consumption. This indicates that depending on the seawater salinity, a salt concentration reduction of 75 to 99 % is required. The water being drinkable if the salt level is less than 500 ppm [2]. Therefore, scientists in several nations are working to create more effective desalination systems in order to generate more drinking water at a cheaper cost [3].

The literature review presents a brief overview of several traditional desalination systems as well as modern improvements. In addition, more information about the membrane distillation method has been given, which is now the main desalination process. Then, special attention has been given to solar-powered MD systems for develop a renewable desalination system that can be used at different countries.

I. 1. Drinking water problem

Water is plentiful on our planet and comes in different forms. During the water cycle, it does really move from one to another. While most of the water consumed comes from lakes, rivers, and groundwater. The oceans, which span 71 percent of the Earth's surface, contain more than 96 percent of the water as shown in (Table I.1) (81 percent in the Southern Hemisphere and 61 percent in the Northern Hemisphere). Therefore, the ocean provides an almost limitless water supply [4].

Table I.1: Major stocks of water on Earth [4].

	Distribution area 10 ³ km ²	Volume 10 ³ Km ³	Percent of Total water, %	Percent of fresh water, %
Total water	510,000	1.386 million	100	-
Total fresh water	149,000	35,000	2.53	100
World oceans	361,300	1.340 million	96.5	-
Saline groundwater	-	13,000	1	-
Fresh groundwater	-	10,500	0.76	30
Antarctic glaciers	13,980	21,600	1.56	61.7
Greenland glaciers	1,800	2,340	0.17	6.7
Arctic islands	226	84	0.006	0.24
Mountain glaciers	224	40.6	0.003	0.12
Ground ice/permafrost	21,000	300	0.022	0.86
Saline lakes	822	85.4	0.006	-
Freshwater lakes	1,240	91	0.007	0.26
Wetlands	2,680	1.5	0.0008	0.03
Rivers (as flows on average)	-	2.12	0.0002	0.006
In biological matter	-	1.12	0.0001	0.0003
In the atmosphere (on average)	-	12.9	0.0001	0.04

Geographically, distribution of water is very differentially around the earth as shown in (Figure I.1). 10 countries share 60 percent of the world's freshwater reserves. Brazil has 12 percent alone. On the opposite, 29 other countries, mostly in the Middle East and Africa, have a chronic shortage of fresh water [5].

Water shortage has been a major issue in recent years, as the situation in most countries with large deserts and highly populated areas has become worrying and causing tensions. The impacted areas are frequently found in developing countries, and they are all the more exposed as a result of high population growth, which adds more demands on the water supply in these areas. However, WHO has defined a critical minimum of 1000 m³ per inhabitant per year, or 2.7 m³ per day, but this level is far from being reached. Furthermore, two billion people are affected by water stress, which is reached between 1000 and 2000 m³ per person and per year. 450 million of them do not have access to the bare minimum of water. It's estimated that by 2050, nearly one-third of the world's population (around 2.8 billion people) will be affected by water scarcity due to changing demography and increased water consumption [6].

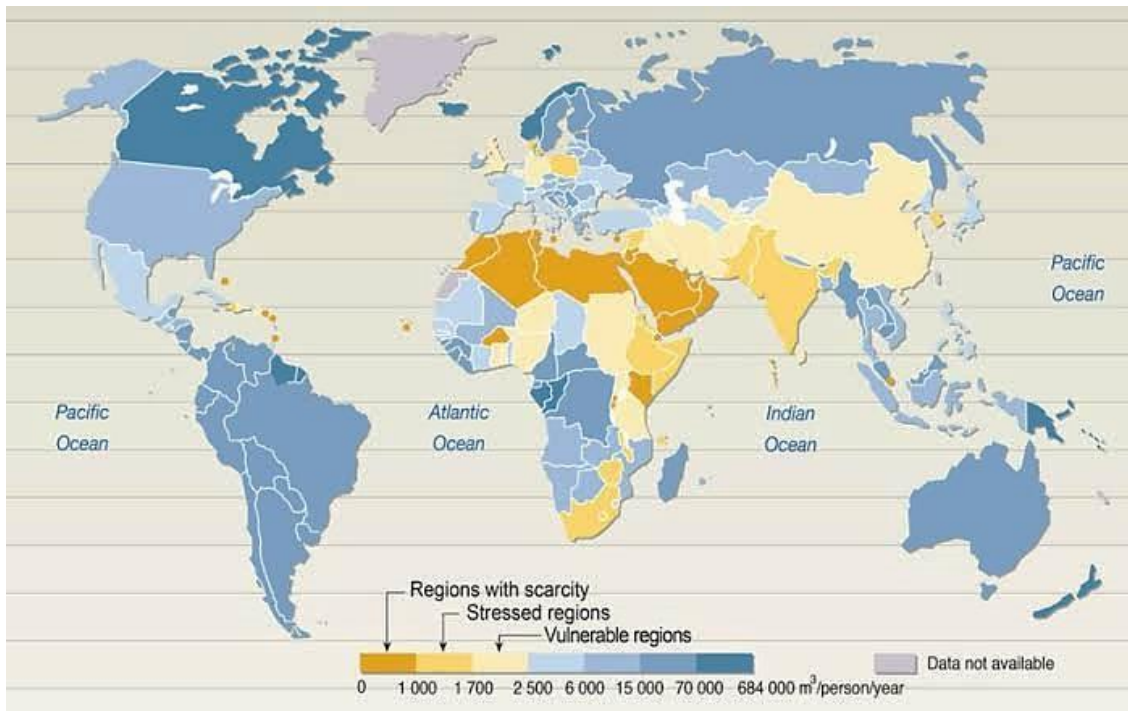


Figure I.1: Availability of fresh water in the world [7].

The total water potential of Algeria is estimated to be 19.4 billion m^3 per year. The groundwater resources (renewable resources) in the north are estimated to be around 2 billion m^3 per year. The annual surface resources are reached 12 billion m^3 [8]. Algeria is therefore among the countries with the greatest water deficit. Its average annual rainfall is predicted to be 89 mm because it's location in North Africa, and the fact that almost all of its lands are classed as desert. Thus, Algeria is one of the thirteen African nations with the most severe water shortages. Furthermore, with less than 500 m^3 per person per year, the country has less than 50 % of the theoretical shortage level [9].

Moreover, the demand for fresh water increases by 4 to 5% each year while natural supplies reduces because increasingly serious pollution problem. This equation demonstrates that demand will be greater than the resources. (Table I.2) shows that the potential for drinking water per person in Algeria has decreased [10].

Table I.2: Variation of drinking water resources per person in Algeria [10].

Year	1962	1990	1995	1998	2000	2020
m^3/person	1500	720	680	630	500	430

I. 2. Suggested solutions for desalination

To face this water scarcity, seawater desalination is regarded as a potential option for producing drinking water to cover the demands of the growing population, as well as industrial and agricultural needs. Seawater desalination technologies have been used for many years, but their expensive cost typically limits them from being used in richer countries. In recent years, desalination plant capacity has increased significantly as a result of technological and economic advancements in this field, which has led to a significant reduction in production costs.

Membrane processes or electrical methods (filtration) and distillation or thermal methods (which require phase change, evaporation and condensation) are the two broad categories of desalination processes (Figure I.2) [11].

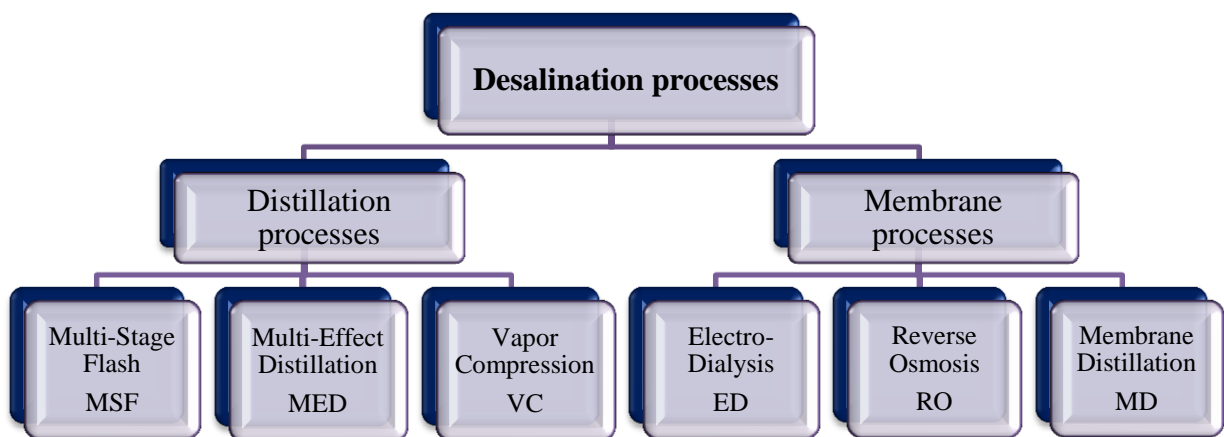


Figure I.2: Main water desalination processes [11].

Membrane distillation and reverse osmosis are two performance technologies for seawater desalination among the processes mentioned above. Furthermore, in the global desalination market, these two processes are the most popular. The other methods have not made significant progress in the field due to problems in energy consumption and the amount of the investments required [12].

I. 3. Desalination

Desalination is the process that produces pure water by removing dissolved solids from seawater, waste and brackish water. The concentration of total dissolved solids (TDS) is generally the amount of salt in water. TDS is the sum of all metals, minerals, anions, and cations dissolved in water. The amount of TDM (total dissolved matter) defines the salinity of water (mg/L) depending the amount of dissolved salt in the water [12].

I. 4. Properties of seawater

Some properties of water are strongly influenced by salts (compressibility, freezing point, density, activity coefficient), while others are unaffected (light absorption, viscosity). Other characteristics are determined by the quantity of salt in the water (osmotic pressure, conductivity). Under the influence of polar currents, the temperature of seawater ranges from -1.9 °C (freezing point of seawater at a concentration of 35 g/L of salts) to 35 °C at the Arabian Peninsula's level [13].

Temperature, pressure, and salinity are the properties of seawater, which they are affected by the depth. Because of the large variations in temperature, salinity, and depth, they can be highly variable from place to other. Except in closed seas, the chemical composition of seawater varies little. The average physicochemical characteristics of standard water are shown in (Table I.3) [14]. Sodium chloride accounts for about 85 percent of the total weight of the salts.

Table I.3: Composition of standard seawater [14].

The composition of standard seawater $S = 35 \text{ g/kg}$, $TA = 2.3 \times 10^{-3} \text{ mol/kg}$ and $pH = 8.1$ at $25 \text{ }^\circ\text{C}$

Species	Concentration		Specific concentration (g/kg)/s
	(g/kg seawater)	(mol/kg seawater)	
Na ⁺	10.7838	0.46907	0.30811
Mg ²⁺	1.2837	0.05282	0.036678
Ca ²⁺	0.4121	0.01028	0.01177
K ⁺	0.3991	0.01021	0.01140
Sr ²⁺	0.0079	0.00009	0.000227
Cl ⁻	19.3529	0.54588	0.55294
SO ₄ ²⁻	2.4121	0.02824	0.07750
HCO ₃ ⁻	0.1070	0.00175	0.00306
Br ⁻	0.0672	0.00084	0.00192
CO ₃ ²⁻	0.0161	0.00027	0.000459
B(OH ⁻) ₄	0.0079	0.00010	0.000225
F ⁻	0.0013	0.000068	0.000037
B(OH) ₃	0.0193	0.00031	0.000551
Total	35.1707	1.1199	1.004877

I. 5. History of seawater desalination

Since antiquity, people have attempted to extract unsalted water from seawater by boiling it and condensing the steam produced, which is the case with sailors in the long distance. Aristotle described a method for evaporating impure water and condensing it to obtain drinking water in the 4th century BC. However, it was not until the 18th century that processes were developed that allowed for production while improving water purity and energy efficiency. Furthermore, the first industrial processes of distillation, solution concentration, and fresh water production by vaporization and condensation did not appear until the early twentieth century [15].

Since the late 1940s, thermal desalination technologies by distillation have been used to desalinate seawater on a large scale. The first industrial desalination pilot plants appeared in the Middle East in the 1950s. Then, in 1959, the University of California developed the reverse osmosis process of the separating salts method from colloids and molasses. This is a membrane process in which fresh water is produced from salt water using pressure in a semi-porous membrane. Commercial membranes appeared around 1970. The two main processes used today for seawater desalination are membrane processes and distillation. There are more than 17,000 desalination units in service now, with a capacity of more than 109 million dem³ of generated water per day with an increase of 12% in the previous five years. More than half of the world's desalination capacity is in the Middle East, particularly Saudi Arabia, which produces 26% of worldwide desalination [15].

I.6. The main water desalination technologies

According to the principle used, current water desalination technologies are divided into two types [16]:

- ❖ Thermal processes including a change of phases: distillation and freezing.
- ❖ The membrane processes: electro dialysis, reverse osmosis and membrane distillation.

I.6.1. Thermal distillation processes

I.6.1.1. Multi-stage flash distillation (MSF)

MSF distillation is a distillation process depended on the instantaneous vaporization principle (flash distillation) as shown in (Figure I.3). The pretreated seawater in the installation is preheated using the condensers in the various stages of the process. Then it's put into a boiler

or heater, where it's heated to 110 degrees Celsius. Moreover, warm seawater is introduced into the first stage's bottom, where the pressure is lower than the saturated vapor pressure.

Therefore, this process operates in instant vaporization by expansion (flash distillation).

As a result, the vapor produced condenses on the condenser's walls and is collected. The seawater then enters the next chamber, which is warmer and has a lower pressure. In this chamber, a new flash distillation takes place. Until the final chamber, the process repeats the phenomenon. The pressure variations between the chambers allow seawater and fresh water flows produced without using pumps to the final chamber [17]. With a salinity of 50 to 100 mg/L and an electrical consumption of 1 to 3 kWh/m³ of produced water, this method obtains 25,000 m³ per day with a salinity of 50 to 100 mg/L.

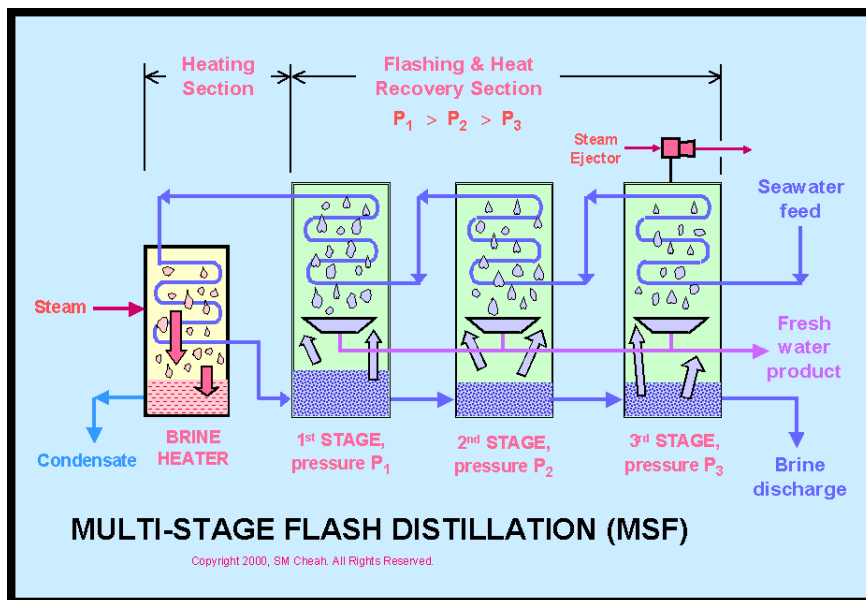


Figure I.3: Multi-stage flash distillation [17].

1.6.1.2. Multi-effect distillation (MED)

MED reproduces the natural water cycle. A heating coil in a closed chamber brings seawater to a boil. When the vapor produced comes into contact with a second coil filled with cold seawater, it condenses. Finally, the incondensable gases are evacuated using an ejector or a pump. Condensed water and concentrated seawater (brine) are drawn off by two electric pump units.

MED is the representation of several cells that operate on the single-effect principle as shown in (Figure I.4). The heat transfer fluid brings the seawater admitted into the first cell to a boil, where the temperature is the highest. The vapor emitted by boiling seawater is transferred to a neighboring cell, which maintains a slightly lower pressure. The seawater in the second cell

is vaporized with the steam from the first effect as the boiling temperature decreases with pressure. In the other effects, the operation can be repeated multiple times [17]. For an energy consumption of 1 to 2 kWh/m³ of produced water, this process allows for a production of 10.000 to 25.000 m³ per day with a salinity of 1 to 50 mg/L.

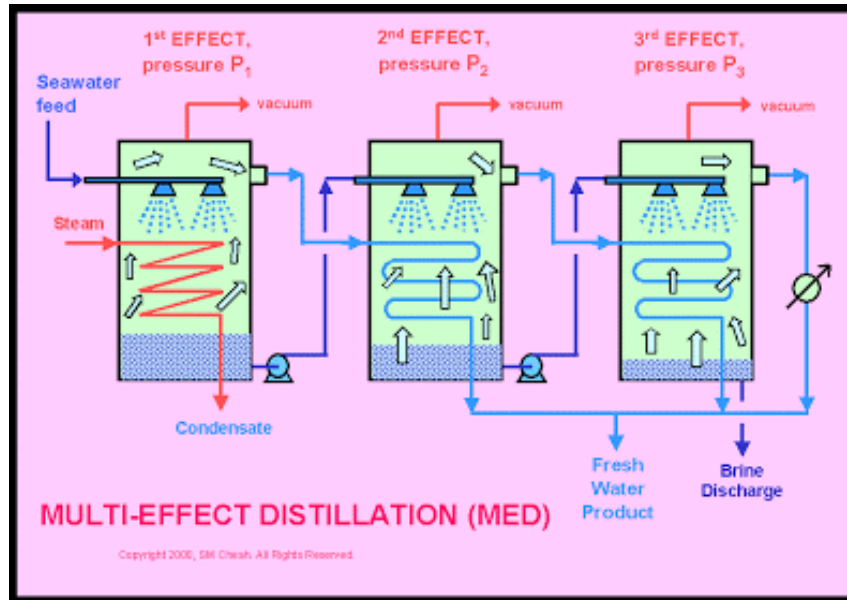


Figure I.4: Multi-Effect distillation (MED) [17].

I. 6. 1. 3. Vapor compression distillation (VCD)

A mechanical compressor (Mechanical Vapor Compression, MVC) can be used to compress vapors. Seawater is brought to a boil in a thermally insulated chamber during vapor compression distillation (Figure I.5). A compressor absorbs the vapor produced, which increases its saturation temperature. This vapor is condensed by passing through a tube bundle at the enclosure's base, causing the salt water to evaporate. For an energy consumption of 12 to 17 kWh/m³ of produced water, this process allows for a maximum production of 5,000 m³ per day with a salinity of 1 to 50 mg/L [17].

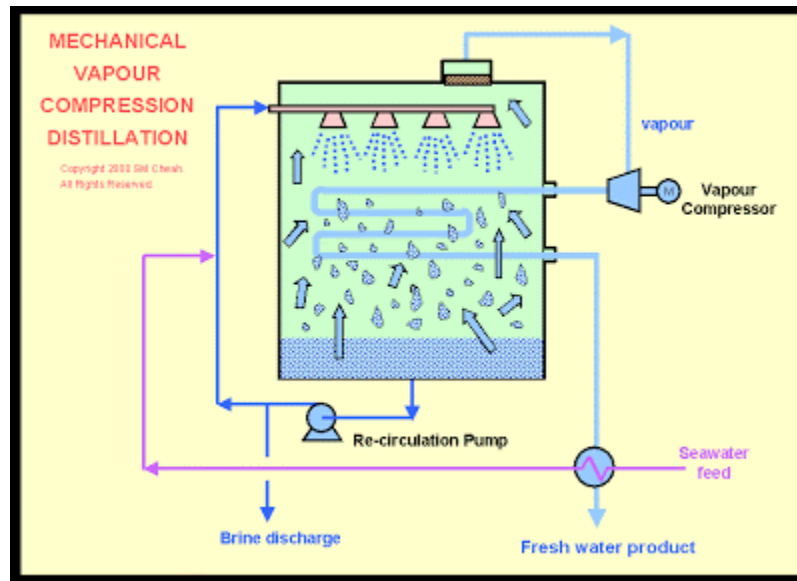


Figure I.5: Mechanical Vapor compression (MVC) [17].

Distillation processes have several technical constraints and high energy consumption. Therefore, the non-condensable gases in the seawater that have evaporated during the distillation process must be evacuated. In addition, pretreatments such as 0.5 mm sieve filtration, chlorination, and anti-scale treatment are also required.

I. 6. 2. Desalination using membrane processes

I. 6. 2. 1. Electrodialysis (ED)

Electrodialysis (ED) is an electro-membrane process that allows of solutions containing charged species to be concentrated and demineralized. A potential gradient is applied between two electrodes as the driving force. Anion and cation exchange membranes alternate between these electrodes. The ions in the water move due to the electric field. These ions are concentrated in one compartment (concentrate) and the other is depleted in salt as shown in (Figure I.6). Electrodialysis is not competitive due to its high power consumption, so it's only used to treat brackish water with a concentration of less than 3 g/L [18].

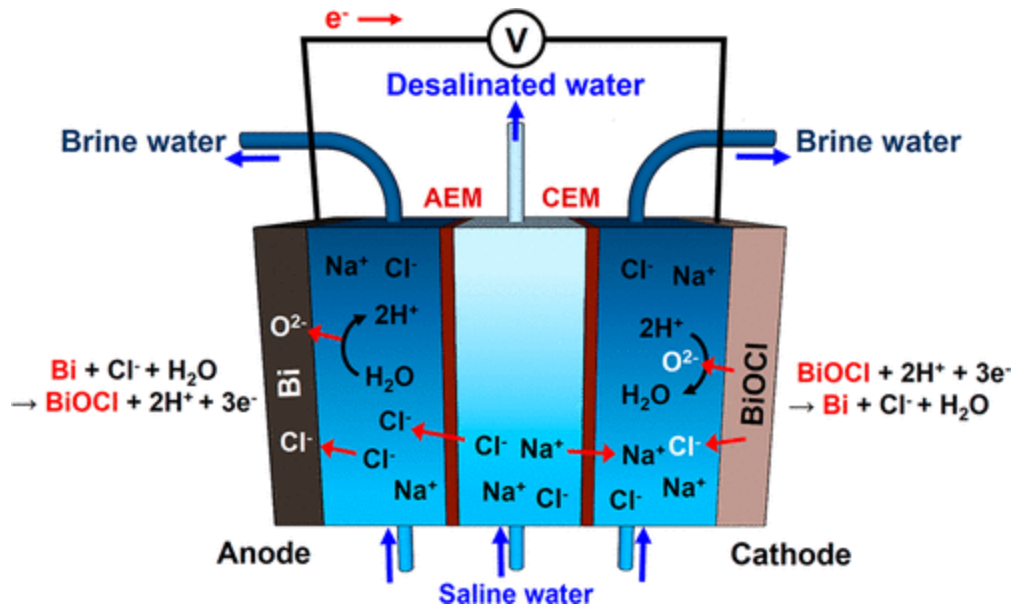


Figure I.6: Electrodeionization (ED) process [19].

I. 6. 2. 2. Reverse osmosis (RO)

The process of separating water and dissolved salts using semi-permeable membranes under pressure (54 to 80 bars) is known as reverse osmosis (RO). There is no phase change in this process, and it does not operate at room temperature. Only water molecules could pass through polymeric membranes and not particles (dissolved salts or organic molecules) larger than 10^{-7} mm as shown in (Figure I.7).

The reverse osmosis process requires only electrical energy, which is primarily consumed by high-pressure pumps. Reverse osmosis water has a salt content of around 0.5 g/l [20].

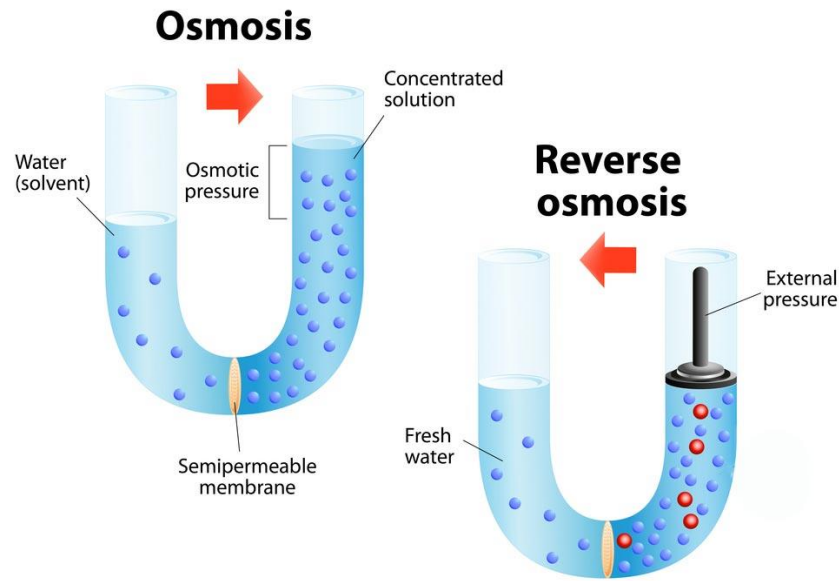


Figure I.7: Reverse osmosis process [21].

I. 6. 2. 3. Membrane distillation (MD)

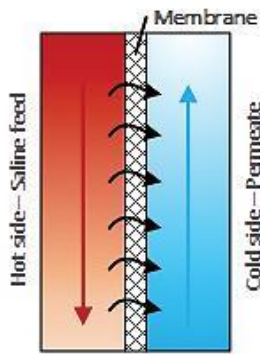
MD is a thermally driven process in which the main driving force is the vapor pressure differential between the hot and cold sides. The feed water solution keeps direct contact with one side of the hydrophobic membrane, preventing penetration through the membrane's dry pores. Water in the feed solution vaporizes at typical operating temperatures (about 80 °C or lower) and passes through a microporous membrane for condensing on the other side [22].

As shown in (Figure I.8), the MD process can be divided based on the various modes of vapor condensation on the cold side: direct contact MD (DCMD), air gap MD (AGMD), vacuum MD (VMD), and sweep gas MD (SGMD). Because of its simplicity of use, DCMD is the most studied MD process. However, due to conduction heat losses, DCMD has low energy efficiency. As in the case of AGMD, a stagnant air gap between the membrane and the cooling surface increases the thermal energy efficiency of the process [23]. However, various issues such as high specific thermal energy demand, AGMD-specific membrane development, and efficient module designs must be addressed for efficient operation of AGMD. In addition, researchers have developed other configurations, including liquid gap MD (LGMD) or permeate gap MD (PGMD), material gap MD (MGMD), and conductive gap MD (CGMD) [24, 25-26].

I. 7. Types of membrane distillation processes

The method varies by which the vapor is recovered after it has passed through the membrane in various MD processes as [27]:

A. Direct Contact Membrane Distillation (DCMD)



Advantages

Possible internal heat recovery

High permeate flux

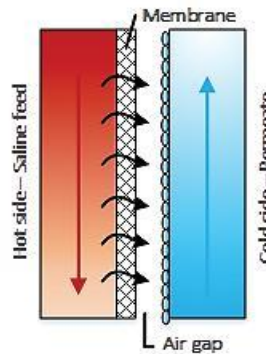
Disadvantages

High temperature polarization

High conductive heat losses

Permeate mass contamination risk

B. Air-Gap Membrane Distillation (AGMD)



Advantages

Low conductive losses

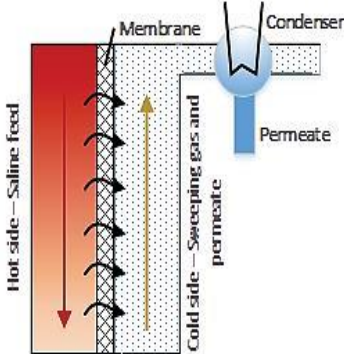
Internal heat recovery possibility

Low polarization Effect

Disadvantages

Low permeate flux due to mass transfer Resistance

C. Sweeping Gas Membrane Distillation (SGMD)



Advantages

High permeate flux

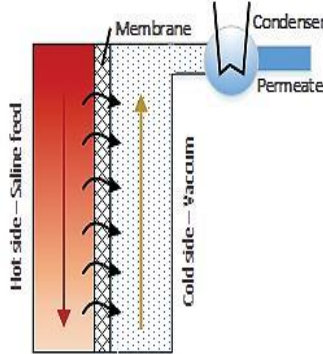
Low conductive heat losses

Disadvantages

Complicate handling of sweeping gas

Difficult heat recovery

D. Vacuum Membrane Distillation (VMD)



Advantages

High permeate flux

Low conductive heat losses

Disadvantages

Risk of pore wetting is high

Difficult heat recovery

Figure I.8: Different configurations of MD process [27].

A. The oldest and most widely used process (DCMD) has liquid phases in direct contact with both sides of the membrane. Because the vapor diffusion path by the membrane's thickness is limited, heat and mass transfer resistances are reduced. Furthermore, condensation into the pores must be avoided by selecting appropriate temperature differences in the membrane.

B. An additional air gap is interposed between the membrane and the condensation surface in AGMD process. Therefore, heat and mass transfer resistances are increased (see Figure I.8). Although heat loss through conduction is reduced, the flux is decreased. However, using the air gap allows higher temperature to be applied through the membrane, which helps to compensate the higher transfer resistances.

C. The permeating vapor is removed in an inert gas steam that passes on the permeate side of the membrane in SGMD process. Condensation is done outside the module and includes large volumes of sweep and vapor steam. This process is similar to the gas membrane stripping process.

D. The permeate-side pressure is lower than the saturation pressure of the evaporating species and the permeate's condensation is done outside the module. Therefore, the vapor is extracted by applying a vacuum on the permeate side in VMD process [27].

I. 8. MD technology developers and promoters

Many developers have worked hard to commercialize efficient MD modules since 1970. As shown in (Table I.4), the commercial MD systems have been increased by several promoters. Despite recent advances in MD configurations, the most of commercial MD systems installed around the world use air-gap or vacuum MD processes, with the most common membrane materials such as polypropylene (PP), polytetrafluoroethylene (PTFE) and polyvinylidene fluoride (PVDF) [28]. As shown in (Figure I.9), these membranes are assembled together to form hollow fiber, spiral wound, plate and frame MD modules.

The Swedish Svenska Utvecklings AB developed the first flat plate AGMD system in 1988 [29]. SCARAB Development AB currently manufactures and sells these modules. Solar spring GmbH (Fraunhofer Institute) develops spiral wound AGMD modules for desalination systems, which have been field tested in Europe, Middle East and North Africa (MENA). A Dutch TNO company has created a multistage AGMD system that can be used in both configurations of spiral wound and plate-and-frame. Various international companies promote these units, which are known as Aquastill and memstill. As well as AGMD, Memsys created flat plate VMEMD systems, and KmX recently released commercial hollow fiber VMD modules [30].

Table I.4: Commercial MD technology developers and process utilized.

Technology developer	MD Process	Notes
Scarab Development AB, Sweden	AGMD	Technology is promoted as XZero, HVR and Elixir water purification systems using flat sheet modules [31]
Solar Springs GmbH, Germany	AGMD	Spin-off from Fraunhofer Institute for Solar Energy Systems/provides complete MD systems [32]
TNO, Netherlands	DCMD, AGMD and PGMD	Developed Memstill technology promoted by Aquastill for spiral wound modules [33], Keppel Seghers and BuleGold technologies promotes flat sheet configuration of Memstill [34].
Memsys GmbH, Germany	VMEMD	Develops multi-effect flat sheet VMD systems licensed to Aquaver. New Concept Holdings Limited (NCHL) acquired assets of Memsys in 2016 [35].
KmX Corporation, Canada	VMD	Aqua-sep™ technology for brine concentration using hollow fiber VMD systems [36].

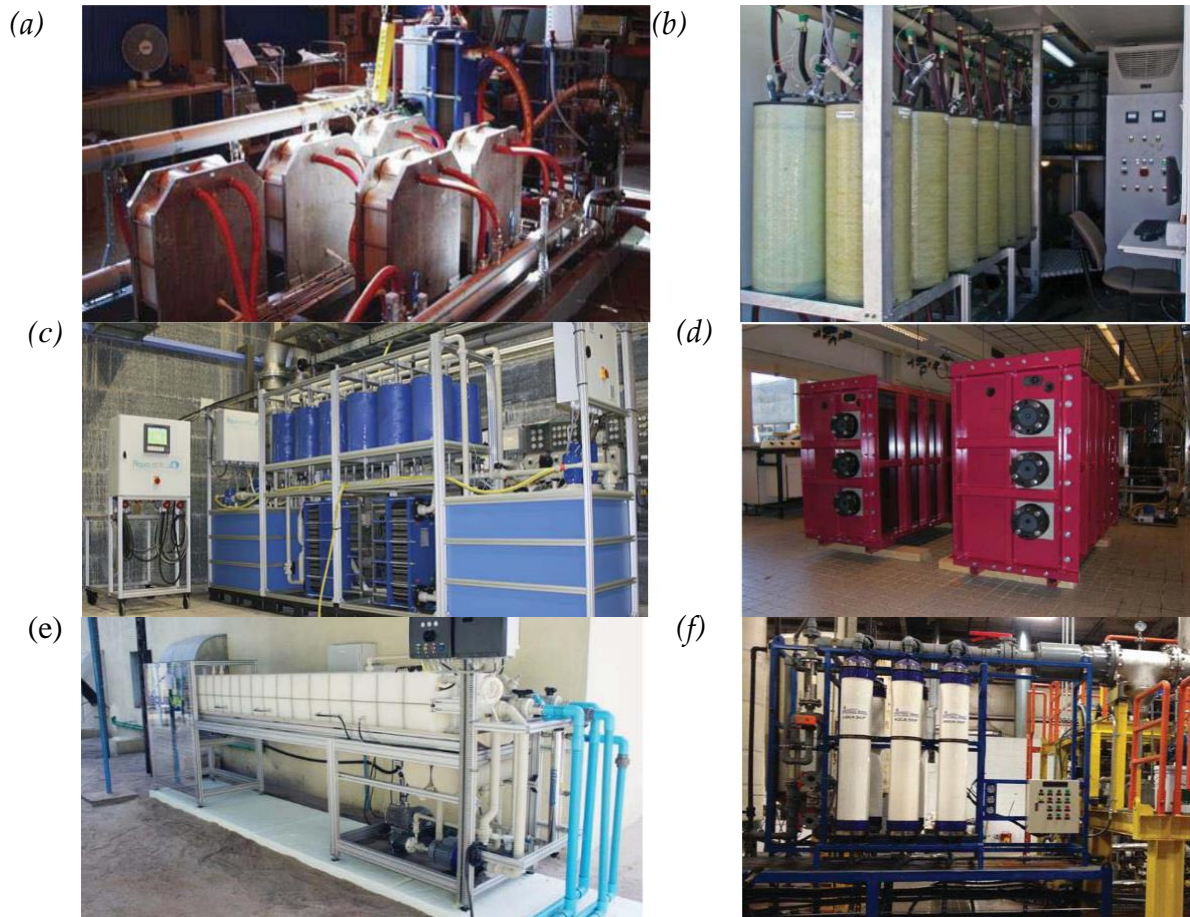


Figure I.9: Pilot plants of MD systems from different suppliers. a) Xerox [31], b) Solar spring AGMD system [32], c) Aquastill pilot system [33] d) Memstill system [34] e) Memsys VMEMD [35] and f) Aqua-sep™ Membranes [36].

I. 9. Advantages of AGMD

AGMD is one of the new MD configurations where both the hot feed stream and the cold permeate stream are in indirect contact with the two membrane surfaces.

In AGMD, the features that make it different from other configurations are [37]:

- The air gap acts as a thermal insulation layer and reduces the heat loss from the membrane, which results in the improvement of thermal efficiency.
- A condenser surface separates distillate and the coolant. Therefore, AGMD can be used to recover components that should not be mixed or diluted with other components.
- Only AGMD permits the latent heat recovery without any external heat exchanger [38].
- AGMD offers higher resistance to mass transfer, and therefore, it is operated at low water flux [39-40].
- Due to higher thermal efficiency, it is the first choice for pilot testing plants which address long-term operational and scale up issues [41].

- AGMD modules can be made with inexpensive polymeric corrosion resistant materials [42].

In a study that compare AGMD and DCMD, it was shown that the thermal efficiency of AGMD is 6% higher, whereas distillate flux is 2.3–4.8 times [43] higher. Another comparison study of AGMD, PGMD, DCMD and VMD revealed that the flux in AGMD is the lowest of all configurations [44-45].

I. 10. Heat and mass transfer in AGMD

I. 10. 1. Heat transfer

All interactions with the heat transfer should be analyzed and quantified. The heat transfer includes heating the feed for rejecting the heat by vapors to the cold fluid. Additionally, the measurement of temperature must be determined at various interfaces and locations throughout the module [46]. Figure I.10 shows the complete heat interactions.

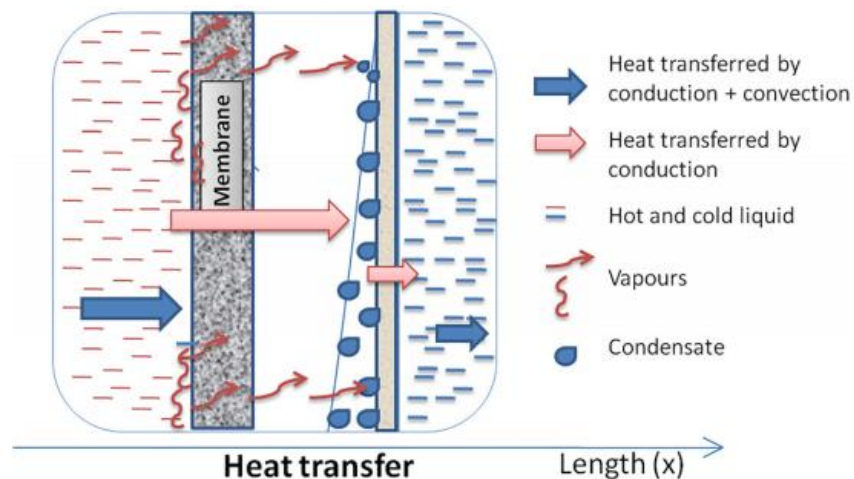


Figure I.10: Heat transfer process in AGMD [37].

Convection and conduction transfer heat from the bulk feed solution to the membrane surface. Feed is evaporated to form vapors at the membrane surface by absorbing the latent heat of vaporization. Heat is also transferred through the air gap in the membrane surface. If the air is considered still, heat is conducted through the air gap to the condenser surface; otherwise, heat is transferred to the condenser surface via convection through the air gap.

The vapor mass transfers some heat from the membrane across the air gap. Additionally, vapors encounter the condensate film, where the total heat is released, which is composed of the latent heat of condensation of permeate flux. The heat is transferred across the membrane and the air gap. The heat is conducted through the condensate film. Then, the total heat is conducted

through the condenser surface to the cold fluid film. Finally, the heat is transferred to the cold fluid [47].

I. 10. 2. Mass transfer

The difference in vapor pressure between feed and cold sides effects on the mass transfer through the membrane. The formula for the relationship is as follows [48]:

$$J = C_M (P_F - P_C)$$

Where C_M is the mass transfer coefficient ($\text{kg}/\text{m}^2 \text{ Pa s}$); P_C and P_F are the vapor pressure (bar) at the cold side and the feed side of the membrane and the condensation section, respectively. Mass transfer is controlled by the hydrodynamics and thermodynamics in the membrane compartments while it occurs mainly by the diffusion across the membrane pores. Through the AGMD modules, mass transfer follows the specified sequence as shown in (Figure I.11):

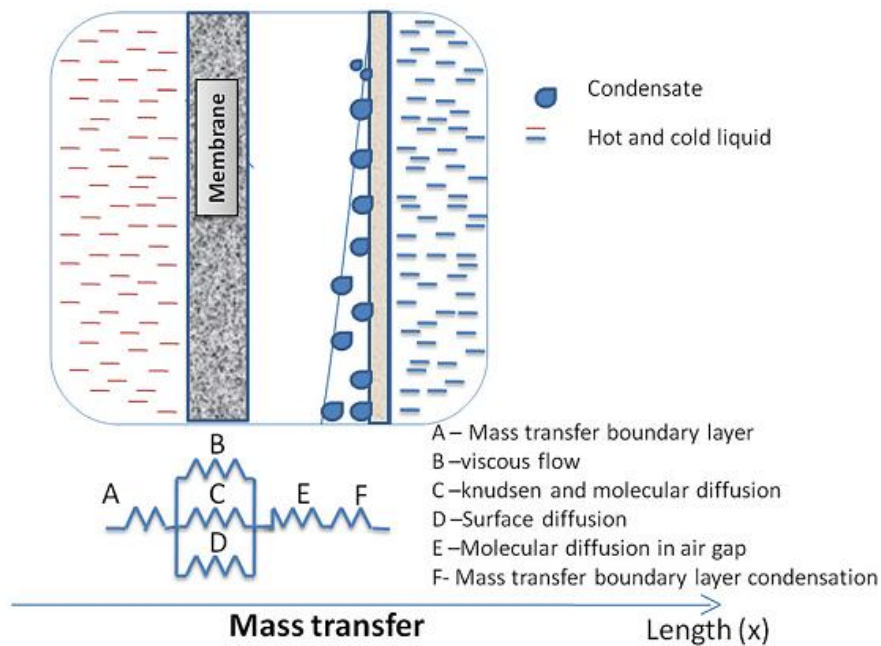


Figure I.11: Mass transfer process in AGMD [37].

At the membrane feed interface, the hot feed evaporates. The combined effects of Knudsen diffusion, Molecular diffusion and viscous flow allow vapors to diffuse into the membrane and pass through the pores. In addition, the air gap allows vapors to diffuse. Then, vapors come into contact with the condensate thin film to converts to permeate on the condenser surface [49].

I. 11. Heat and mass transfer analysis

The differences in thermodynamic property or in vapor pressure across the membrane are considered as driving force in the membrane distillation [50]. For heat and mass transfer analyses, individual regions are illustrated in (Figure I.12):

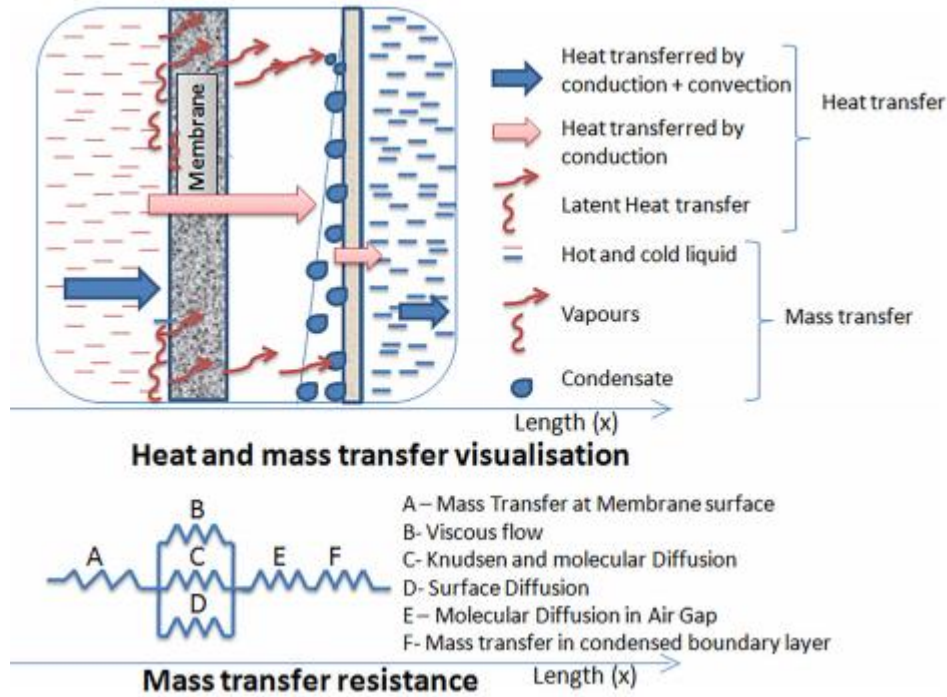


Figure I.12: Heat and mass transfer of AGMD [37].

A. Bulk feed region:

Heat is transferred to the membrane surface via convection from the hot feed [51]:

$$Q_f = \frac{Q}{A} = h_f(T_1 - T_2)$$

When diffusive heat transfer is determined [52]:

$$Q_f = (J_w - C_{pf}) \times (T_1 - T_2)$$

B. Membrane:

Membrane thermal conductivity varies depending on the membrane [53].

$$K_m = \varepsilon K_g + (1 - \varepsilon)K_s$$

The porosity of the membrane affects its thermal conductivity because these pores contain air, which reduces the effective conductivity.

The Knudsen number is used to determine the dominant mechanism of mass transfer across membrane pores. The Knudsen number (kn) is the ratio of the mean free path of the transported molecules and the membrane's pore size.

$$K_n = \frac{S}{d}$$

For $kn < 1$; Knudsen - molecular diffusion transition mechanism; for $kn > 1$; Knudsen diffusion governs the flow; and $kn < 0.01$, molecular diffusion completes vapor transport through membrane pores. In the air gap, molecular resistance dominates over other resistances during vapor transport.

- Heat conduction across the membrane polymer [54],

$$q_{mc} = \frac{Q_m}{A} = K_m \frac{(T_1 - T_2)}{\delta_m}$$

- Transfer of latent heat with vapors that passing through the membrane [52],

$$q_{ml} = J \times h_{fg}$$

- Sensible heat transfer: this mode is often neglected in many research because latent heat transfer is always much higher than sensible heat transfer.

$$q_{sensible} = J \times C_p(T_1 - T_2)$$

- The mass flux in the membrane is presented as [55]:

$$J_m = C_1 \frac{(T_2 - T_3)}{\delta_m}$$

C_1 is a constant that determines the mass transfer mechanism mode inside the membrane. It is different in Knudsen diffusion, combined diffusion, molecular diffusion and Poiseuille flow [56]. The dusty gas model is another way to describe mass transfer across the membrane [57].

C. Air gap:

Heat is transported through the air gap via convection, conduction, and latent heat. The Rayleigh number should be used to determine the dominant mode of heat transfer. Natural convection is ignored for $Ra < 1000$ [53-58],

$$\text{Conduction } q_{ac} = K_a \frac{(T_3 - T_4)}{\delta_a}$$

$$\text{Convection } q_{aconv} = C_a(T_3 - T_4)$$

$$\text{Latent heat } q_{al} = J \times h_{fg}$$

The mass transfers through the air gap by diffusion are calculated as follows:

$$J_a = C_2 \frac{(T_3 - T_4)}{\delta_a}$$

In the air gap, C2 is the molecular diffusion coefficient [58].

D. Condensate film:

We can assume that only conduction is dominant when the condensate film has a very thin thickness [59],

$$q_c = K_c \frac{(T_4 - T_5)}{\delta_c}$$

By using convection, it can be obtained as follows:

$$q_c = h_c(T_4 - T_5)$$

The heat transfer coefficient across the condensate film is determined by h_c .

E. Condenser plate:

The heat is transferred across the cooling plate via conduction [60].

$$q_p = K_p \frac{(T_5 - T_6)}{\delta_p}$$

F. Coolant fluid:

The heat is transferred from the plate to the first layer of fluid via conduction, and then to the bulk fluid via convection. We can neglect the heat transfer by conduction in this case [61].

$$q_{co} = h_{co}(T_6 - T_7)$$

I. 12. AGMD Configurations

Membrane polymers must be packaged into a configuration known as a device or element in order to be effective. Tubular, capillary fiber, spiral wound, and plate and frame are the most common element configurations [62]. The configurations of these elements are described below as shown in (Figure I.13):

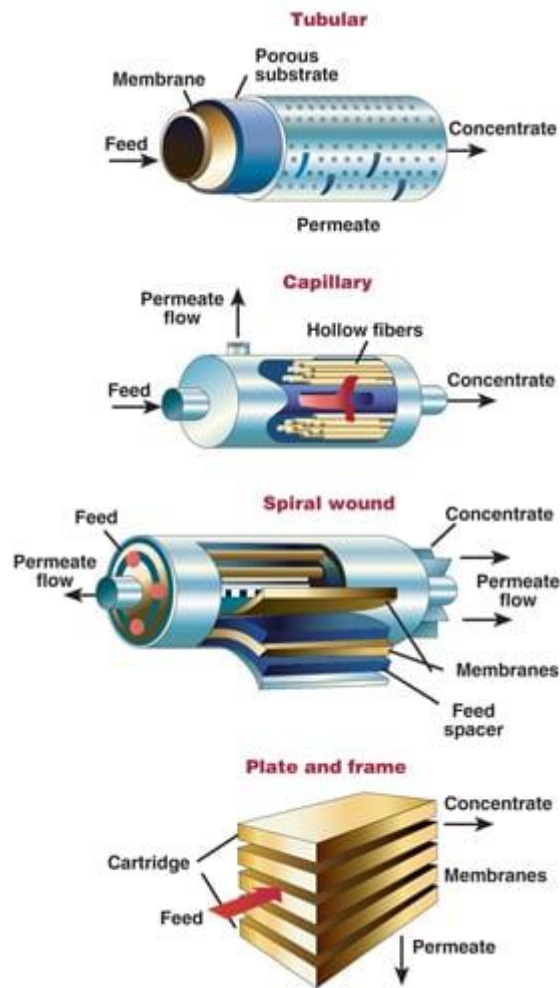


Figure I.13: Membrane element configurations [62].

Tubular

These tubes that are made of carbon, stainless steel, ceramics, or a number of thermoplastics, have inside diameters ranging from six to about 25 mm. The feed solution flows from one end of the tube to the other via the interior (MD) under pressure. Then, the permeate passes across the wall and collected outside of the tube. In addition, the membrane is typically coated on the inside of the tube.

Capillary (hollow) fiber

These elements are designed similarly to tubular elements, but have a smaller diameter. They are often ceramics or membrane polymers that require support on both ends from an epoxy 'potting' of a bundle of fibers within a cylinder. The flow of feed has to be either down the inside of the fiber (lumen feed) or around the outside of the fiber where is from outside to inside (circumferential feed) [62].

Spiral wound

This element is made up of a sheet membrane envelope wound around a permeate tube that is perforated to allow the permeate to be removed. Water is purified by passing through one layer of the membrane and flowing into the permeate tube in a spiral pattern. In water purification applications, the element of spiral wound is the most common configuration.

Plate and frame

This device uses a sheet membrane stretched over a frame to separate the layers and make it easier to collect the permeate, which is directed to the collection tube [62].

Packing density

From the viewpoint of cost and convenience, it's useful to package as much membrane area as possible into a small volume, which is known as packing density. Generally, the larger membrane area increases the packing density and decreases the cost. The disadvantage of high-packing density membrane elements is their higher propensity for fouling. Table I.5 compares the packing densities of the various element configurations [62].

Table I.5: Membrane element configuration comparison.

Element configuration	Packing density*
Capillary fiber	Medium
Plate and frame	Low
Spiral wound	Medium
Tubular	Low

*Membrane area unit volume.

I. 13. Renewable energy sources for desalination

Desalination is an energy-intensive process with large demands due to the high tonnage of desalination plants. These energy needs are currently using very expensive fossil fuels, which are contributing significantly to global warming. Therefore, to supply the growing demand for desalination, it will be necessary to look for alternative energy sources in the future. The developed sustainable desalination application requires the reduction in energy consumption using renewable energy sources. Moreover, less developed countries can be able to obtain sufficient amounts of fresh water [63].

Solar and wind power are the most common renewable energy sources. Desalination using renewable energy sources is currently very limited. Desalination estimates only about 0.02 percent of all renewable energy sources used globally [64]. Most of the countries in MENA, including Algeria, suffer from severe water shortage. Therefore, renewable energy is the best option, especially solar power in the MENA region. However, this technology must be optimized to decrease its limitation because it's currently more expensive than fossil fuel [65].

I.14. Definition and typology

Renewable energies are those whose consumption does not decrease as they are produced. Therefore, the advantage of renewable energy sources is available with unlimited quantities. They can be used to supply energy needs while also protecting the environment. Solar, wind and geothermal energies are the most common renewable energy sources [66].

Renewable energies are those that reach us from the Sun, either directly or indirectly in various forms: the radiation is the vector to transfer the usable energy during the photosynthesis or the water cycle which allows hydropower. The energies of wind, wave and underwater currents are used for motors and tidal turbine, etc. In addition, thermal energy of the seas, osmotic, geothermal and tidal energies are the forms of renewable energy.

I. 14. 1. Solar energy

Many coastal and inland areas around the world receive a lot of sunlight but lack pure water. Solar desalination using seawater or brackish water is the reasonable solution to the problem. Solar energy can be combined with solar distillation and MED to produce clean water [67-68]. Solar basins and parabolic troughs are the most common among various systems. Solar power for the MED for the MED is still unable to compete with fossil fuels at current market prices, with the exception of sunny areas, where solar power can be an effective alternative.

Photovoltaic panels are currently the most promising technology in the various solar energy systems.

Solar energy is converted to electricity through the transfer of electrons in photovoltaic networks. Many small photovoltaic power plants are developed in recent years. Reverse osmosis systems using photovoltaic power plants are the most common system in solar desalination, which are already commercialized. Many applications of photovoltaic reverse osmosis (PV-RO) systems can be found in the literature [69].

I. 14. 2. Wind power

Windmills are turned by wind energy, which produces mechanical energy that can be converted to electrical energy. The wind speed should be higher than 5 m/s for optimal efficiency. Therefore desalination using wind energy can be a best option for windy islands like the Canary Islands, where wind energy is used for both seawater desalination and power generation [70]. Additionally, the use of wind power is also suited electro dialysis and MVC systems. However, it's not possible to use this energy in RO systems because they must be operated continuously. Therefore, a significant investment must be made in wind power systems [71].

I. 14. 3. Geothermal energy

There are three types of geothermal energy resources: thermal, hydraulic, and methane gas. Geothermal energy can be used in many processes as thermal desalination applications or to generate electricity [72].

I. 15. Renewable energies in the world

According to the International Renewable Energy Agency (IRENA), the global renewable electricity production reached 1,700 GW in 2013, accounting for 30% of total installed production. Renewable energy technologies have improved in terms of reliability and efficiency, and they can now generate electricity even in less-than-ideal conditions like low sunlight or low wind speed. Solar photovoltaic energy prices have dropped by 80% since 2008, making it increasingly competitive with other resources without the need for government subsidies. In addition, since 2009, the cost of wind electricity has decreased by 18%. Therefore, turbine costs decreased a nearly 30% where this energy has become the least source of

electricity in growing markets. As a result, the development of renewable energies will be a significant role to limit global warming [7].

I. 16. The development of renewable energies in Algeria

The dimension of sustainability has been integrated in the national development policy of Algeria through planning instruments in order to maintain the socio-economic development using natural resources especially water and energy [73].

In fact, the use of renewable energy sources is still very low in Algeria. Unfortunately, our country currently has all primary sources for the development of renewable energy systems. However, Algeria's strategy aims to raise renewable energy to 5% of electricity production by 2025. Several projects will be created and developed, which are included solar water heaters, solar or wind-powered pumps, and about twenty solar villages (Adrar, Tamanrasset, Tindouf, and Illizi), etc. About 2000 photovoltaic panels are installed for lighting and 200 solar pumping systems for drinking water and irrigation in the many countries of Algeria [73]. In addition, there are wind farms in Adrar, which has a capacity of 10 MW. With around 450 MW of solar power installed, Algeria would need to add 5,000 MW to reach the solar capacity objective in 2028. To meet the stated 2030 objectives, a total of 22,000 MW of renewable power would have to be produced as shown in (Figure I.14) [74].

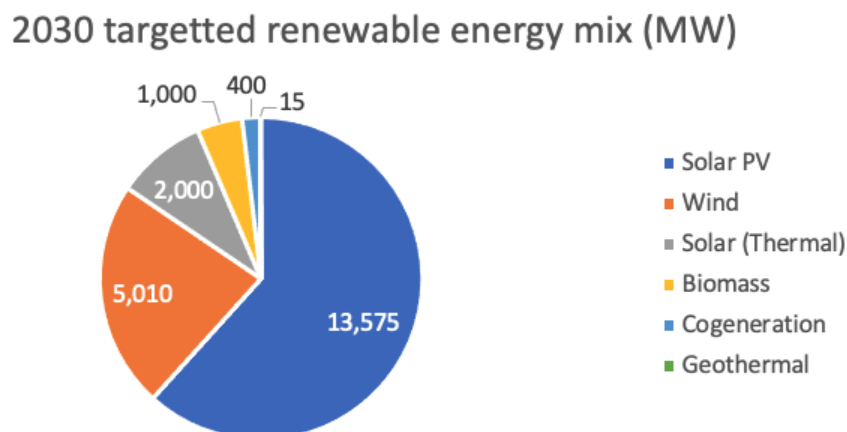


Figure I.14: Targeted renewable energy mix (2030) [74].

I. 17. Solar desalination systems

Using renewable energy sources in stand-alone desalination systems, such as the sun (Thermal Collector and Photovoltaic) and wind, has been widely discussed [75-76].

Desalination can be a promising application that involves widely fields of study. Therefore, many solutions have been proposed in these applications. Even if desalination applications are used renewable energy sources and different specific methods, there are many options based on the configuration of the final system. The most common desalination techniques using renewable energy sources are shown in (Figure I.15):

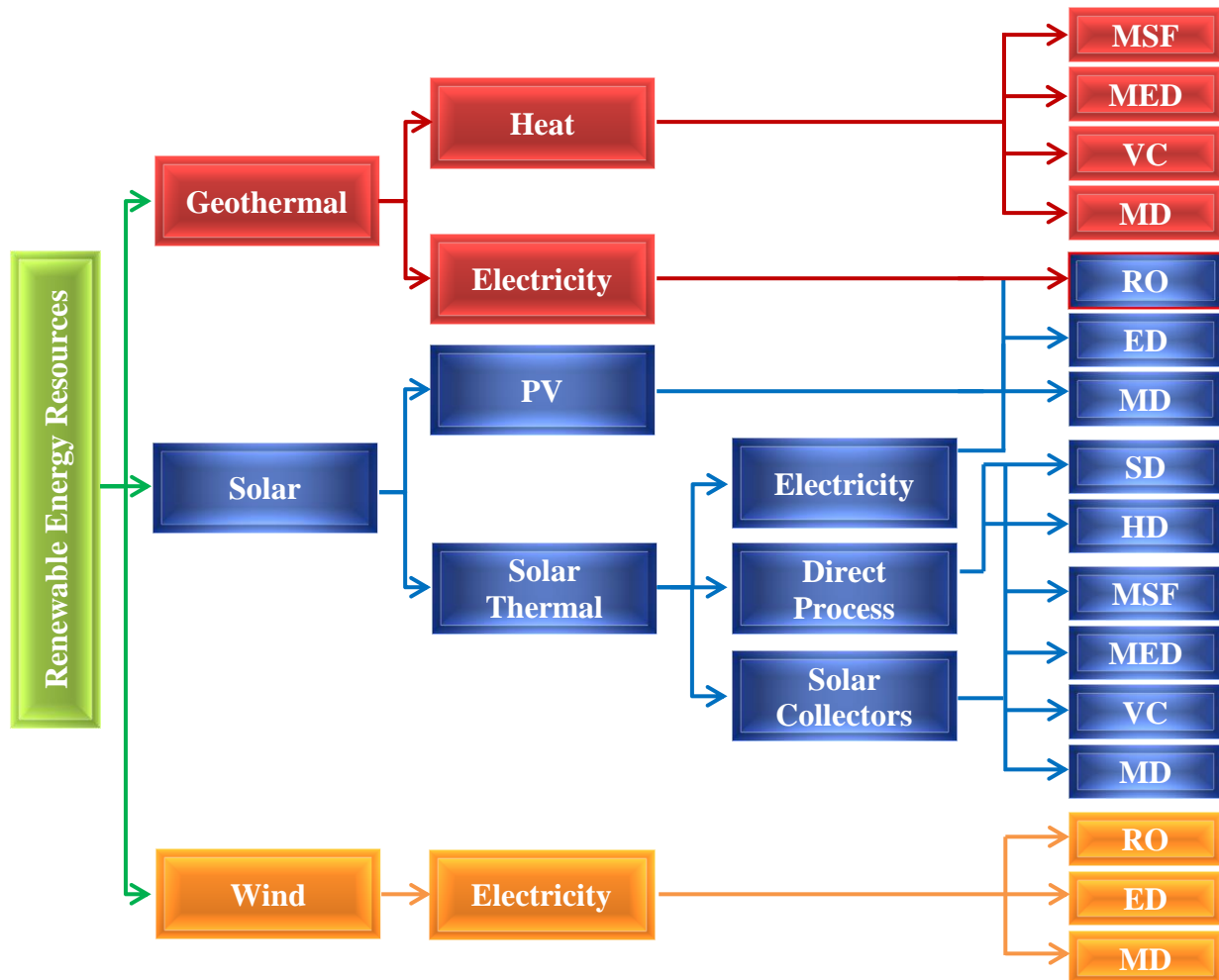


Figure I.15: Representation of some possible combinations of renewable energy sources and desalination processes [12].

Solar and wind energy are renewable energy sources that are increased significantly in desalination processes. The distillation process using thermal and membrane methods is one of the most applications used. Furthermore, reverse osmosis membranes are the most popular, followed by MED and MSF processes in renewable desalination systems [77]. Figure I.16 illustrates the contribution of renewable energy resources in desalination for freshwater production processes.

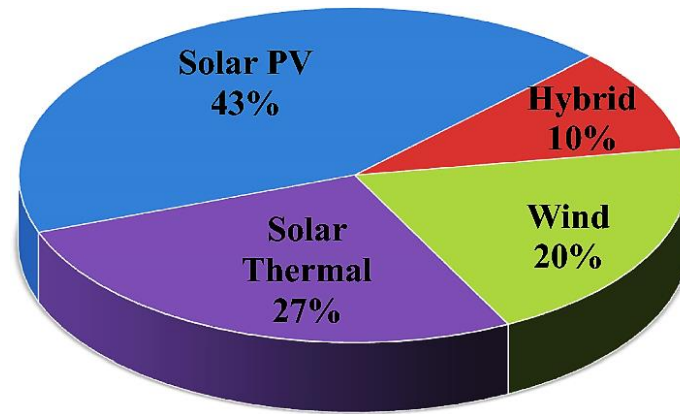


Figure I.16: The contribution of renewable energy resources in desalination [78].

On the other hand, there are a few factors that limit the use of all renewable energy sources in desalination systems. The first problem is the unpredictability of renewable resources, which cannot always supply the fresh water demand. In addition, the most desalination applications are unsuitable for variable-wattage operation. Moreover, the size of the installation has a significant impact on the energy source selected [77].

I. 18. Solar Membrane Distillation (SMD)

In decentralized areas, solar membrane distillation (SMD) is regarded as a suitable water supply option. Many researchers have considered flat plate (FPC) and evacuated tubular (ETC) collectors as a thermal source for MD, which have low grade thermal energy absorbing properties. However, solar gradient ponds, solar stills, and compound parabolic collectors (CPC) [79,80-81] have been used for various MD systems. Therefore, conventional desalination systems could be combined with solar collectors (thermal or PV) to create a solar desalination system, depending on the scale of operation and the operational temperature range [82].

The study of proposes an integrated solar MD system as shown in (Figure I.17) [83]. The system includes vacuum glass tubes to efficiently transfer absorbed energy, and a tubular MD module to more effectively. The results show that the maximum thermal efficiency was 78 percent, and the energy efficiency varied between 4 and 5 percent in summer for a remarkable period of time starting from 10:30 AM to 3 PM. According to the experimental and numerical results, the solar thermal system was able to supply the required thermal energy for the MD system.

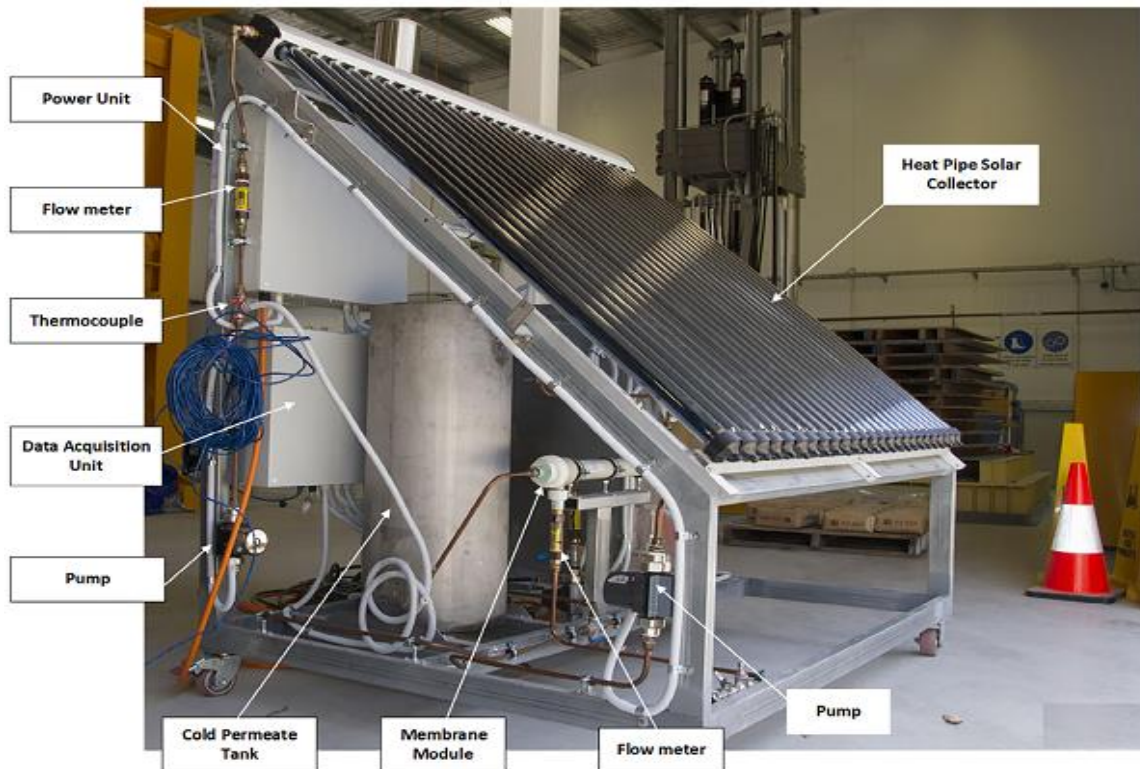


Figure I.17: The experimental rig manufactured and used in the solar tubular MD module [83].

A solar combined MD (SCMD) system was experimentally studied for single household application in Kumar's paper et al [84]. The system produced 250 L/day of hot water and 20 L/day of distillate water as shown in (Figure I.18). Individual operation of solar heaters and solar MD were compared using the efficiency of the co-production system. The results showed that the combined operation of Solar Domestic Hot Water (SDHW) and SMD increased collector efficiencies with higher solar fraction throughout the year. In addition, the average distillate production can be increased marginally using the SCMD system and DHW operation.

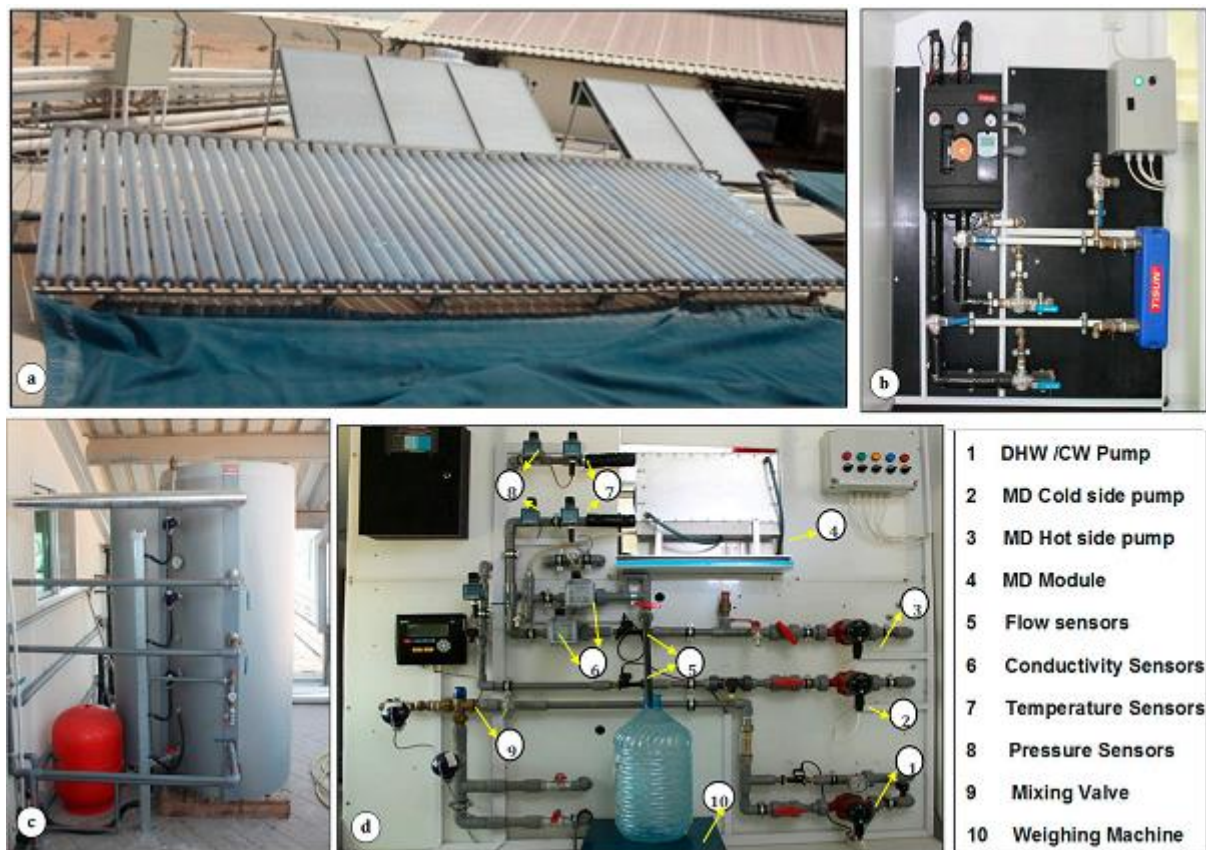


Figure I.18: A Pilot solar combined MD (SCMD) system installed at UAE: (a) Solar thermal collectors; (b) Station circuit; (c) Storage tank; and (d) MD module with all instrumentation[84].

I. 19. Solar AGMD systems

The solar-driven AGMD systems have been studied by focusing on air-gap MD module configuration in the literature search. Additionally, AGMD applications have been widely studied using solar-powered systems because the simplicity in design and the advantage of low heat losses [85]. Hogan et al [86] was one of the first to discuss the connection between MD and solar heating. Later, the European Commission (EC) supported the development of solar MD systems and funded research projects such as SMADES, MEDIRAS, MEDESOL, and MEMDIS. Several solar-powered AGMD pilot plants have been developed with capacities ranging from 0.5 to 5 m³/day as shown in (Table I.6):

Table I.6: Pilot scale solar driven AGMD systems.

Project/Company	Location	Capacity	Energy Source	Notes
SCARAB	El-paso, USA	-	Solar pond	Pilot plant
SMADES/Solar Spring (a)				
Compact systems	Jordan, Morocco and Egypt	0.12 m ³ /day	Solar FPC+PV	STED: 200-300 kWh/m ³ Water cost: 15\$/m ³
Large system	Aqaba, Jordan	1 m ³ /day	Solar FPC+PV	Flux: 2-11 l/m ² .day Water cost: 18\$/m ³
MEMDIS/Solar Spring (b)				
Compact system	Gran Canaria	8 l/h	Solar FPC+PV	Air gap is filled with condensed vapor thus making it PGMD system
Large system	Gran Canaria	70 l/h	Solar FPC+PV	
MEDIRAS /Solar Spring (c)				
Compact system	Tunisia	0.15 m ³ /day	Solar FPC+PV	Coupled with UV disinfection system
Compact system	Spain	1.4 m ³ /day	Solar FPC+PV	
Two-loop system	Spain	3.69 m ³ /day	Solar FPC+PV	STED: 300 kWh/m ³
Two-loop system	Italy	5 m ³ /day	FPC (20%) + Waste heat (80%)	STED: 271 kWh/m ³
MEDESOL/Scarab (d)				
Multistage AGMD	Almeria, Spain	1-2m ³ /day	Solar CPC	STED: 800-1200 kWh/m ³ Flux: 7 l/m ² .day

a) Banat et al.; 2007 [87], b) Subiela et al.; 2009 [88], c) Zhani et al.; 2016 [89], d) Galveza et al.; 2009 [90]

SMADES and MEMDIS projects were created to provide people that living in remote areas away from the public grid by the fresh water supply. Therefore, eight pilot plants with capacities ranging from 0.1 to 1 m³/day were installed at different regions using spiral wound AGMD modules. MEDIRAS was a follow-up to the MEMDIS project, in which five solar MD systems were installed increasing the total capacity to 5 m³/day of drinking water [89]. In the MEDESOL project, the multi-stage AGMD system coupled with three CPC modules have been investigated by Galveza et al [90]. Each one from CPC modules has an effective membrane area of 2.8 m² for producing a distillate flux of 7 kg/m² h [91].

Horta et al [92] investigated the use of commercial low-temperature solar collectors in various layouts, as well as the optimal system dimensioning in terms of water production costs at various locations. They came to the conclusion that the costs of solar energy supply are highly dependent on specific energy demand in different desalination systems. According to the researchers, the specific thermal energy demand of MD ranges from 100 to 9000 kWh/m³ with low GOR (gain output ratio) values. Additionally, the water costs of solar MD systems range between 0.3 \$/m³ and 130 \$/m³ based on the energy demand. Depending on MD system configuration, specific electrical energy demand varies from 0.5 to 2 kWh/m³ [93]. Therefore, solar MD systems can be used when the cost of membranes, PV panels, collectors, solar heaters, and other fixed capital costs are optimized and reduced. However, to improve the

performance of solar-powered MD systems must be used the low heat losses and shall be installed based on the location and raw water conditions.

I. 20. Summary of literature review

The literature review presents a brief overview of several traditional desalination systems as well as modern improvements. In addition, more information about the membrane distillation method has been given, which is now the main desalination process to face the problem of increasing fresh water demand every year.

Solar seawater desalination has gained popularity in the MENA region in the recent years. It's competitive with traditional thermal desalination processes today because of its performance and energy costs. However, the technical challenge is to develop more efficient processes using renewable energy, in order to approach the minimum consummation energy in desalination with remaining the environment.

Renewable energy technologies can now generate electricity under less optimal conditions. Therefore, they allow possibilities for their development in desalination processes. As a result, the literature review identifies the integration of low-grade solar thermal energy with membrane distillation technology for desalination. Then, special attention has been given to solar-powered MD systems for develop a renewable desalination system that can be used at different countries.

References

- [1] Abdullah Najib, Jamel Orfi, Emad Ali, Jehad Saleh. Thermodynamics analysis of a direct contact membrane distillation with/without heat recovery based on experimental data. *Desalination* 466 (2019) 52–67.
- [2] Usman, M., Rehman, Z., Seong, K., & Song, M. H. (2021). Vacuum degassing of aqueous tetrafluoroethane (R134a) solution during seawater desalination utilizing gas hydrate. *Desalination*, 498, 114754. doi:10.1016/j.desal.2020.114754
- [3] M.A. Sharaf, A. Nafey, L. García -Rodríguez, Exergy and thermo-economic analyses of a combined solar organic cycle with multi effect distillation (MED) desalination process, *Desalination* 272 (2011) 135–147
- [4] Peter H. Gleick et Meena Palaniappan, Peak water limits to freshwater withdrawal and use, *Proceedings of the National Academy of Science* (2010) 107 11155–11162. (doi: 10.1073/pnas.1004812107).
- [5] V. RENAUDIN, «Le dessalement de l'eau de mer et des eaux saumâtres», *Dossiers Chimie et question de société sur le site Culture Sciences chimie : site de ressources scientifiques pour les enseignants en chimie*, Novembre 2003
- [6] C. LARUE, A. LIBERMANN, «L'eau : une ressource en péril», *Les dossiers des Yeux du Monde – Numéro 1 – Janvier 2014*.
- [7] www.irena.org
- [8] www.mre.gov.dz (Site du Ministère des Ressources en Eau).
- [9] B. MOUHOUCHE, «Maîtrise de la pratique de l'aridoculture comme palliatif au manque d'eau en Algérie », 9ème Conférence Internationale « EURO -RIOB 2011 » sur l'application actuelle et future de la Directive - Cadre Européenne sur l'Eau, Porto, Portugal, 27–30 Septembre 2011.
- [10] A. KETTAB, «Les ressources en eau en Algérie : stratégies, enjeux et vision». *Desalination* 136 (2001) 25–33.
- [11] A.MAUREL. «Dessalement de l'eau de mer et des eaux saumâtres», édition technique et documentation, 2001.
- [12] O. CHARROUF, «Optimisation d'Un Système De Dessalement Renouvelable», Mémoire de magister en Electrotechnique Option : Energies Renouvelables, Université Mohamed Khider – Biskra, p 4, 2012.
- [13] J.P. MERIQ, «Approche intégrée du dessalement d'eau de mer : Distillation membranaire sous vide pour la réduction des rejets salins et possibilités de couplage avec l'énergie solaire», Thèse de doctorat en Génie des Procédés et de l'Environnement, UNIVERSITÉ DE TOULOUSE, p 33, 2009.
- [14] LE GUERN, P. LACHASSAGNE, Y. NOEL, F. PERSIN et L. DE BUVSSCHER, « Dessalement et recharge artificielle : synthèse technico-économique », Rapport BRGM/RP-52262-FR, 2003, 80 p.
- [15] C. TANSAKUL, «Procédés hybrides à membranes pour le prétraitement d'eau de mer avant dessalement par osmose inverse», Thèse de doctorat en Génie des Procédés et de l'Environnement, UNIVERSITÉ DE TOULOUSE, p 22, 2009.

- [16] K. A. AL-SHAYJI, «Modeling, Simulation, and Optimization of Large- Scale Commercial Desalination Plants», Thèse de doctorat de Virginia Polytechnic Institute and State University, 1998.
- [17] <https://sites.google.com/site/kjdesalination/vacuum-distillation>
- [18] P. DANIS, «Dessalement de l'eau de mer», Techniques de l'ingénieur traité Génie des Procédés, J2700. Juin 2003.
- [19] J.P. BRUN; «procédés de séparation par membranes» ; MASSON ; 1989.
- [20] C .GALUS, «les techniques de dessalement de l'eau de mer prennent de l'essor», extrait du monde, p 23, 2000.
- [21] Z .TRIKI, «Études, Analyses et Optimisation de la Consommation Énergétique des Unités de Dessalement pour les Sites Isolés», Thèse de doctorat en Sciences Spécialité : Génie Climatique, Université Constantine 1, p 38, 2014.
- [22] Cipollina A, di Sparti M.G, Tamburini A, and Micale G, Development of a membrane distillation module for solar energy seawater desalination. Chem. Eng. Res. Des., 90 (2012) 2101–2121.
- [23] Alkhudhiri A, Darwish N, and Hilal N, Membrane distillation: A comprehensive review. Desalination, 287 (2012) 2–18.
- [24] Francis L, Ghaffour N, Alsaadi A A and Amy G.L, Material gap membrane distillation: A new design for water vapor flux enhancement.J. Membrane Sci., 448 (2013) 240–247.
- [25] Essalhia M and Khayet M, Application of a porous composite hydrophobic/hydrophilic membrane in desalination by air gap and liquid gap membrane distillation: A comparative study. Sep. Purif. Technol., 133 (2014) 176-186.
- [26] Swaminathan J, Chung H.W, Warsinger D.M, AlMarzooqi F.A, Arafat H.A and Lienhard J.H, Energy efficiency of permeate gap and novel conductive gap membrane distillation. J. Membrane Sci., 502 (2016) 171–178.
- [27] Uday Kumar N T. Integration of Membrane Distillation and Solar Thermal Systems for Coproduction of Purified Water and Heat. Thesis, 2017.
- [28] Eykens L, De Sittera K, Dotremonta C, Pinoy L and Van der Bruggen B, Membrane synthesis for membrane distillation: A review. Sep. Purif. Technol., 182 (2017) 36-51.
- [29] Alklaibi A.M and Lior N, Membrane-distillation desalination: status and potential. Desalination, 171 (2004) 111–131.
- [30] Thomas N, Mavukkandy M.O, Loutatidou S and Arafat H.A., Membrane distillation research & implementation: Lessons from the past five decades. Separation and Purification Technology, 189 (2017) 108–127.
- [31] Scarab Development AB. Available online: <http://www.scarab.se/> (accessed on June 2015)
- [32] Fraunhofer ISE. 2014. Available online: <https://www.ise.fraunhofer.de/en/press-media/pressreleases/2014/new-applications-for-membrane-distillation.html>
- [33] Aquastill Netherlands, Available online: <http://aquastill.nl/portfolio/> (accessed on July 2017)

- [34] Hanemaaijer J H., van Medevoort J, and Jansen A.E., Memstill membrane distillation – a future desalination technology. *Desalination*, 199 (2006).
- [35] Aquaver, “Aquaver-case study”. Available online: <http://www.aquaver.com/knowledge-center/articles/membrane-distillation-a-low-cost-breakthrough-technology-for-water-treatment/> (accessed on November 2016).
- [36] KmX Corporation, Aqua-sep Membranes. Available online: <http://kmxcorporation.wixsite.com/kmxcorporation/aqua-sep> (accessed on July 2017)
- [37] Vandita T. Shahu, and S. B. Thombre. Air gap membrane distillation: A review. *J. Renewable Sustainable Energy* 11, 045901 (2019)
- [38] H. C. Duong, P. Cooper, B. Nelemans, T. Y. Cath, and L. D. Nghiem. Evaluating energy consumption of air gap membrane distillation for seawater desalination at pilot scale level. *J. Sep. Purif. Technol.* 166, 55 (2016)
- [39] P. Wang and T.-S. Chung. Recent advances in membrane distillation processes: Membrane development, configuration design and application exploring. *J. Memb. Sci.* 474, 39 (2015)
- [40] J. Minier-Matar, A. Hussain, A. Janson, F. Benyahia, and S. Adham. Field evaluation of membrane distillation technologies for desalination of highly saline brines. *Desalination* 351, 101 (2014).
- [41] R. Schwantes, A. Cipollina, F. Gross, J. Koschikowski, D. Pfeifle, M. Rolletschek, and V. Subiela. Membrane distillation: Solar and waste heat driven demonstration plants for desalination. *Desalination* 323, 93 (2013).
- [42] A. S. Alsaadi, N. Ghaffour, J. D. Li, S. Gray, L. Francis, H. Maab, and G. L. Amy. Modeling of air-gap membrane distillation process: A theoretical and experimental study. *J. Membr. Sci.* 445, 53 (2013).
- [43] A. M. Alklaibi and N. Lior. Comparative Study of Direct-Contact and Air-Gap Membrane Distillation Processes. *Ind. Eng. Chem. Res.* 46, 584 (2007)
- [44] L. Eykens, T. Reyns, K. De Sitter, C. Dotremont, L. Pinoy, and B. Van der Bruggen. How to select a membrane distillation configuration? Process conditions and membrane influence unraveled. *Desalination* 399, 105 (2016).
- [45] L. Eykens, I. Hitsov, K. De Sitter, C. Dotremont, L. Pinoy, and B. Van der Bruggen. Direct contact and air gap membrane distillation: Differences and similarities between lab and pilot scale. *Desalination* 422, 91 (2017)
- [46] Z. Liu, Q. Gao, X. Lu, L. Zhao, S. Wu, Z. Ma, and H. Zhang. Study on the performance of double-pipe air gap membrane distillation module. *Desalination* 396, 48 (2016)
- [47] F. Korminouri, M. Rahbari-Sisakht, D. Rana, T. Matsuura, and A. F. Ismail. Study on the effect of air-gap length on properties and performance of surface modified PVDF hollow fiber membrane contactor for carbon dioxide absorption. *Sep. Purif. Technol.* 132, 601 (2014)
- [48] H. C. Duong, A. R. Chivas, B. Nelemans, M. Duke, S. Gray, T. Y. Cath, and L. D. Nghiem. Treatment of RO brine from CSG produced water by spiral-wound air gap membrane distillation - A pilot study. *Desalination* 366, 121 (2015)
- [49] C. Zhu, G. L. Liu, C. S. Cheung, C. W. Leung, and Z. C. Zhu. Ultrasonic stimulation on enhancement of air gap membrane distillation. *J. Membr. Sci.* 161, 85 (1999)

- [50] L. Francis, N. Ghaffour, A. A. Alsaadi, and G. L. Amy. Material gap membrane distillation: A new design for water vapor flux enhancement. *J. Membr. Sci.* 448, 240 (2013)
- [51] M. H. Sharqawy, J. H. Lienhard, and S. M. Zubair. Thermophysical properties of seawater: a review of existing correlations and data. *Desalin. Water Treat.* 16, 354 (2010)
- [52] A. Khalifa, D. Lawal, M. Antar, and M. Khayet. Experimental and theoretical investigation on water desalination using air gap membrane distillation. *Desalination* 376, 94 (2015).
- [53] A. Alklaibi and N. Lior. Transport analysis of air-gap membrane distillation. *J. Membr. Sci.* 255, 239 (2005)
- [54] H. Geng, Q. He, H. Wu, P. Li, C. Zhang, and H. Chang. Experimental study of hollow fiber AGMD modules with energy recovery for high saline water desalination. *Desalination* 344, 55 (2014)
- [55] H. Geng, L. Lin, P. Li, C. Zhang, and H. Chang. Study on the heat and mass transfer in AGMD module with latent heat recovery. *Desalin. Water Treat.* 57, 15276 (2015)
- [56] R. Aryapratama, H. Koo, S. Jeong, and S. Lee. Performance evaluation of hollow fiber air gap membrane distillation module with multiple cooling channels. *Desalination* 385, 58 (2016)
- [57] M. Khayet and C. Cojocar. Artificial neural network modeling and optimization of desalination by air gap membrane distillation. *Sep. Purif. Technol.* 86, 171 (2012)
- [58] M. S. El-Bourawi, Z. Ding, R. Ma, and M. Khayet. A framework for better understanding membrane distillation separation process. *J. Membr. Sci.* 285, 4 (2006)
- [59] M. N. Chernyshov, G. W. Meindersma, and A. B. de Haan. Modelling temperature and salt concentration distribution in membrane distillation feed channel. *Desalination* 157, 315 (2003)
- [60] K. Charfi, M. Khayet, and M. J. Safi. Numerical simulation and experimental studies on heat and mass transfer using sweeping gas membrane distillation. *Desalination* 259, 84 (2010)
- [61] H. Chang, C. L. Chang, C. Y. Hung, T. W. Cheng, and C. D. Ho. Optimization Study of Small-Scale Solar Membrane Distillation Desalination Systems (s-SMDDS). *Int J. Environ. Res Public Health* 11, 12064 (2014)
- [62] Available online: <http://wcponline.com/2007/05/10/water-reuse-technologies-wave-future-part-1/>
- [63] B. VAN DER BRUGGEN, C. VANDECASTEELE, «Removal of pollutants from surface water and groundwater by nanofiltration: overview of possible applications in the drinking water industry», *Environmental Pollution*, No 122 (2003), 435- 445
- [64] G.R. LOURDES, «Seawater desalination driven by renewable energy», *A review*, *Desalination*, No 143 (2002), 103-113.

- [65] H.MAHMOUDI, and N. GHAF FOUR, «Capacity building strategies and policy for desalination using renewable energies in Algeria», *Renewable and Sustainable Energy Reviews*, (2008)
- [66] N. BOUBOU-BOUZIANI, «Problématique de gestion de l'eau et déficit énergétique», In *Revue LJEE*, N°24&25, Blida, Juin-Décembre 2014, P50
- [67] A. E I-NASHAR «The economic feasibility of small solar MED seawater desalination plants for remote arid areas», *Desalination*, No 134 (2001), 173-186
- [68] E.S. HRAYSHAT and A.E. AL-RAWAJFEH, «A solar multiple effect distiller for Jordan», *Desalination*, No 220(2008), 558-565
- [69] D.HEROLD, «Small scale photovoltaic desalination for rural water supply- Demonstration plant in Gran Canaria», *Renewable Energy*, No 14(1998), 293-298
- [70] A.G.GOTOR, I.PESTANA, and C.A.ESPINOZA, «Optimization of RO desalination systems powered by renewable energies», *Desalination*, No 156(2003), 351- 360
- [71] J. A.CARTA, J. GONZALEZ, and V.SUBIELA, «Operational analysis of an innovative wind powered reverse osmosis system installed in the Canary Islands», *Solar Energy*, No 75 (2003), 153-168
- [72] Goosen, M., Mahmoudi, H., & Ghaffour, N. (2010). Water Desalination Using Geothermal Energy. *Energies*, 3(8), 1423–1442. doi:10.3390/en3081423
- [73] N. BOUBOU-Bouziani, «Les énergies renouvelables et l'eau en Algérie», *Communication Science & technology* vol 17. July 2016
- [74] Available online: <https://www.mei.edu/publications/algeria-charts-path-renewable-energy-sector-development>
- [75] M.TURKI, A.BEN RHOUMA, J.BELHADJ, «Control strategy of an autonomous desalination unit fed by PV-Wind hybrid system. », *J. Electrical Systems* 4-2(2008):1-12
- [76] Q.WEI, L.JINFENG and D. PANAGIOTIS CHRISTOFIDES, «Supervisory Predictive Control for Long-Term Scheduling of an Integrated Wind/Solar Energy Generation and Water Desalination System», *IEEE*,10.1109/TCST.2011.2119318
- [77] «Entreprises et Industrie», Magazine de la Commission européenne, ISSN 1831-1245, Septembre 2014, P10.
- [78] <https://link.springer.com/article/10.1007/s13201-020-1168-5>
- [79] Lu H, Walton J C, and Swift A H P, Desalination coupled with salinity-gradient solar ponds. *Desalination*, 136 (2001) 13–23
- [80] Banat F, Jumah R and Garaibeh M, Exploitation of solar energy collected by solar stills for desalination by membrane distillation, *Renew. Energy*. 25 (2002) 293–305

- [81] Burrieza E G, Alarcón D C, Palenzuela P and Zaragoza G, Techno-economic assessment of a pilot scale plant for solar desalination based on existing plate and frame MD technology. *Desalination*, 374 (2015) 70–80
- [82] Sharon H and Reddy KS, A review of solar energy driven desalination technologies. *Renew. Sustainable Energy Rev.*, 41 (2015) 1080-1118
- [83] Abdellah Shafieian, Mehdi Khiadani. A novel solar-driven direct contact membrane-based water desalination system. *Energy Conversion and Management* 199 (2019) 112055
- [84] Nutakki Tirumala Uday Kumar and Andrew R. Martin. Co-Production Performance Evaluation of a Novel Solar Combi System for Simultaneous Pure Water and Hot Water Supply in Urban Households of UAE. *Energies*. April 2017 DOI: 10.3390/en10040481
- [85] Khayet M and Matsura T, *Membrane Distillation: Principle and Applications*, 2011
- [86] Hogan P, Sudjito A, Fane G and Morrison G. Desalination by solar heated membrane distillation. *Desalination*, 81 (1991) 81-90.
- [87] Banat F, Jwaied N, Rommel M, Koschikowski J and Wiegghaus M, Performance evaluation of the “large SMADES” autonomous desalination solar-driven membrane distillation plant in Aqaba Jordan. *Desalination*, 217 (2007) 17–28
- [88] Subiela VJ, de la Fuente J, Piernavieja G and PeñateB, Canary Islands Institute of Technology (ITC) experiences in desalination with renewable energies (1996–2008). *Desalin. Water Treat.*, 7 (2009) 220-235
- [89] Zhani K, Zarzouma K, Ben Bachaa H, Koschikowski J and Pfeifle D, Autonomous solar powered membrane distillation systems: state of the art. *Desalin. Water Treat.*, 57 (2016) 23038–23051
- [90] Gálveza J, García-Rodríguez L and Martín-Mateos I, Seawater desalination by an innovative solar powered membrane distillation system: the MEDESOL project. *Desalination* 246 (2009) 567–576
- [91] Camacho L, Dumée L, Zhang J, Li J-d, Duke M, Gomez J and Gray S, *Advances in Membrane Distillation for Water Desalination and Purification Applications*. *Water*, 5 (2013) 94-196
- [92] Horta P, Zaragoza G and Alarcón-Padilla D.C, Assessment of the use of solar thermal collectors for desalination. *Desalination and Water Treatment*, 55 (2015) 2856–2867
- [93] Saffarini R B, Summers E K, Arafat H A, and Lienhard V J H, Economic evaluation of stand-alone solar powered membrane distillation systems. *Desalination*, 229 (2012) 55–62



CHAPTER II:

**Effects of operating parameters on the AGMD module for
desalination**

A. MARNI SANDID

DOCTORAL THESIS

2023



II. Introduction

Desalination using membrane distillation (MD) can be described as the water treatment procedure applied by the temperature gradient over the microporous, hydrophobic membrane between the hot feed and the cold stream (permeate) [1]. Recently, the use of membrane distillation MD has been applied as a practical alternative solution to the use of conventional distillation and reverse osmosis (RO). The process occurs through the simultaneous transfer of mass and heat across the membrane: the water is evaporated on the hot side, while the water vapor is transported through the membrane. At the cold side, the water vapor is condensed [2].

Concerning the advantages of MD desalination we can mention: a low operating temperature (less than 100 °C), high level of salt waste with low fouling, and low operating pressure [3]. Recent studies indicated that the materials used in the manufacture of MD technology are mainly polyvinylidene fluoride (PVDF), polytetrafluoroethylene (PTFE), or polypropylene (PP). The MD industry has been greatly developed within the last five decades [4].

It is worth noting that the various commercial configuration of MD such as DCMD, AGMD, vacuum distillation (VMD), and gas scavenging distillation (SGMD) are used in industrial scale [5]. DCMD is one of the most widely used techniques due to the simplicity of operation as its efficiency is related to energy use (thermal efficiency of the membrane). In MD application, AGMD technology's membrane thermal efficiency is higher than DCMD [6]. The AGMD technology has higher thermal energy efficiency because the overlapping of the air gap that exists between the condensation zone and the membrane [7].

Due to the air gap between condensation surfaces and the membrane, AGMD configuration has the lowest heat transfer required when compared to other MD. It also has better internal heat recovery, hence lower energy requirement, which makes it the first choice for a pilot plant for the work of Marni et al. [8]. Although the effects of operating conditions have been reasonably studied, it is important to define parameter interactions and optimize the MD system in order to increase process performance and reduce energy consumption.

The MD configuration has been examined in the majority of CFD-based DCMD investigations. One reason for this could be the technology's simplicity when compared to other MD, particularly for desalination and water/wastewater treatment [9]. On the other hand, Xu et al. [10] looked into CFD simulations of AGMD-based desalination in order to anticipate both heat and mass transport characteristics utilizing the carbon membrane. On the hot side, they investigated the profiles of mass flux and temperature polarization next to the tubular

membrane surface under various Reynolds numbers. The obtained results found that the temperature polarization can be decreased the distillate flux. It can be optimized by increasing the feed stream turbulence.

However, it should be noted that CFD simulation for the feed side in AGMD can produce the same results as DCMD technology. Besides, more efforts should be made to simulate the distilled side in AGMD, particularly the condensing surface [11]. Furthermore, because the mass and heat transfer of AGMD technology may be more complicated than other technologies due to the mass/heat transfer resistance enforced by the air-gap, more attempts at CFD simulation for this technology must be investigated.

The present paper investigate the mass and heat transfer in the liquid boundary layer of the PVDF membrane AGMD application using the commercial CFD code ANSYS-FLUENT with a new approach for this study. The present numerical modeling has allowed to examine the effect of the nature of materials (Polyvinylidene fluoride (PVDF) polymers, copolymers and blends) used on the thermal properties. Then, the effects of feed and cold inlet temperatures with flow rates on distillate flux average have been studied for seawater desalination. In addition, the mass flux, efficiency and temperature polarization coefficient (TPC) have been calculated using different areas and flow regimes (laminar and turbulent) of the AGMD process. Besides, effects of membrane physical properties and operating parameters (Temperatures and velocities), which occur on the membrane surface have an important significance for developing new membrane in the future.

II. 1. Presentation of "Fluent":

"Fluent" is a code for modeling fluid flows and heat transfers in complex geometries. It can solve flow problems with structured or unstructured meshes, which can be produced for complex geometries with relative ease. The types of meshes supported are meshes, in 2D, triangular or quadrilateral, or in 3D and mixed meshes [12]. "Fluent" is written based on the programming language "C" and utilizes of the flexibility and power offered by this language (dynamic memory allocation). Furthermore, it uses an architecture that allows it to run as multiple processes on the same or on separate workstations, for more efficient execution. "Fluent" is used through a graphical interface. The experienced user can adapt or augment the interface as needed by writing macros and menu functions to automate certain procedures. Thus, not exhaustively, it has the following modeling capabilities [12]:

- 2D or 3D flows.
- Permanent or transitory states.
- Incompressible or compressible flows including all speed regimes (subsonic, transonic, supersonic and hypersonic).
- Inviscid, laminar or turbulent flows.
- Newtonian flows or not.
- Forced heat transfer, by conduction, convection or radiative.
- Flows with phase changes
- Flows in porous areas.

This code uses the finite volume method as a discretization process. The integral equations which govern the flow, such as the equation of continuity, the equation of conservation of the mass, that of the energy as well as other scalars, like turbulence, are solved by this statistical method. Using this technique based on a control volume, "Fluent" deals with the following steps [12]:

- Division of the domain into discrete control volumes using a calculation grid (mesh).
- Integration of the governing equations on the individual control volumes in order to build the algebraic equations for the dependent discrete variables, (the unknowns), such as speeds, pressure, temperature...
- Linearization of the discretized equations and resolution of the resulting system of linear equations to be able to update the values of the dependent variables (unknowns).

II. 2. Procedure under "Fluent":

When loading the mesh under "Fluent", first of all, we have to scale the geometry (millimeter, centimeter or meter). The software also makes it possible to reorder nodes, surfaces and cells in memory, so that they have the same arrangement in the grid and in memory to improve the performance of the calculation and the efficiency of the access to the memory [12].

II. 3. Turbulence models:

There are different levels of models that differ in their degree of complexity; that means by the number of additional transport equations introduced for the turbulent quantities to close the problem: we thus speak of turbulent models with zero, one or two equations. The most

widely used turbulence models at present in CFD codes are 2-equation models, and more particularly the standard k- ϵ turbulent model which is the most recommended [12].

$$\frac{\partial(\rho k)}{\partial t} + \frac{\partial(\rho k u_i)}{\partial x_i} = \frac{\partial}{\partial x_i} \left[\frac{\mu_t}{\sigma_k} \frac{\partial k}{\partial x_i} \right] + 2\mu_t E_{ij} E_{ij} - \rho \epsilon \quad (1)$$

$$\frac{\partial(\rho \epsilon)}{\partial t} + \frac{\partial(\rho \epsilon u_i)}{\partial x_i} = \frac{\partial}{\partial x_j} \left[\frac{u_t}{\sigma_\epsilon} \frac{\partial \epsilon}{\partial x_j} \right] + C_{1\epsilon} \frac{\epsilon}{k} 2\mu_t E_{ij} E_{ij} - C_{2\epsilon} \rho \frac{\epsilon^2}{k} \quad (2)$$

*** This numerical simulation was carried out through a turbulent model called k- ϵ Standard.

Three turbulence models are available in Fluent:

- The standard k- ϵ model
- The RSM model
- The RNG k- ϵ model

II. 3. 1. k- ϵ model:

II. 3. 1. 1. Standard k- ϵ model

The standard k- ϵ model is based on the concept of Bousinesq 1877. Reynolds stress terms are estimated by Laufer & Spalding 1974 [12]:

$$\rho \overline{u_i u_j} = 2\mu S_{ij} - \frac{2}{3} \rho K \delta_{ij} - \frac{2}{3} \mu_t \delta_{ij} \frac{\partial u_k}{\partial x_k} \quad (3)$$

$$S_{ij} = \frac{1}{2} \left(\frac{\partial u_i}{\partial x_j} + \frac{\partial u_j}{\partial x_i} \right) \quad (4)$$

S_{ij} Introduces the strain tensor

The turbulent viscosity is given by [12]:

$$\mu_t = \rho c_\mu \frac{K^2}{S} \quad (5)$$

It can be seen from equation (3) that the Reynolds stresses are considered proportional to the rate of dissipation reduced by the kinetic energy of the vortices.

Usually, molecular viscosity μ and turbulent viscosity μ_t are combined with effective viscosity by the relationship [12]:

$$\mu_{eff} = \mu + \mu_t \quad (6)$$

The turbulent kinetic energy k is defined by [12]:

$$k = \frac{1}{2} \overline{u_1^2 + u_2^2} \quad (7)$$

Its dissipation rate ε is given by [12]:

$$\varepsilon = \nu \overline{\left(\frac{\partial u_i}{\partial x_j} \frac{\partial u_i}{\partial x_j} \right)} \quad (8)$$

The coefficients of the model are shown in the (Table II.1) [12]:

c_μ	$c_{\varepsilon 1}$	$c_{\varepsilon 2}$	σ_k	σ_ε
0.09	1.44	1.92	1.0	1.3

Table II.1: Values of the constants of the k- ε model.

It is essential to know that the k- ε model is applicable to high Reynolds number flows.

II. 3. 1. 2. RNG k- ε model:

The k- ε RNG (renormalization group) model is the same form as the standard model except that the coefficients are differently specified Choudhury, (1993). In the Fluent code, the RNG k- ε model uses the concept of Boussinesq (Equations 3 and 5) and adopts the following relations for the closure of the turbulence problem studied [12]:

$$\rho u_i \frac{\partial k}{\partial x_i} = \frac{\partial}{\partial x_i} \left(\alpha_p (\mu + \mu_t) \frac{\partial k}{\partial x_i} \right) + \mu_t S^2 - \rho \varepsilon \quad (9)$$

$$\rho u_i \frac{\partial \varepsilon}{\partial x_i} = \frac{\partial}{\partial x_i} \left(\alpha_p (\mu + \mu_t) \frac{\partial \varepsilon}{\partial x_i} \right) + C_{\varepsilon 1} \frac{\varepsilon}{k} \mu_t S^2 - C_{\varepsilon 2} \rho \frac{\varepsilon^2}{k} - R \quad (10)$$

α_p is the inverse of the Prandtl number for the turbulent transfer, it is calculated using the following equation [12]:

$$\left| \frac{\alpha_p - 1.3929}{-0.3929} \right|^{0.6321} \left| \frac{\alpha_p - 2.3929}{3.3929} \right|^{0.3679} = \frac{\mu}{\mu_t} \quad (11)$$

The rate of the stress term R is given by [12]:

$$R = \frac{C_{\mu} \rho \eta^3 \left(1 - \frac{\eta}{\eta_0} \right) \eta^2}{1 + \beta \eta^3} \quad (12)$$

η is given by $\eta = SK/\varepsilon S^2 = 2S_{ij}$

S_{ij} is the module of the strain tensor rate expressed by relation eq.(3)

The expression (9) adds term function of the strain tensor rate η to the dissipation rate equation thus making it less diffusive.

The constants of the RNG model have the value as shown in (Table II.2) [12].

C_μ	$C_{\varepsilon 1}$	$C_{\varepsilon 2}$	η_0	β
0.0845	1.42	1.68	4.38	0.012

Table II.2: Values of the constants of the RNG k- ε model.

In contrast to the RNG model, the k- ε standard model is valid only for fully turbulent flow.

In the RNG model, the size of the turbulent scales is taken into account to determine the part of the energy which will be transported and dissipated. The small scales of turbulence which dissipate all their energy are modeled while the large scales are studied precisely.

II. 3. 1. 3. Realizable model k- ε

The realizable model k- ε is the nonlinear version of the model k- ε . It is proposed in order to improve the deficits of the standard model k- ε . This model maintains two equations of the model k- ε , but also extends the model by integrating additional effects to explain the anisotropy Reynolds stresses.

This model shows that the turbulence does not always adjust instantaneously while moving through the flow domain, meaning that the Reynolds stress depends partially on the average strain rate itself. This means that the realizable k- ε nonlinear model takes into account turbulence slowing phenomena that influence the balance of turbulence production and dissipation [12].

The coefficients of the model illustrated in (Table II.3) [12]:

$C_{\varepsilon 1}$	$C_{\varepsilon 2}$	σ_k	σ_ε
1.44	1.9	1	1.2

Table II.3: Values of the constants of the realizable model k- ε .

II. 4. Principle of the finite volume method

The finite volume method is used by the majority of computer codes, it is based on the subdivision of the field study into the finite number of control volumes (mesh) on which the conservation equations are integrated [12]. In addition, the finite volume method consists:

- The integration of the governing equations on the individual control volumes, in order to construct algebraic equations for the discrete dependent variables (the unknowns), such as velocities, pressure, temperatures and other conserved scalars.

- The linearization of discretized equations.
- Solving the system of resulting linear equations.

II. 5. Reminder on the finite volume method

The calculation domain is divided into the finite number of elementary sub-domains called control volumes. Each one of them includes a node called the main node as shown in (Figure II.1) [12].

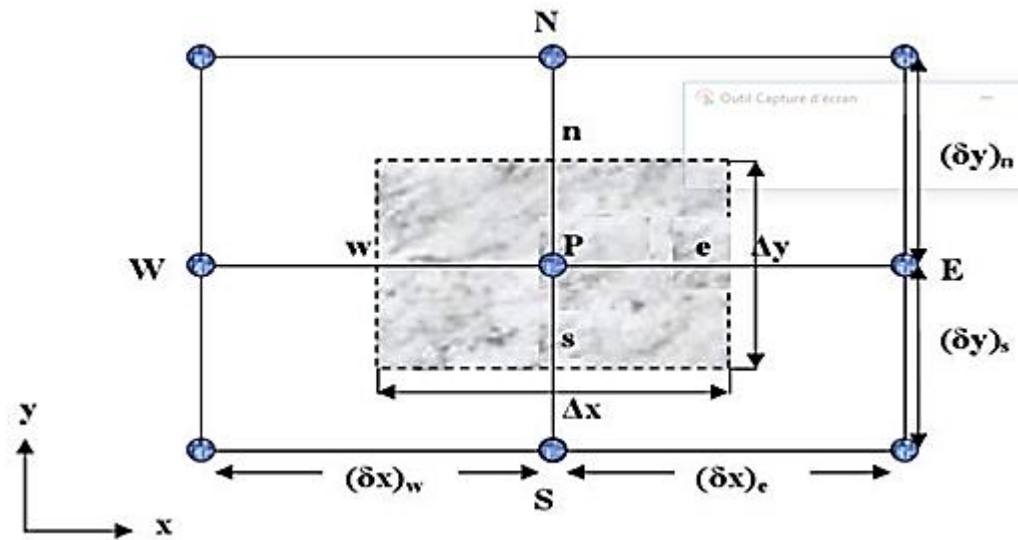


Figure II.1: Two-dimensional control volume [12].

For a main node P, the points E and W (E=East, W= West) are neighbors in the x direction, while N and S (N=North, S=South) are neighbors in the y direction.

II. 6. Mesh

It is the subdivision of the field study into longitudinal and transverse grids whose intersection represents a node, where the components u and v of the vector velocity are in the middle of the segments connecting two adjacent nodes. The discretization of the domain is obtained by a mesh made up of a network of points [12].

The scalar quantities pressure and temperature are stored in the node P of the mesh, while vector quantities u and v are stored in the middles of the segments connecting the nodes.

The general transport equation is integrated on the control volume associated with the scalar variables and the momentum equations are integrated on the control volume associated with the velocity components. The control volume of the longitudinal component u is offset along the x direction relative to the main control volume, while the transverse component v is offset along the y direction as shown in (Figure II.2) [12].

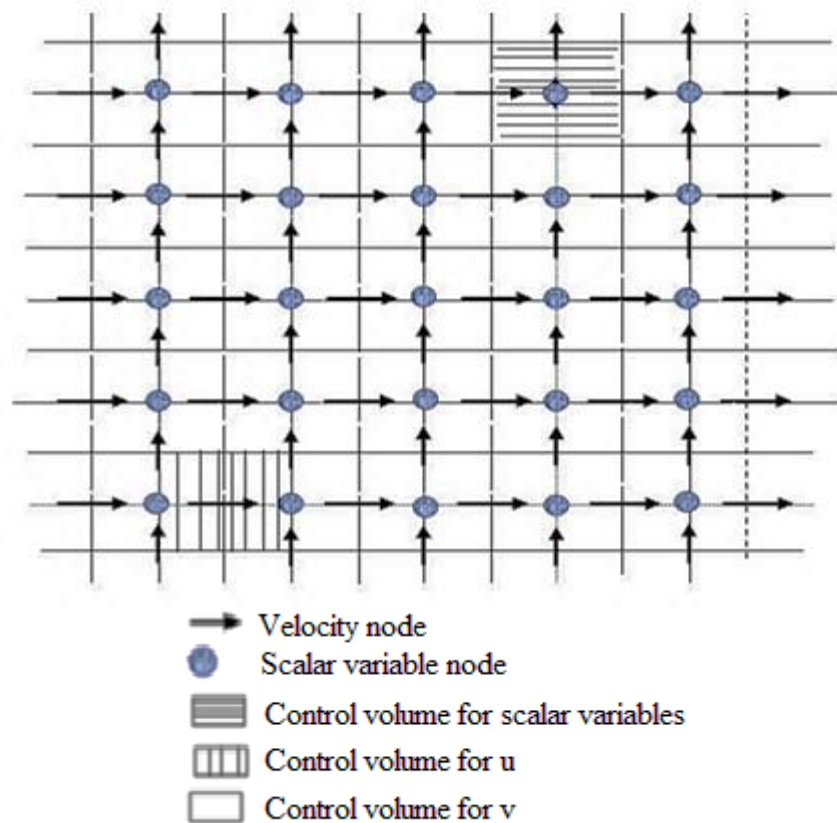


Figure II.2: Diagram of the mesh [12].

II. 7. Reynolds number

The Reynolds number is a dimensionless number used in fluid mechanics. It was highlighted in 1883 by Osborne Reynolds. It characterizes a flow, in particular the nature of its regime (laminar, transient, and turbulent) [12].

II. 7. 1. Laminar flow

When the Reynolds number is small, the inertia forces are small compared to the forces of viscosity. It may even be negligible for very low values of this number. Therefore, the flow is called "LAMINAR". If the Reynolds number is less than 2000, this flow is even reversible; the inertia forces cannot modify the structure of the fluid due to the viscosity forces [12].

For a Reynolds number between 2000 and 3000, the flow remains laminar but it is no longer reversible. If the direction of the current is reversed, the fluid particles do not return to their initial position. The highly viscous and the low-velocity fluids cause the laminar flows.

II. 7. 2. Transient flow

Transient flow refers a flow whose properties vary over time. For example, when you open a faucet, the flow is not instantaneously stable [12].

II. 7. 3. Turbulent flow

For values greater than 3000, the flow of the fluid is called "TURBULENT". Turbulence results from inertial forces which become more important than viscosity forces and the structure of the fluid tends to change irreversibly and significantly. The fluids with low viscosity and at high speed cause the turbulent flows [12].

In a conduit:

The flow regimes vary according to:

Velocity, viscosity, duct section, roughness, density.

They are determined by the Reynolds number.

- If $Re < 2000$, the regime is laminar.
- If $2000 < Re < 3000$, the regime is transient.
- If $2000 < Re < 10^5$, the flow is turbulent.

II. 8. Equations and methodology

II. 8. 1. Governing equations

The governing equations for the system are the conjugated steady incompressible Navier-Stokes and energy equations are written as [13]:

Continuity:

$$\frac{\partial u}{\partial x} + \frac{\partial v}{\partial y} = 0 \quad (13)$$

x-Momentum:

$$\frac{\partial u}{\partial t} + u \frac{\partial u}{\partial x} + v \frac{\partial u}{\partial y} = -\frac{1}{\rho} \frac{\partial p}{\partial x} + \nu \left(\frac{\partial^2 u}{\partial x^2} + \frac{\partial^2 u}{\partial y^2} \right) \quad (14)$$

y-Momentum:

$$\frac{\partial v}{\partial t} + u \frac{\partial v}{\partial x} + v \frac{\partial v}{\partial y} = -\frac{1}{\rho} \frac{\partial p}{\partial y} + \nu \left(\frac{\partial^2 v}{\partial x^2} + \frac{\partial^2 v}{\partial y^2} \right) + \rho g_y \quad (15)$$

Energy:

$$\rho C_p \left(\frac{\partial T}{\partial t} + u \frac{\partial T}{\partial x} + v \frac{\partial T}{\partial y} \right) = k \left(\frac{\partial^2 T}{\partial x^2} + \frac{\partial^2 T}{\partial y^2} \right) + S_h \quad (16)$$

Where u and v are the velocity components, ρ is the density, μ is the viscosity, g_y is the gravitational acceleration, C_p is the specific heat, k is the thermal conductivity, and S_h is a source term of energy transport which is defined as follows:

$$\begin{cases} S_h = \frac{Q_{La}}{\delta_y} \times \frac{y_{mo}}{y_{mi}}; & \text{if } y = y_{mi} \\ S_h = -\frac{Q_{La}}{\delta_y} & ; \text{if } y = y_{mo} \\ 0 & ; \text{otherwise} \end{cases} \quad (17)$$

Where Q_{La} is transmembrane latent heat flux at the hot side membrane surface, and y_{mo} and y_{mi} are distance at y-direction of the inner and outer layer of membrane, respectively. δ_y signifies the grid quantity in the y-direction.

II. 8. 2. Mass flux

The saturated pressure differential along membrane surfaces occurs because of temperature polarization while it drives mass transfer through the porous membrane.

The general mass flux expression is as follows [13, 14]:

$$J = c_m (P_f^{sat} - P_p^{sat}) \quad (18)$$

Where c_m is the membrane mass coefficient, P_f^{sat} and P_p^{sat} are the saturated water vapor pressures at the feed and permeate membrane surface, respectively.

The vapor pressure of distilled water and its temperature is described by the Antoine equation [15] within the range of the MD operation following a monotonic form and is written as:

$$P_{i(pure)}^{sat} = \exp \left(23.238 - \frac{3841}{T-45} \right), \quad i \{f, p\} \quad (19)$$

Three essential membrane coefficient models in literature is stated to characterize the mass transfer across the microporous hydrophobic membrane [16]: the Knudsen, the Poiseuille flow, and the molecular diffusion models. However, in this paper a combination of Poiseuille and Knudsen models is simultaneously used following the work of Chen et al [14] and is described by:

$$c_m = c_k + c_p = 1.064 \alpha(T) \frac{\varepsilon r_p}{\tau \delta_m} \sqrt{\frac{M_w}{R T_m}} + 0.125 \beta(T) \frac{\varepsilon r^2}{\tau \delta_m} \frac{M_w P_m}{R T_m \mu_v} \quad (20)$$

Where $\alpha(T)$, and $\beta(T)$ are Knudsen diffusion and Poiseuille flow models contributions, respectively. T_m is mean membrane temperature ($^{\circ}\text{C}$), M_w is molar mass of the water in kg/mol, P_m is mean pressure, R is gas constant, δ_m thickness of the membrane, μ_v is gas viscosity, τ is tortuosity factor, r_p is pores radius, and ε is the membrane porosity.

II. 8. 3. Heat flux

The heat transfer in MD is characterized by three thermal resistances: Combined transfer over the membrane, convective and conductive transfers through the feed and permeate boundary layers [17]. The total heat flux in MD (Q_m) is assigned to latent heat of the evaporation (Q_v) and a combination of the conduction (Q_c). It is expressed as:

$$Q_m = Q_v + Q_c \quad (21)$$

Whereas the bulk membrane material is responsible for conduction, the membrane pores are responsible for evaporation. Taking ΔH_m to be the enthalpy change because the latent heat of the transmembrane mass flux, it is described by Termpiyakul et al [18]:

$$Q_v = J \Delta H = J (H_{m,f} - H_{m,p}) \quad (22)$$

The conductive heat flux fraction is written by Fourier heat equation as:

$$Q_c = -\frac{k_m}{\delta_m} (T_{m,f} - T_{m,p}) \quad (23)$$

Where k_m is the equivalent thermal conductivity of the membrane. k_b and k_g are the bulk conductivity and the vapor conductivity of the weighted volume average. The subscripts f and p signify the feed and permeate, respectively.

II. 8. 4. Thermal efficiency and temperature polarization coefficient

The latent heat of evaporation used the total heat flux of equation (20) and the thermal efficiency is represented as [10]:

$$\eta = \frac{Q_v}{Q_m} = \frac{J \Delta H_m}{Q_m} \quad (24)$$

Where the ratio of membrane boundary layer resistance over the total and bulk heat transfer resistance is defined by TPC or θ as [19]:

$$\theta = \frac{T_{m,f} - T_{m,p}}{T_{b,f} - T_{b,p}} = \frac{\Delta T_m}{\Delta T_b} \quad (25)$$

Where the subscripts m , p , f , and b indicate the membrane, permeate, feed and bulk surfaces, respectively. A small value of θ (≤ 0.2) signifies a limited heat transfer MD system.

II. 9. AGMD module

A numerical study is performed on AGMD by using ANSYS-FLUENT (CFD). Dimensions of 1 mm height and 210 mm length per channel with the thickness of 130 μm , and an air gap of 0.05 for the AGMD module simulation. A schematic diagram of the counter-current flows modules are illustrated in (Figure II.3).

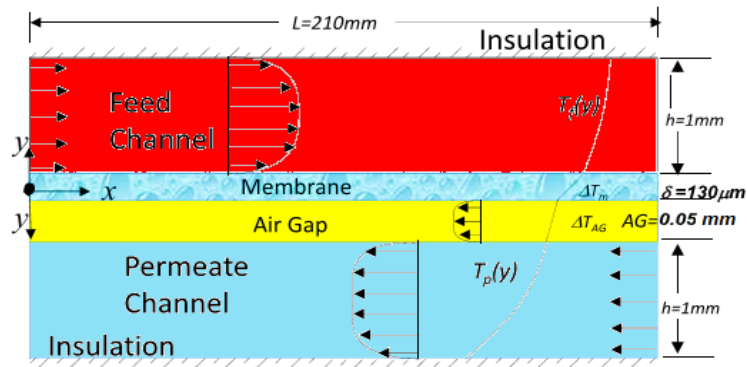


Figure II.3: Schematic diagram of the AGMD module.

The solution is calculated using the commercial CFD (code FLUENT) that based on segregated solver and finite volume approach. The semi-implicit method for pressure equations (SIMPLE algorithm) is used for second order upwind spatial derivatives and pressure-velocity coupling. Convergence residuals is set very tight of 10^{-12} for all scalar equations, (energy, continuity, x- and y-momentums). All membrane, fresh feed, and saline permeate properties are listed in (Table II.4) [20], whereas summary of the boundary conditions are shown in (Table II.5) [21].

Table II.4: Summary of PVDF, vapor, and total membrane thermo-physical properties [20].

Material	Density (kg/m^3)	Specific heat (J/kg K)	Conductivity (W/m K)	Viscosity (pas)
PVDF [5]	1175	1325	0.2622	-
Vapor	0.554	2014	0.0261	-
Membrane	302.2	1896.9	0.0662	-
Saline sea water [22]	1013.2	4046.8	0.642	$5.86 \cdot 10^{-4}$
Pure water [23]	995.2	4182.1	0.613	$8.38 \cdot 10^{-4}$

Table II.5: Summary of boundary conditions for AGMD [21].

Boundary conditions		Feed channel	Permeate channel	Air-gap channel
Inlet channel	Kinetic	0.1 to 1 m/s	0.1 to 1 m/s	0.1 to 1 m/s
	Thermal	50 to 90 °C	5 to 35 °C	5 to 35 °C
Outlet channel		Zero pressure, $dV/dx = 0$	Zero pressure, $dV/dx = 0$	Zero pressure, $dV/dx = 0$
Upper wall	Kinetic	Stationary/no-slip	Stationary / no-slip	Stationary/no-slip
	Thermal	Zero heat flux (insulated)	Coupled	Coupled
Lower wall	Kinetic	Stationary/no-slip	Stationary / no-slip	Stationary/no-slip
	Thermal	Coupled	Zero heat flux (insulated)	Coupled

II. 10. Grid Independent

Because the temperature and velocity profiles along the membrane's walls are so important, the grids are closely refined at those sides using the inflating layer. A grid independence study is carried out by putting various distributions to the test. For this study, the heat transfer coefficient (h) is calculated using several grids and the trends of the change are shown in (Figure II.4):

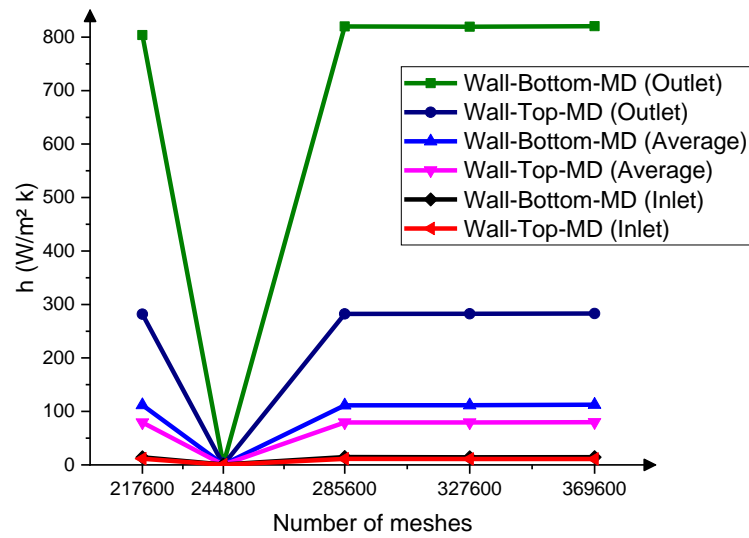


Figure II.4: Heat transfer coefficients (h) at various mesh sizes.

As shown by (Figure II.4), meshing with 285,600 grids presented the optimal results. Therefore, they are considered the chosen mesh in all cases using reasonable resolutions and a structured-quadrilateral type. The symmetrical 2D flow system is discretized in (Figure II.5):

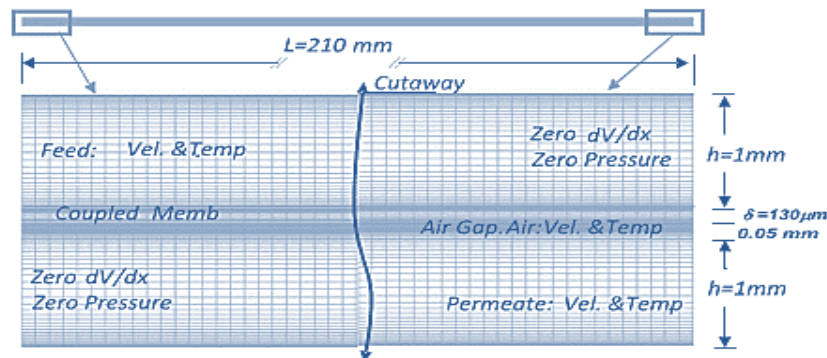


Figure II.5: The models discretization mesh of AGMD.

II. 11. Conclusion

Symmetrical 2D flow systems are performed on AGMD module using non-isothermal CFD coupled thermally with the solid porous membrane. In the membrane surfaces temperatures, the outlet hot temperatures are more important in counter-current flow. Therefore, the thermal behavior of the fluid in AGMD module notes that the exchange is more important the more presides over the wall and especially at the outlets of the AGMD module. In the AGMD module, the concentration of the condensed permeate in AGMD isn't never in direct contact with the membrane surface, hence there isn't risk of membrane wetness on the permeate side. This effective study will be useful to develop and optimize in the future both the small and large scales MD processes for desalination.

Remarque:

Chapter II includes our Article:

- **A. Marni Sandid, D. Nehari, T. Nehari. Effective study of operating parameters on the membrane distillation processes using various materials for seawater desalination. Membrane and Water Treatment. Under Review**

References

- [1] A. G. Fane, Membranes for water production and wastewater reuse, *Desal.* 106 (1) (1996) 1–9
- [2] R.W. Schofield, A.G. Fane and C. J. Fell, Heat and mass transfer in membrane distillation, *J. Membr. Sci.* 33 (1987) 299–313.
- [3] J. Phattaranawik, R. Jiratananon, A. Fane, Heat transport and membrane distillation coefficients in direct contact membrane distillation, *J. Membr. Sci.* 212 (2003) 177-193
- [4] M. Teoh, T. Chung, Membrane distillation with hydrophobic macrovoid-free PVDF-PTFE hollow fiber membranes *Separation and Purification Tech.* 66 (2) (2009) 229-236.
- [5] A. Alkudhiri, N. Darwish, N. Hilal, Membrane distillation: a comprehensive review, *Desal.* 287 (2012) 2–18
- [6] A. Marni-Sandid, M. Bassyouni, D. Nehari, Y. Elhenawy, Experimental and simulation study of multichannel air gap membrane distillation process with two types of solar collectors, *Energy Conversion and Manag.* 243 (2021) 1-14
- [7] A. Marni-Sandid, T. Nehari, D. Nehari, Simulation study of an air-gap membrane distillation system for seawater desalination using solar energy, *Desal. Water Treat.* 229 (2021) 40-51
- [8] A. Marni-Sandid, D. Nehari, A. Elmeriah A, A. Remlaoui, Dynamic simulation of an air-gap membrane distillation (AGMD) process using photovoltaic panels system and flat plate collectors, *Journal of Thermal Engineering* 7 (2021) 117-133
- [9] Y. Guan, J. Li, F. Cheng, J. Zhao, X. Wang, Influence of salt concentration on DCMD performance for treatment of highly concentrated NaCl, KCl, MgCl₂, and MgSO₄ solutions, *Desalination* 355 (2015) 110–117.
- [10] Z. Xu, Y. Pan, Y. Yu, CFD simulation on membrane distillation of NaCl solution, *Front. Chem. Eng. Chin.* 3 (2009) 293–297.
- [11] D.E.M. Warsinger, J. Swaminathan, L.A. Maswadeh, J.H. Lienhard V, Super hydrophobic condenser surfaces for air gap membrane distillation, *J. Membr. Sci.* 492 (2015) 578–587
- [12] A. Marni Sandid and Abdelkader Ismaili. Etude numérique d'un écoulement turbulent à l'intérieur d'un échangeur de chaleur muni d'ailettes. *Memoire de Master 2018 .Centre Universitaire Belhadj Bouchaib d'Ain-Temouchent*
- [13] B.L. Pangarkar, M.G. Sane, Heat and mass transfer analysis in air gap membrane distillation process for desalination, *Membr. Water Treat.* 2 (2011) 159–173.
- [14] T. C. Chen, C.D. Ho, H. M. Yeh, Theoretical modeling and experimental analysis of direct contact membrane distillation, *J. Membr. Sci.* 330 (2009) 279–287.
- [15] R.M. Felder, R.W. Rousseau, *Elementary principles of chemical processes*, 3rd edn., John Wiley & Sons, New York (2000).
- [16] I. Janajreh, D. Suwwan, Numerical simulation of Direct Contact Membrane Desalination (DCMD): II, *Int. J. Eng. Res. Innov.* 6 (2014) 21–33.
- [17] M. Khayet, Membranes and theoretical modeling of membrane distillation: A review, *Adv. Colloid Interface Sci.* 164 (2011) 56–88.

- [18] P. Termpiyakul, R. Jiratananon, S. Srisurichan, Heat and mass transfer characteristics of a direct contact membrane distillation process for desalination, *Desal.* 177 (2005) 133–141.
- [19] J. M. Za'arate, A. Vela'zquez, L. Pen~a, J.I. Mengual, Influence of Temperature Polarization on Separation by Membrane Distillation, *Sep. Sci. Technol.* 28 (7) (1993) 1421–1436
- [20] I. Janajreh, D. Suwwan, R. Hashaikeh, Assessment of direct contact membrane distillation under different configurations, velocities, and membrane properties, *Appl. Energy* 185 (2017) 2058–2073.
- [21] I. Janajreh, K. ElKadi, R. Hashaikeh, R. Ahmed, Numerical investigation of air gap membrane distillation (AGMD): Seeking optimal performance, *Desal.* 424 (2017) 122–130
- [22] B.S. Sparrow, Empirical equations for the thermodynamic properties of aqueous sodium chloride, *Desal.* 159 (2003) 161–170.
- [23] C. L. Yaws, *Chemical Properties Handbook: Physical, Thermodynamic, Environmental, Transport, Safety and Health Related Properties for Organic and Inorganic Chemicals*, 1st ed, (1999)



CHAPTER III:

**Simulation, controlling and optimization study of the
solar AGMD system small scale**

A. MARNI SANDID

DOCTORAL THESIS

2023



III. Introduction

Several technologies are used to produce potable water in different places of the world, and membrane distillation (MD) is a new process of producing distilled water that had been used many years ago. MD process appears as an attractive solution with a free energy source (solar energy) [1]. MD is a thermally driven separation process in which only the vapor molecules pass through a microporous hydrophobic membrane [2]. The driving force in the MD process is the vapor pressure difference induced by the temperature difference across the membrane surface. This process has various applications such as desalination, wastewater treatment and the food industry [3-4]. The advantages of MD desalination via working on low-grade temperature sources (less than 100 °C), 100% salt rejection with low fouling and operating pressure make it more efficient methods for desalination application [5]. Until now, the most employed studies of MD hydrophobic micro-porous membranes commercially available have been based on polypropylene (PP), polyethylene (PE), polytetrafluoroethylene (PTFE), or polyvinylidene fluoride (PVDF) [6].

In light of the review of work done by Verma SK et al [7], the efficiency of the membrane decreases due to its contamination by agglomeration of particles. Self-cleaning smart nanomaterials may be a suitable choice to solve the problem. Therefore, photocatalytic methods of purification can be modified by adopting hybrid nanomaterials photocatalytic, which can widen the absorption of ultraviolet-visible spectra for producing reactive oxygen radicals, which damage the cell wall of harmful bacteria and simultaneously absorb more heat energy at the higher temperature to raise the rate of the process.

Recently, various MD processing technics have appeared as solutions have a free energy source and diversity of membrane distillations technologies such as Direct Contact Membrane Distillation (DCMD), Vacuum Membrane Distillation (DMV), Air Gap Membrane Distillation (AGMD), and Sweeping Gas Membrane Distillation (SGMD) [8]. According to the high-energy costs associated with existing desalination methods, there is a great demand for technologies that can use low-temperature sources like waste heat or solar energy. DCMD is the most MD configuration technology studied due to the simplicity and ease of handling, where its energy efficiency, called the membrane thermal efficiency (MTE), is commonly related to the operating conditions [9]. In the MD process field, the DCMD process has a lower MTE against the AGMD procedure because of conduction heat losses.

The mechanism functions of the AGMD systems based on the stagnant air gap interposition between the membrane and condensation area, which leads to an inherently increasing of the thermal energy efficiency of the process [10]. Consequently, the first patent to

discuss the principle of AGMD appeared with G. L. Hassler [11] and P. K. Weyl [12] for the basics knowledge, in which the concept and behavior of AGMD systems can be found in different literature studies [13, 14, 15]. Hanemaaijer et al [16] introduced an idea of internal heat recovery that is called memstill membrane distillation. Sequentially, Duong et al [17, 18] conducted a study that allowed only AGMD to restore the latent heat without any external heat exchanger. Minier-Matar et al [19] found through their study that AGMD provides a higher resistance to mass transfer and runs at low water flow.

Schwantes et al [20] gave the high thermal efficiency in AGMD; it was the first choice for experimental test stations dealing with long-term operation and expansion problems, where these AGMD modules can be made with cheap polymeric corrosion-resistant materials [21].

Although recent developments in AGMD configurations, the first flat plate AGMD system was developed by the Swedish Svenska Utvecklings AB in 2016 [22], while such modules today are manufactured and commercialized by Scarab Development. Each module is made up of 10 planar cassettes with an overall membrane surface of 2.3 m² and a global capacity of 1–2 m³/d of distillate water [23]. The single-stage consists of injection-molded plastic frames containing two parallel membranes, feed and exit channels for warm water and two condensing walls [22, 24]. Achmad Chafidz et al. [25] developed a portable hybrid solar-powered membrane distillation system for the production of freshwater using Vacuum Multi-Effect Membrane Distillation. The total volume distillate output during the test was approximately 70 L with an approximate conductivity of 4.7 $\mu\text{S}/\text{cm}$. The average distillate output rate was 11.53 L/h with a maximum of 15.94 L/h at noontime, whereas the distillate flux was in the range of 1.5–2.6 L/m² h.

Kullab et al [26] studied the solar thermal integrated AGMD unit having non-concentrating solar thermal collectors. The trials were conducted on this test facility with different parametric analyses (feedstock, Total Dissolved Solid levels, temperature, and flow rates) and the data from the experiments and related studies demonstrated that the MD unit performance remains insensitive to variations in feedstock qualities (e.g. PH, TDS levels).

On the other hand, Banat and Simandl [27] used membranes of different porosities for desalinating water by using Air Gap Membrane Distillation (AGMD) technique. The results demonstrated that the permeate flux increased exponentially with the increase in hot side temperature. Khan et al [28] conducted experimental analysis from arsenic removal using single cassette AGMD with an effective membrane area of 0.2 m² and reported fluxes of 20 L/m²h at a temperature difference of 50°C between hot and cold inlet temperatures. He et al [29] applied factorial design and RSM to analyze the relationships between operating parameters (hot and

cold inlet temperatures, feed flow rate) on performance indicators including distillate flux and gained output index of a hollow fiber AGMD module.

In Kumar's work et al [30], a single cassette air-gap membrane distillation (AGMD) module characterized to identify the effect of process parameters on distillate flux and thermal efficiency. Favorable conditions to obtain a distillate flow rate of 5–6 kg/h determined on a bench-scale experimental setup. The developed RSM regression model tested by analysis of variance (ANOVA) and validated using experimental results of Asim et al [31]. Parametric optimization carried out as well to identify suitable conditions for operating MD with constant or dynamic energy supply (e.g. solar thermal energy). Then, experiments on a solar MD system were carried out in October during which maximum radiation would be incident on solar collectors installed in the United Arab Emirates (UAE).

In this chapter, two cases of the solar AGMD small scale systems are studied, controlled and optimized. In the first case, the solar AGMD system is studied and controlled for product a constant distilled water flow on different days throughout the year using TRNSYS program. In the second case, optimized parametric conditions were used to operate the solar thermal driven membrane distillation system in Ain-Temouchent City, Algeria. Accordingly, the purpose of this study is the use of solar panels in the photovoltaic system with the energy storage batteries to produce all necessary electrical energy. Therefore, the optimal AGMD system with a controlled distilled water flow can make this contemporary model usable and suitable to be a system compatible in the future with all intermittent climatic conditions and all over the world.

III. 1. Description of the TRNSYS software

TRNSYS is a commercially available transient systems simulation program since 1975 [32], continues to develop by the international collaboration from the United States (Thermal Energy System Specialists and the University of Wisconsin-Solar Energy Laboratory), Germany (TRANSSOLAR Energietechnik), and France (Centre Scientifique et Technique du Bâtiment). TRNSYS is a flexible energy modeling software package by allowing:

- (1) The addition of mathematical models.
- (2) The availability of add-on components.
- (3) The ability to link with other simulation programs.

TRNSYS has been widely used to model solar energy applications, biological systems, and conventional buildings. TRNSYS is a dynamic simulation system that enables the fine-grained simulation of the behavior of complex thermal systems as buildings. TRNSYS has been in operation since 1975. It has inspired several innovations in other simulation tools (Energy +,

Energy 10, HVACSIM +, CA-SIS, etc...) that employ either its general solver, or parts of its models, or both [33].

TRNSYS simulation software consists a collection of mathematical models of physical components in the TRNSYS library. The components can be created using FORTRAN program, however TRNSYS 17 permits the use of any programming language capable of generating a Windows - C DLL, C ++, etc...

TRNSYS 17 has a significant number of standard models (Solar collectors, Thermal Storage, Heat Exchangers, Regulators, Electrical / Photovoltaic components, Hydraulics, Loads and Structures, etc...). To define a simulation project, just interconnect them in a project editor. In addition, there are many building models that can be simulated the thermal behavior of a multi-zone building a very detailed way (ambient temperature, air humidity, energy requirements for each surface and each zone; gains by ventilation, convective coupling with other zones; latent energy needs; appreciable variation in energy; solar energy entering through the windows; etc...). Many components are included in the TRNSYS standard library such as solar (photovoltaic and thermal), HVAC, hydrogen systems and many others [33]

III. 1. 1. Advantages and disadvantages of the TRNSYS software

The TRNSYS program has many advantages such as [34]:

- A large amount of documentation and realization feedback.
- The ability to edit the source code yourself in order to customize your model.
- The ability to connect to other applications such as CFD, Matlab, SketchUp, Excel, ESS, etc...
- Possibility of the control in the simulation period, including the ability to select the time step at the start and the end of the simulation.
- The user is required to enter all of the data specifying the building systems.
- Simplifying the heat exchange gradient by utilizing a standard temperature approach.

On the other hand, TRNSYS doesn't checks errors on the regions and volumes entered into the software. Therefore, some disadvantages must be considered in the program while assuming and interpreting the results.

III. 2. Equations and methods of the solar AGMD system small scale

III. 2. 1. AGMD module

- The most significant influential design variables on the AGMD performance are the feed inlet temperature (T_{Hin}), the cooling inlet temperature (T_{Cin}) which is condensation temperature, the feed flow rate (V_f) and feed concentration (C_f). The selected performance indicators of the AGMD process are distillate flux (J_d) and specific performance ratio (SPR), whereas J_d is calculated by [30]:

$$J_d = \frac{M_d}{S.t} \quad (1)$$

Where M_d (kg) is the mass of distillate water collected within the time t , and S (m^2) is the effective membrane surface area of evaporation.

- The regression quadratic model with coded parameters can be expressed as [30]:

$$Y = \beta_0 + \beta_1 X_1 + \beta_2 X_2 + \beta_3 X_3 + \beta_{12} X_1 X_2 + \beta_{13} X_1 X_3 + \beta_{23} X_2 X_3 + \beta_{11} X_1^2 + \beta_{22} X_2^2 + \beta_{33} X_3^2 \quad (2)$$

- Kumar et al [30] determined the final regression equations for J_d and T_{Hout} in terms of actual operating parameters as follows:

$$J_d = -6.57 + 0.16 * T_{Cin} + 0.15 * T_{Hin} - 5.86 * 10^{-3} * V_f - 5.77 * 10^{-3} * T_{Cin} T_{Hin} - 2.5 * 10^{-4} * T_{Cin} V_f + 3.44 * 10^{-4} * T_{Hin} V_f + 2.48 * 10^{-3} * T_{Hin}^2 \quad (3)$$

$$T_{Hout} = 3.097 + 6.82 * 10^{-2} * T_{Cin} + 0.772 * T_{Hin} + 3.5 * 10^{-3} * V_f + 1.42 * 10^{-3} * T_{Cin} T_{Hin} \quad (4)$$

Table III.1: Operational conditions of tested AGMD module [30].

Operational parameter	Specification
Feed flow rate, L/min	4, 6 and 8
Hot water operation temperature, °C	40–80
Coldwater operation temperature, °C	10–50
Tap water conductivity, $\mu S/cm$	500–10,000

- The bulk temperature of the feed is used for calculating the latent heat of evaporation. Therefore, the thermal efficiency of the MD unit is given by [35]:

$$EE = mp \times Hv / Q_{in} \quad (5)$$

Where H_v is Latent heat of vaporization (J/kg), mp is permeate flux (kg/s).

$$Q_{in} = mf \times C_p \times (T_{feed,in} - T_{feed,out}) \quad (6)$$

where mf is the feed-water flow rate (kg/h), C_p is the feed-water heat capacity (kWh /kg °C), $T_{feed,in}$ is the evaporator inlet temperature (°C) and $T_{feed,out}$ is the evaporator outlet temperature (°C).

H_v is estimated by [36]:

$$H_v = 2501.897149 - 2.407064037 \times T + 0.001192217 \times T^2 - 0.000015863 \times T^3 \quad (7)$$

where T is the average temperature at the evaporator entrance and the exits of the condenser (°C).

III. 2. 2. Solar thermal system

- The basic method of measuring collector performance is to expose the operating collector to solar radiation and measure the fluid inlet and outlet temperatures and the fluid flow rate. The useful gain is [37]:

$$\dot{Q}_u = m_0 C_{pf} (T_0 - T_i) \quad (8)$$

Where m_0 is the solar fluid mass flow rate (kg.hr-1), C_{pf} is the specific heat capacity of solar fluid (KJ.hr-1), T_0 and T_i are the inlet and outlet temperature of the solar fluid (K).

- The efficiency of flat plate collectors is expressed as follows [37]:

$$\eta = \eta_0 - a_0 * \frac{(T - T_{amb})}{G} - a_1 * \frac{(T - T_a)^2}{G} \quad (9)$$

With G : the solar flux (W/m²), T_a : the ambient temperature (°C), a_0 and a_1 are characteristic constants of the efficiency of the collector.

- Heat exchanger counter flow effectiveness is [38]:

$$\varepsilon = \frac{1 - \exp\left(-\frac{UA}{C_{min}}\left(1 - \frac{C_{min}}{C_{max}}\right)\right)}{1 - \left(\frac{C_{min}}{C_{max}}\right)\exp\left(-\frac{UA}{C_{min}}\left(1 - \frac{C_{min}}{C_{max}}\right)\right)} \quad (10)$$

UA is the overall loss coefficient between the heater and its surroundings during operation ($\text{kg}\cdot\text{hr}^{-1}$), C_{max} is the maximum capacity rate ($\text{KJ}\cdot\text{hr}^{-1}\cdot\text{K}$), C_{min} is the minimum capacity rate ($\text{KJ}\cdot\text{hr}^{-1}\cdot\text{K}$).

Required heating rate including efficiency effects in the auxiliary heaters is [38]:

$$Q_{aux} = Q_{loss} + Q_{fluid} \quad (11)$$

With:

$$Q_{loss} = UA(\bar{T} - T_{env}) + (1 - \eta_{htr})Q_{max} \quad \text{and} \quad Q_{fluid} = \dot{m}_0 C_{pf}(T_{set} - T_i)$$

Q_{aux} is the required heating rate including efficiency effects ($\text{kg}\cdot\text{hr}^{-1}$), Q_{fluid} is the rate of heat addition to fluid stream ($\text{kg}\cdot\text{hr}^{-1}$), Q_{loss} is the rate of thermal losses from the heater to environment ($\text{kg}\cdot\text{hr}^{-1}$), Q_{max} is the maximum heating rate of the heater ($\text{kg}\cdot\text{hr}^{-1}$), η_{htr} is an efficiency of the auxiliary heater, m_0 is the outlet fluid mass flow rate ($\text{kg}\cdot\text{hr}^{-1}$), C_{pf} is the fluid specific heat ($\text{KJ}\cdot\text{hr}^{-1}$), T_i is the fluid inlet temperature (K), (\bar{T}) brackish water average temperature T_{set} set temperature of heater internal thermostat (K), T_{env} is the temperature of heater surroundings for loss calculations (K).

III. 2. 3. Solar PV system

The use of solar energy considerably reduces the operating costs; however, its intermittent nature requires a non-stationary optimal operation that can be achieved through advanced control strategies. In this study, the control and model of the thermal system of the membrane make with the use of Photovoltaic panels for cost savings. Therefore, to reduce the operating cost, the photovoltaic system uses the storage battery that replaces the power load of the auxiliary heater. Then, the following output parameters, which are the outlet temperature of solar collector and auxiliary power supplied to the storage tank. The control and model of the thermal system of the distillation membrane also make with the use of Photovoltaic panels

device for cost savings. In this study, a TRNSYS program [39] is used to predict the long-term performance of the solar water heating systems in different locations for distillation membrane, and they can simulate the system performances under different weather, among them the operating conditions in the weather of the state Ain-Temouchent, Algeria.

- The PV system is calculated based on the following equations [40]:
The peak power of the autonomous photovoltaic installation

$$P_c = P_{pv} = \frac{D}{N * F} \quad (10)$$

P_c Power of the PV field, D Daily need kWh/jour, F Form factor, N number of hours equivalent.

$$N = \frac{G_T(t)}{G_{T,STC}} \quad (11)$$

$G_T(t)$ is the solar radiation incident on the solar -PV array in the current time step kW/m^2 . $G_{T,STC}$ is the incident radiation at standard test conditions kW/m^2 .

- The size of the inverter from 25 to 30% must be greater than the total quantity of devices. In the case of a device or compressor, the size of the inverter must be at least 3 times the capacity of these devices and must be added to the capacity of the inverter to handle the surge current during startup [41].
- The storage capacity of the battery is calculated according to the following relation [41]:

$$C(Ah) = \frac{D * 1000 * N_j}{n_b * P_d * P_r} \quad (12)$$

Where D is the total Watt-hours per day used, N_j : Autonomy number of days without radiation, P_r : Nominal voltage of the batteries, n_b : Battery efficiency, P_d : Depth of the discharge.

III. 3. Main specifications of the solar thermal integrated MD system

MD system determines the distillate production flow rate along with MD hot side outlet temperature. Other main components of the solar thermal MD system are the solar collectors, a heat exchanger, three pumps and a hot water storage tank. The heat exchanger transfers heat from the collectors to the MD feed water stored in a small tank from where the feed pumps to the MD module. Cold-water pumps to MD from a cold-water storage tank having temperatures according to the ambient conditions of the location [30].

Tables (III.2) and (III.3) show the main specifications considered for the components of the solar thermal MD system. Five flat plate collectors having a total area of 12.75 m² considered for both experiments and the simulation model. A simple storage tank with fixed inlets and uniform heat losses use for feeding water storage. The temperature differential controller uses to control the flow of heat transfer fluids in the solar thermal system. This model studies throughout the year, especially in December when the minimum radiation is incident on solar collectors in Ain-Temouchent.

Table III.2: Main specifications of the solar thermal integrated MD system [30].

component	Parameter	Value	Unit
Flat plate collectors	Collector absorber area	12.75	m ²
	Collector efficiency	0.781	-
	Tilt angle	35	Degrees
Heat exchanger	Effectiveness	0.5	-
MD hot water store	Volume	100	L
MD hot pump	Flow rate	420	kg.hr ⁻¹
Auxiliary heaters	Maximum heating rate	1500	W
	Efficiency of the auxiliary heater	1	-

Table III.3: Technical characteristics of the PV system [37].

Component	Parameter	Value	Unit
PV panel	Module area	1.6	m ²
	Power tolerance	± 5	%
	Solar Cells	36	cells
	Module open-circuit voltage at reference conditions	38.9	V
	Module short-circuit voltage at reference conditions	9.31	Amperes
Battery	Tolerance for iterative calculations	16.7	Ah
	Charging efficiency	0.8	-
Inverter	High limit on the fractional state of charge (FSOC)	1	-
	Regulator efficiency	0.78	-

III. 4. Simulation and controlling of the solar AGMD system during the year “CASE 1”

In this chapter (Case1), a numerical model of desalination that depends on single cassette air-gap membrane distillation (AGMD) module integrated solar thermal system is validated with simulation results of Kumar et al [30] which was carried out experiments on solar MD system only in October on solar collectors installed in UAE as previously mentioned [31]. Therefore, this model is dynamically simulated with the TRNSYS (transient system simulation) program to be an ideal model of obtaining a constant distilled water flow rate at different times at changing climatic conditions throughout the year in Ain-Temouchent weather. Then, the auxiliary heater adds to compensate the lost thermal energy in cold climatic conditions, and the photovoltaic system adds the energy storage battery for the auxiliary heater needs. Thus, it saved costs by relying on solar energy only as renewable energy for this model used in desalination throughout the year using modern membrane distillation technology (AGMD). Therefore, this model is suitable to be a compatible system with all intermittent weather climatic conditions in Ain-Temouchent, Algeria.

III. 4. 1. System Description

III. 4. 1. 1. AGMD process

AGMD is a configuration of membrane distillation (MD) in which an air layer is interposed between a porous hydrophobic membrane and the condensation surface. In the process, volatile compounds (including water) present in a warm feed evaporate at the liquid/vapor interface formed at the membrane surface. The vapor is transferred through the membrane pores and the air gap then finally condenses on a cold surface inside the membrane module. The driving force of the mass transfer in AGMD is the difference in vapor pressure on both sides of the membrane. The present work utilizes a bench-scale AGMD unit with a single membrane cassette developed in collaboration with an industrial research partner. Figure III.1 shows the layout of components in the bench-scale MD module and shows the picture of the module fitted with the cassette in a plate and frame configuration. Specifications of the membrane cassette are [30]:

Material: hydrophobic PTFE membrane.

Pore size: 0.2 μm ; thickness: 280 μm ; total membrane area: 0.2 m^2 .

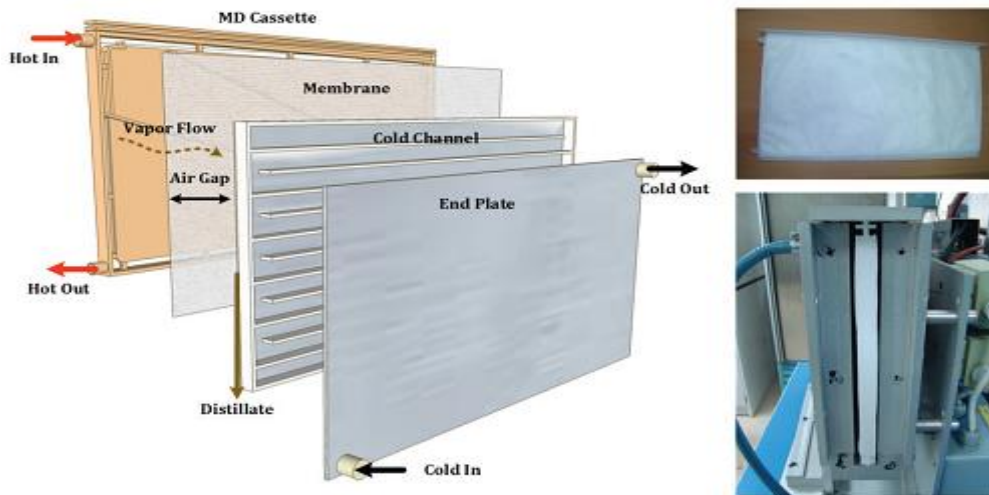


Figure III.1: Bench-scale MD module and pictures of cassette fitted into module [30].

III. 4. 1. 2. Thermal system

The studied system contains the thermal energy loop, as shown in (Figure III.2). The system incorporating a flat plate collector (FPC) with an area of 12.75 m^2 , heat exchanger internal, and auxiliary heaters providing heat via freshwater heat transfer fluid to MD hot water store containing 100L with a pump and a controller in differential temperature as shown in (Figure III.2).

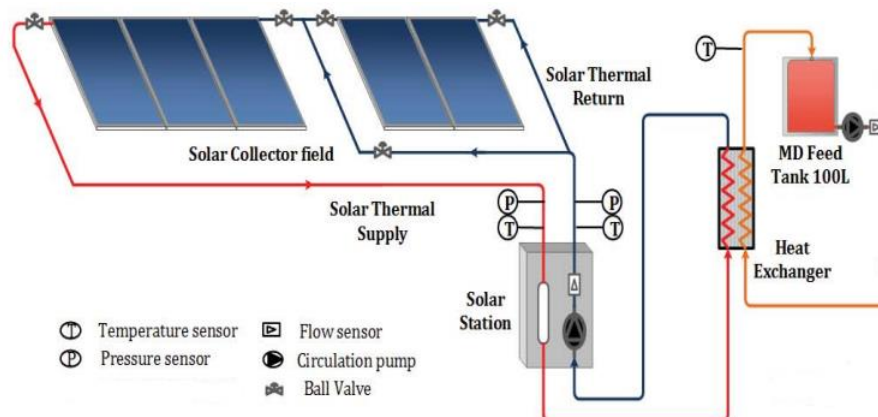


Figure III.2: Schematic showing an operation of solar domestic hot water (SDHW) [42].

III. 4. 1. 3. Photovoltaic (PV) system

The solar PV system consists of different components that must be selected according to the type of system, the location of the site and the applications. The main components of the solar photovoltaic system are the solar charge controller, the inverter, the group of batteries, the auxiliary power sources and the loads (devices) as shown in (Figure III.3).



Figure III.3: Synoptic representation of the structure of a photovoltaic system with storage [43].

III. 4. 1. 4. Weather data

This model has been studied in Ain-Temouchent weather, Figure III.4 shows changing climate conditions throughout the year. The weather in the Ain-Temouchent state is pleasant, warm and moderate in general. At an average temperature of 25.7 degrees Celsius, August is the hottest month of the year. At 10.8°C on average, January is the coldest month of the year. Therefore, in (Figure III.4a), we notice a change in temperature throughout the year, which reaches up to 40 degrees Celsius in August, and we note that the wind is moderate and does not exceed the velocity of 15 m/s. For the irradiation, it changes during the months of the year and reaches up to 220 KWh/m² in August and July as shown in (Figure III.4b), because the temperature is high in this period of the year. This study has been simulating for a full year and the results will appear on different days (11/12, 11/03, 11/08, and 11/10).

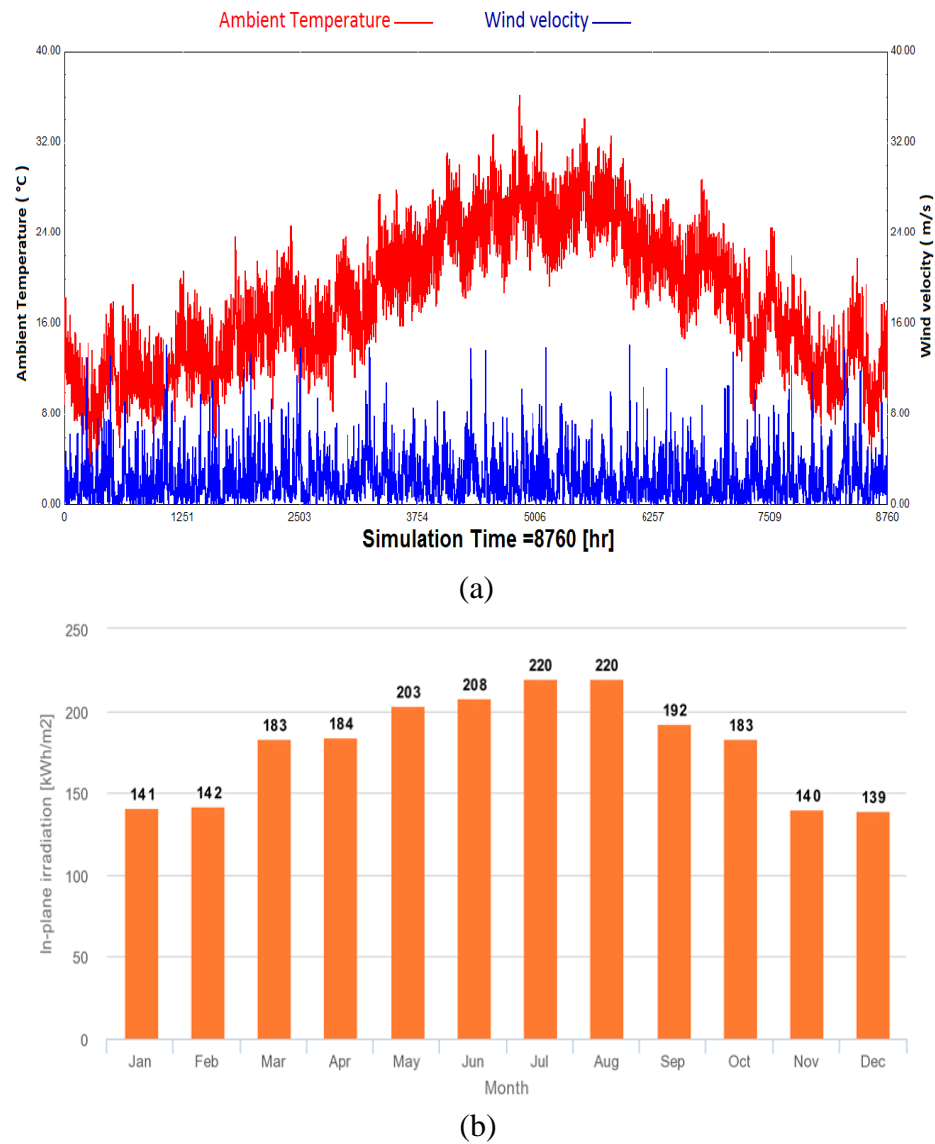


Figure III.4: (a) Ambient temperature, wind velocity and (b) irradiation in the weather of Ain-Temouchent.

III. 4. 1. 5. TRNSYS Model

The model of solar thermal membrane distillation system with AGMD and the photovoltaic system is developed using TRNSYS software, which is a quasi-steady-state simulation program. TRNSYS enables system components represented as preformats to be selected and interconnected in any desired manner to construct a system's model. To facilitate the selection of the system components, it is important to develop an information flow diagram. The information flow diagram for the models is shown in (Figure III.5). The main component of the model is the AGMD unit, which is represented by a new equation in TRNSYS. Additional components to the model include TYPE109-TM2 reading and processing of

meteorological data, Type 91 heat exchanger, Type 39 storage tank, Type 1 flat plate collector, Type 2 differential temperature controller, Type 3 single speed pump, Type 6 auxiliary heaters, Type 94 photovoltaic panels, Type 47 storage battery, Type 48 inverter, Type 14 forcing functions, Type 57 unit conversion and Type 65 online plotter. Tables (III.1) and (III.2) show the values of parameters used in the TRNSYS model.

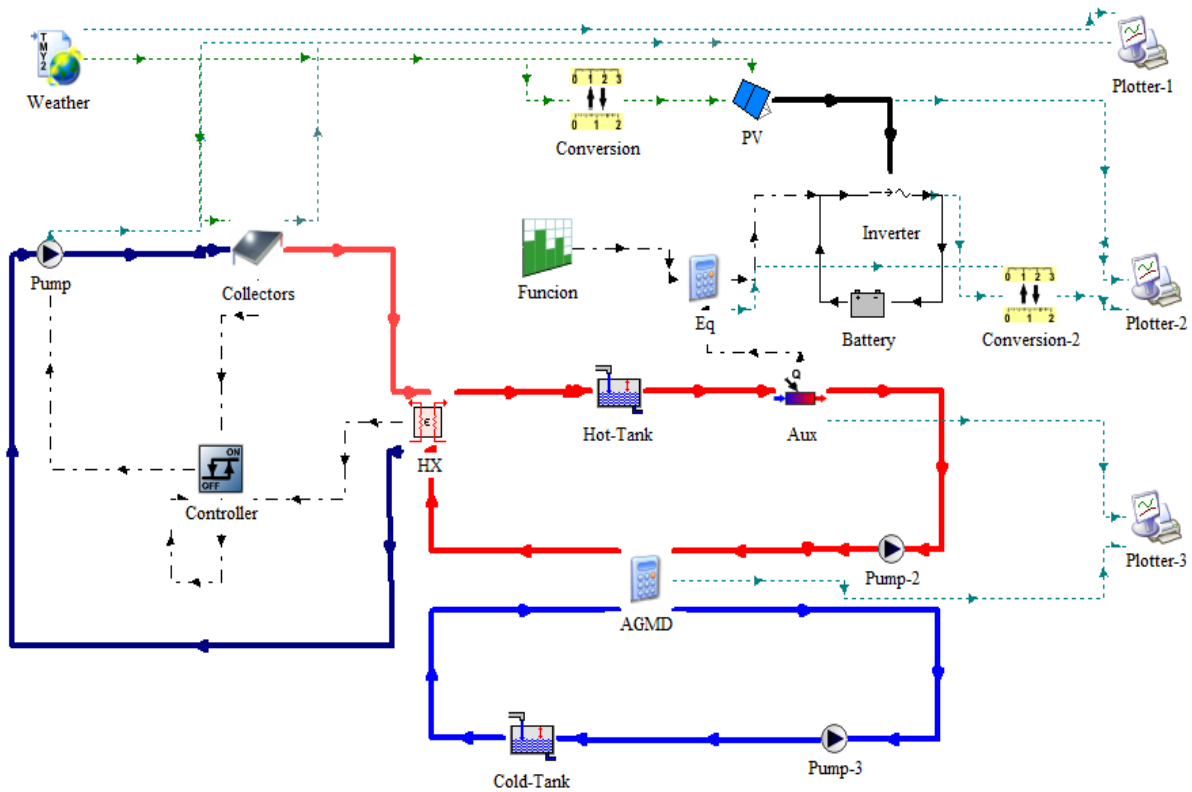


Figure III.5: Assembly diagram of the AGMD system in the TRNSYS simulation.

- To obtain good harmonic results, we have chosen the time from 8 am to 6 pm to operate the AGMD system as show in (Figure III.6). In this time, the solar radiation required by both solar and photovoltaic panels is present in the winter season with various changing climatic conditions in Ain-Temouchent, Algeria.

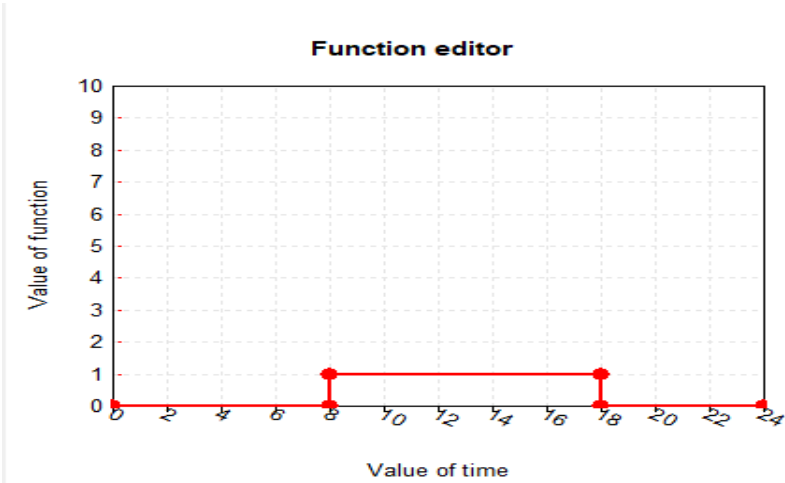


Figure III.6: The time value for operation of the AGMD system with ON / OFF control.

III. 5. Development and optimization of the solar AGMD system during the year “CASE 2”

A solar AGMD system is studied in this chapter for optimizing the operation of a Solar Membrane Distillation (SMD), in terms of thermal efficiency, distillate production, and cost savings. Besides, the brine that contains the high salt concentration is completely dispensed with this process. Therefore this chapter presents a numerical study to investigate the solar membrane distillation (MD) system for seawater desalination using solar energy. The solar MD system includes both flat plate collectors and photovoltaic panels. Additionally, the TRNSYS program software [39] is used to predict the long-term performance of the solar AGMD system at different times throughout the year in Ain-Temouchent weather, Algeria.

III. 5. 1. Description of the AGMD system

Figure III.7 shows a schematic presentation of the principle of the seawater air-gap membrane desalination process using solar energy. The three major components in the solar AGMD system are:

- (1) AGMD system
- (2) Solar-thermal system
- (3) Solar photovoltaic (PV) system

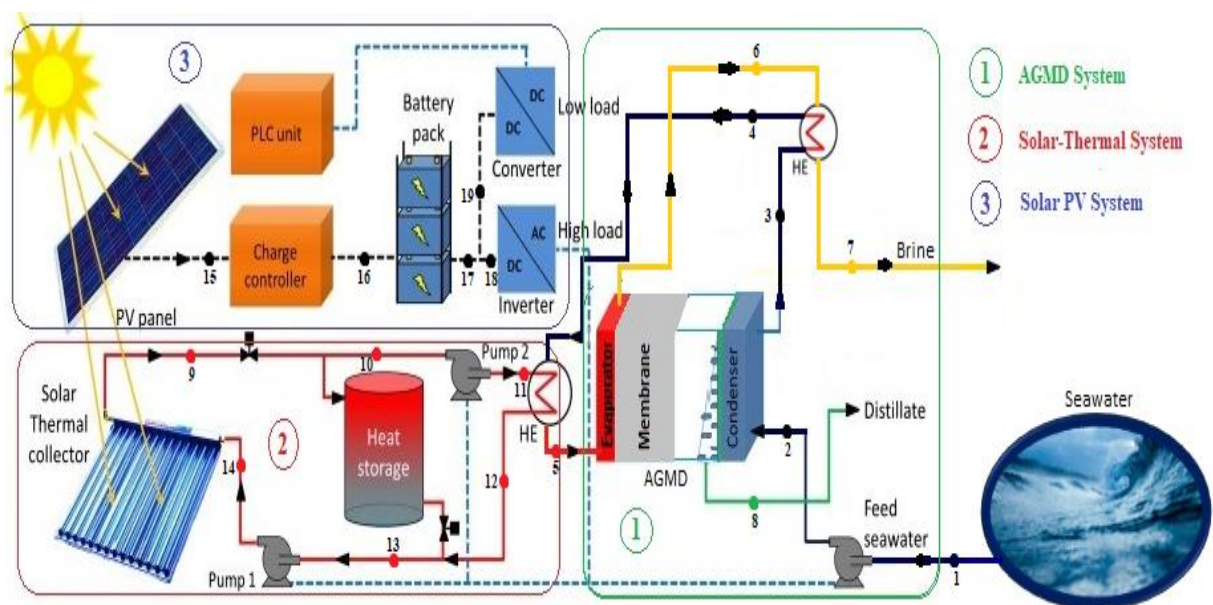


Figure III.7: Schematic of the solar AGMD System for seawater desalination.

III. 5. 1. 1. Solar-thermal system

The studied system contains the thermal energy loop, as shown in (Figure III.7). The system incorporates five flat plate collectors (FPC) with a total area of 12.75 m² with a controller, a counter-flow heat exchanger, a controller in differential temperature, and pumps. The water flow rate is controlled by an ON / OFF controller to optimize thermal energy harvesting and setting time. Due to the convergence of climatic changes between Algeria and the UAE, we chose five flat plate collectors in order to obtain a suitable temperature to provide a flow rate of 5 L/h of distilled water in the weather of the state Ain-Temouchent (latitude 35°3'0" N, longitude 1°1'0" E), Algeria.

III. 5. 1. 2. Solar photovoltaic (PV) system

The solar PV system consists of different components that must be selected according to the type of system, the location of the site, and the applications. The main components of the solar photovoltaic system are the solar charge controller, the inverter, the group of batteries, the auxiliary power sources, and the loads (devices) as shown in (Figure III.7). An installed DC/AC converter converts 24-V DC from the battery into 24-V DC as required by (low load) equipment such as sensors, whereas a DC/DC inverter inverts the 24-V DC into 220-V AC (high load) that is used by pumps.

III. 5. 1. 3. The AGMD module

AGMD is a configuration of membrane distillation (MD) in which an air layer is interposed between a porous hydrophobic membrane and the condensation surface. Figure III.8 shows the picture of the module fitted with the cassette in a plate and frame configuration and shows the layout of components in the bench-scale MD module. The cassette of the AGMD module the following specifications: hydrophobic PTFE membrane with a pore size of 0.2 μm, the thickness of 280 μm, and total membrane area: 0.2 m² [30].

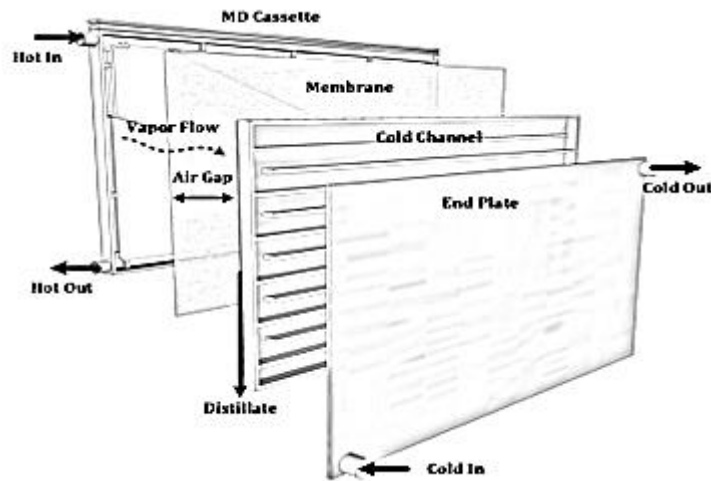


Figure III.8: Pictures of cassette fitted into the module and bench-scale AGMD module [30].

In the AGMD system, seawater is circulated through the AGMD module by the pump. It is responsible for cooling the vapor coming out from the AGMD process. The hot seawater from the AGMD process is exchanged using the thermal system via a counter-flow heat exchanger. However, to avoid losing the heat energy coming out from the evaporator, another recovery exchanger is added. Therefore, it is used to give heat energy to the cold seawater coming from the pump. However, the high salt concentration damages the distillation membrane and reduces the distilled water flow. Therefore, the saltwater leaves the membrane, and cannot returns to the process of distillation (in membrane). Furthermore, from this water we recover the remaining heat via an additional heat exchanger. Thus, the brine that contains the high salt concentration is completely dispensed with this AGMD process as shown in (Figure III.7).

In addition, the salt rejection in the membrane distillation process remains high in all cases. An experimental study was conducted to evaluate the performance of the membrane distillation in the work's Noor et al [36]. High saline water feed of up to 200 g/L NaCl was used in this study at various operating conditions by changing the feed temperature and feed concentration. The results estimated showed excellent conformity with the experimental results. The salt rejection remained high in all cases.

III. 5. 2. The solar AGMD system in the TRNSYS simulation

The model of solar thermal membrane distillation system with AGMD and the photovoltaic system is developed using TRNSYS software, which is a quasi-steady-state

simulation program. TRNSYS enables system components represented as preformats to be selected and interconnected in any desired manner to construct a system's model. To facilitate the selection of the system components, it is important to develop an information flow diagram. The information flow diagram for the models is shown in (Figure III.9). The main component of the model is the AGMD unit, which is represented by a new equation in TRNSYS. Additional components to the model include TYPE109-TM2 reading and processing of meteorological data, Type 91 heat exchanger, Type 1 flat plate collector, Type 2 differential temperature controller, Type 3 single speed pump, Type 94 photovoltaic panels, Type 47 storage battery, Type 48 inverter, Type 14 forcing functions, Type 57 unit conversion and Type 65 online plotter. Tables (III.1) and (III.2) show the values of parameters used in the TRNSYS model.

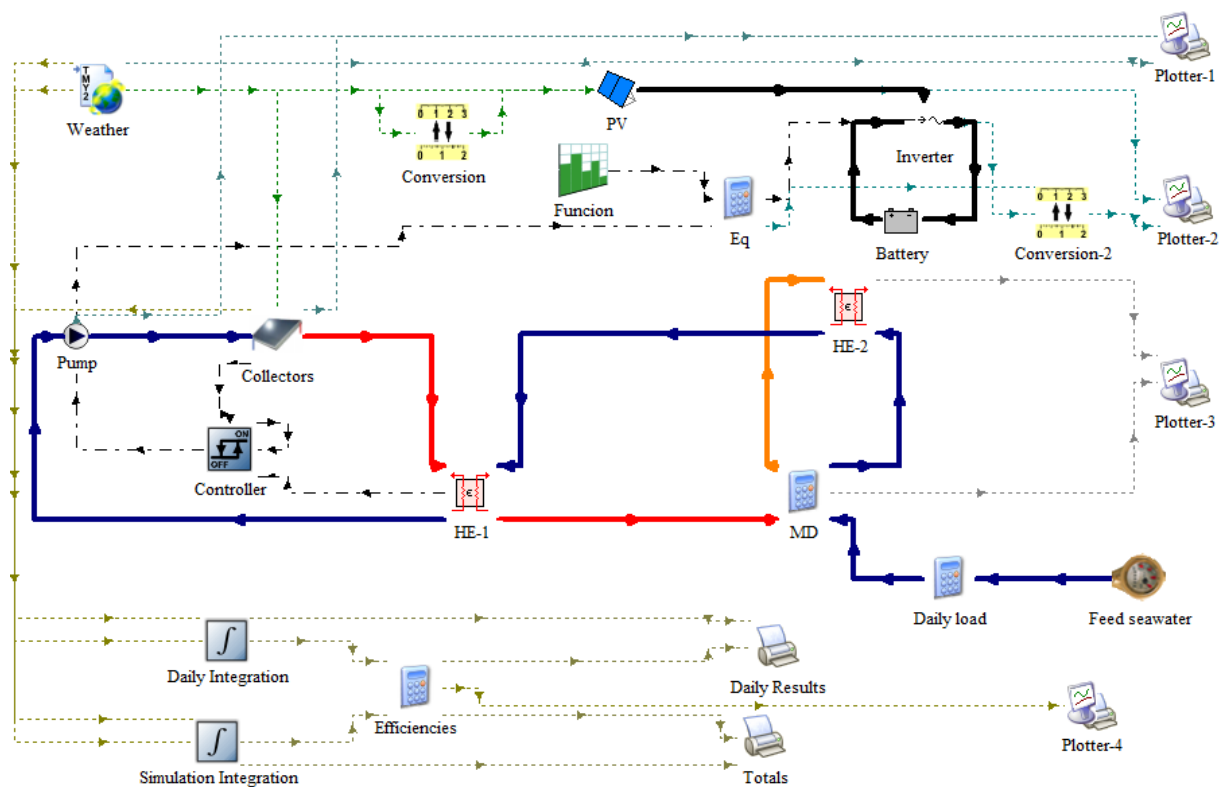


Figure III.9: Diagram of the solar AGMD system in the TRNSYS program.

- In addition, in this study with these equations, a TRNSYS program is used to predict the long-term performance of the solar water heating system for the AGMD process. A complete test rig to evaluate the performance of membrane distillation module is driven by solar energy using the flat plate collectors in Ain-Temouchent weather, Algeria. Where Ain-Temouchent is near the north coast of Algeria affected by the Mediterranean Sea.

III. 6. Conclusion

In this chapter, the AGMD systems have been studied, controlled and optimized. In the first case, a dynamic simulation of the membrane distillation module integrated solar thermal system has been reported along with validation of the system model by comparing it with the experimental data obtained from a pilot-scale setup located in UAE [30]. The solar AGMD system was studied and controlled for product a constant distilled water flow on different days throughout the year using TRNSYS program. Therefore, the AGMD system with a controlled distilled water flow can make this contemporary model usable and suitable to be a system compatible in the future with all intermittent climatic conditions and all over the world.

A TRNSYS model develops solar water heating systems using flat plate collectors with an area of 12.75 m², heat exchanger, storage tanks, the auxiliary heater, and the photovoltaic panels; each one has an area of 1.6 m² with the energy storage batteries (12V, 100Ah).

In the second case, optimized parametric conditions were used to operate the solar thermal driven membrane distillation system in Ain-Temouchent City, Algeria. Accordingly, the purpose of this study is the use of solar panels in the photovoltaic system with the energy storage batteries (12V, 100Ah) to produce all necessary electrical energy. Therefore, this optimal AGMD system using solar energy for seawater desalination will be useful for further simulations or applications of the technology.

Remarque:

Chapter III includes our Articles:

- **A. Marni Sandid, D. Nehari, A. Elmeriah, A. Remlaoui.** Dynamic simulation of an air-gap membrane distillation (AGMD) process using photovoltaic panels system and flat plate collectors. **Journal of Thermal Engineering** 7 (2021) 117-133
DOI: 10.18186/thermal.870383
- **A. Marni Sandid, T. Nehari, D. Nehari.** Simulation study of an air-gap membrane distillation system for seawater desalination using solar energy. **Desalination and Water Treatment** 229 (2021) 40-51
DOI: 10.5004/dwt.2021.27394

References

- [1] Alkhudhiri A, Darwish N, Hilal N. Membrane distillation: A comprehensive review. *Journal of Desalination* 2012;287:2-18. doi: 10.1016/j.desal.2011.08.027
- [2] Amir G, Nasim H, Alireza N, Parisa H. Exergy Based Optimization of a Biomass and Solar Fuelled CCHP Hybrid Seawater Desalination Plant. *Journal of Thermal Engineering* 2017;3:1034-1043. doi: 10.18186/thermal.290251
- [3] Hadi G, Ghader A. Performance Analysis and Thermodynamic Modeling of a Poly Generation System by Integrating a Multi-Effect-Desalination Thermo-Vapor Compression (MED-TVC) System with a Combined Cooling, Heating and Power (CCHP) System. *Journal of Thermal Engineering* 2018;4:1963-1983. <https://doi.org/10.18186/journal-of-thermal-engineering.410264>
- [4] Omid M, Ali K, Chaiwat J, Phubate T, Somchai W, Raviwat S. Solar Distillation Practice For Water Desalination Systems. *Journal of Thermal Engineering* 2015;1:287-288. doi: 10.18186/jte.93924
- [5] Phattaranawik J, Jiratananon R, Fane A. Heat transport and membrane distillation coefficients in direct contact membrane distillation. *Journal of Membrane Science* 2003;212:177-193. doi: 10.1016/S0376-7388(02)00498-2
- [6] Teoh M, Chung T. Membrane distillation with hydrophobic macrovoid-free PVDF-PTFE hollow fiber membranes. *Separation and Purification Technology* 2009;66:229-236. doi:10.1016/j.seppur.2009.01.005
- [7] Verma SK, Singhal P, Chauhan DS. A synergistic evaluation on application of solar-thermal energy in water purification: Current scenario and future prospects. *Journal of Energy Conversion and Management* 2019;180:372-390. doi:10.1016/j.enconman.2018.10.090
- [8] Mohamed K, Takeshi M. *Book of Membrane Distillation* 2011;1:1-16. doi:10.1016/b978-0-444 53126-1.10001-6
- [9] Ruh U, Majeda K, Richard JE, James TM, Mohammad A, Mohamed G, Vahedi TH. Energy efficiency of direct contact membrane distillation. *Journal of Desalination* 2018;433:56–67. doi: 10.1016/j.desal.2018.01.025
- [10] Qtaishata M, Matsuura T, Kruczek B, Khayet M. Heat and mass transfer analysis in direct contact membrane distillation. *Journal of Desalination* 2008;219:272–292 doi:10.1016/j.desal.2007.05.019
- [11] Hassler G L. U.S. patent US3129146A (14 April 1964).
- [12] Weyl P K. U.S. patent US3340186A (5 September 1967).
- [13] Jonsson AS, Wimmerstedt R, Harrysson AC. Membrane Distillation—A Theoretical Study of Evaporation Through Microporous Membranes. *Journal of Desalination* 1985;56:237. doi:10.1016/0011-9164(85)85028-1
- [14] Gostoli C, Sarti GC, Matulli S. Low Temperature Distillation Through Hydrophobic Membranes. *Journal of Separation and Purification Technology* 1987;22: 855. doi:10.1080/01496398708068986
- [15] Banat FA, Al-Rub FA, Jumah R, Shannag M. Theoretical investigation of membrane distillation role in breaking the formic acid-water azeotropic point: Comparison between

Fickian and Stefan-Maxwell-based models. *International Communications in Heat and Mass Transfer* 1999;26:879–888. doi:10.1016/s0735-1933(99)00076-7

[16] Hanemaaijer JH, Van MJ, Jansen AE, Dotremont C, Sonsbeek E, Yuan T, De RL. Memstill membrane distillation – a future desalination technology. *Journal of Desalination* 2006;199:175–176. doi:10.1016/j.desal.2006.03.163

[17] Vandita TS, Thombre S. Air gap membrane distillation: A review. *Journal of Renewable and Sustainable Energy* 2019;11:45-90. doi: 10.1063/1.5063766

[18] Duong HC, Cooper P, Nelemans B, Cath TY, Nghiem LD. Evaluating energy consumption of air gap membrane distillation for seawater desalination at pilot scale level. *Journal of Separation and Purification Technology* 2016;166:55. doi:10.1016/j.seppur.2016.04.014

[19] Minier-Matar J, Hussain A, Janson A, Benyahia F, Adham S. Field evaluation of membrane distillation technologies for desalination of highly saline brines. *Journal of Desalination* 2014 ;351:101–108. doi:10.1016/j.desal.2014.07.027

[20] Schwantes R, Cipollina A, Gross F, Koschikowski J, Pfeifle D, Rolletschek M, Subiela V. Membrane distillation: Solar and waste heat driven demonstration plants for desalination. *Journal of Desalination* 2013;323:93–106. doi:10.1016/j.desal.2013.04.011

[21] Alsaadi AS, Ghaffour N, Li JD, Gray S, Francis L, Maab H, Amy GL. Modeling of air-gap membrane distillation process: A theoretical and experimental study. *Journal of Membrane Science* 2013;445:53–65. doi:10.1016/j.memsci.2013.05.049

[22] Swaminathana J, Chunga HW, Warsingera DM, AlMarzooqib FA, Arafatb HA. Energy efficiency of permeate gap and novel conductive gap membrane distillation. *Journal of Membrane Science* 2016;502:171–178. doi:10.1016/j.memsci.2015.12.017

[23] Alklaibi AM, Lior N. Membrane-distillation desalination: Status and potential. *Journal of Desalination* 2005;171:111–131. doi:10.1016/j.desal.2004.03.024

[24] Camacho L, Dumée L, Zhang J, Li J-d, Duke M, Gomez J, Gray S. Advances in Membrane Distillation for Water Desalination and Purification Applications. *Journal of Water* 2013;5(1):94–196. doi:10.3390/w5010094

[25] Chafidz A, Esa DK, Irfan W, Yasir K, Abdelhamid A, Saeed MA. Design and fabrication of a portable and hybrid solar-powered membrane distillation system. *Journal of Cleaner Production* 2016;133:631–647. doi:10.1016/j.jclepro.2016.05.127

[26] Kullab A, Chuanfeng L, Andrew R. Martin. Solar desalination using membrane distillation: Technical evaluation case study, In *Solar World Congress 2005: Bringing Water to the World, Including 34th ASES Annual Conference and 30th National Passive Solar Conference*; Orlando, FL, United States 2005; 2732-2737.

[27] Banat B, Fawzi A, Jana S. Theoretical and experimental study in membrane distillation. *J of Desalination* 1994;95(1):39–52. doi:10.1016/0011-9164(94)00005-0

[28] Khan EU, Martin AR. Water purification of arsenic-contaminated drinking water via air gap membrane distillation (AGMD). *Journal of Periodica Polytechnica Mechanical Engineering* 2014;58(1):47–53. doi:10.3311/ppme.7422

[29] He Q, Li P, Geng H, Zhang C, Wang J, Chang H. Modeling and optimization of air gap membrane distillation system for desalination. *Journal of Desalination* 2014;354:68–75. doi:10.1016/j.desal.2014.09.022

- [30] Uday KN, Martin A. Experimental modeling of an air-gap membrane distillation module and simulation of a solar thermal integrated system for water purification. *Journal of Desalination and Water Treatment* 2017;84:123-134. DOI:10.5004/dwt.2017.21201
- [31] Asim M, Uday KN, Martin A. Feasibility analysis of solar combi-system for simultaneous production of pure drinking water via membrane distillation and domestic hot water for single-family villa: pilot plant setup in Dubai. *Journal of Desalination and Water Treatment* 2015;57(46):21674–21684. doi:10.1080/19443994.2015.1125806
- [32] Klein, S.A. et al. 2006. TRNSYS 16: A Transient System Simulation Program, SEL, University of Wisconsin, Madison USA
- [33] Matthew J. Duffy, Marion Hiller, David E. Bradley, Werner Keilholz, Jeff W. Thornton. TRNSYS – features and functionality for building simulation. Eleventh International IBPSA Conference Glasgow, Scotland July 27-30, 2009
- [34] Marc, A., Journée Thématique SFT, présentation TRNSYS. 2005
- [35] J. Koschikowski, M. Wieghaus and M. Rommel Solar thermal-driven desalination plants based on membrane distillation, *Desal.*, 156 (2003) 295–304.
- [36] A.M.A. Noor, S.S. Ibrahim, Q.F. Alsahy and A. Figoli, Highly Saline Water Desalination Using Direct Contact Membrane Distillation (DCMD): Experimental and Simulation Study, *Water.*, 12 (2020) 15–75.
- [37] A. Remlaoui, D. Nehari, M. Laissaoui, A. Marni Sandid, Performance evaluation of a solar thermal and photovoltaic hybrid system powering a direct contact membrane distillation: TRNSYS simulation, *Desal. Water Treat.*, 194 (2020) 37–51.
- [38] N.T. Uday Kumar and A. Martin, Techno-economic optimization of solar thermal integrated membrane distillation for co-generation of heat and pure water, *Desal. Water Treat.*, 98 (2017) 16–30.
- [39] TRNSYS, Transient System Simulation, Univ. of Wisconsin Madison, WI: Solar Energy Laboratory, 2017;2:1–129.
- [40] Mahmoud MM, Ibrik IH. Techno-economic feasibility of energy supply of remote villages in palestine by PV-systems, diesel generators and electric grid. *Journal of Renewable and Sustainable Energy Reviews* 2006;10:128-138. doi:10.1016/j.rser.2004.09.001
- [41] Stuart RW, Martin AG, Muriel EW, Richard C. *Applied photovoltaics* second edition first published by earth scan in the UK and USA in 2007 copyright © 2007;arc, ISBN-10:1-84407-401-3
- [42] Nutakki Tirumala Uday Kumar and Andrew R. Martin. Co-Production Performance Evaluation of a Novel Solar Combi System for Simultaneous Pure Water and Hot Water Supply in Urban Households of UAE. *Energies*. April 2017 DOI: 10.3390/en10040481
- [43] N. Abdullah AlShemmary, Laith M. Kadhom, Wajeesh Judi Al-Fahham. Information Technology and Stand-alone Solar Systems in Tertiary Institutions. *Energy Procedia* 36 (2013) 369 – 379



CHAPTER IV:

Experimental, simulation and economical study of the
solar AGMD system large scale

A. MARNI SANDID

DOCTORAL THESIS

2023



IV. Introduction

Due to the rapid demand for high-quality water resources, more than one billion people worldwide cannot use drinking water that meets safety standards [1]. Solar thermal collectors can be used to run membrane distillation (MD), as collectors exhibit high efficiency and good performance at feed temperatures varying from 60 °C to 90 °C. Sample measurements for clear and cloudy days indicate a high productivity of 11.2 L/m².day for a total solar energy of 7.25 kWh/m² day [2].

The MD process in a previous study yielded a salt rejection percentage of about 99.5%, process efficiency of approximately 90%, and solar collector efficiency of about 50% [3]. Solar-powered MD system that uses a parabolic solar concentrator with a capacity of 0.5–50 m³/ day was developed [4]. Constructed pilot plant consists of three commercial MD modules coupled with a static solar collector field and tested the MD systems [5]. The operating temperature of the MD process is 50 °C – 80 °C, which is the temperature at which solar collectors exhibit high efficiency. In addition, such membranes withstand fouling and scaling better than reverse osmosis membranes. Intermittent operation does not damage the membrane module, and no damage occurs if such membranes dry out.

The Swedish company Scarab Development AB has built and produced MD modules. Each module has a flat sheet air gap membrane distillation (AGMD) system with a membrane surface area of 2.8 m². The maximum variation in distillate flux is around 7 L/h m². The modules showed a maximum specific distillate flux of 6.5 L/h m² (65 °C as delta T, 1 g/L salt solution as a feed), productivity decay of around 14% with increasing salinity (from 1 g/L to 35 g/L). A linear flux increases with the delta T across the membrane, with only a slight dependence on the hot-side absolute temperature. However, the specific fluxes and the influence of salt concentration on performance and thermal efficiency are considerably worse than those from laboratory-scale experiments in the literature.

Although the MD technology of Scarab AB is suitable for coupling with solar energy, its thermal efficiency and salt rejection are key factors to be improved to enable the application of this technology to seawater desalination. It was reported that a small device with a 7.2 m² spiral-wound direct contact membrane distillation (DCMD) module and a 22.6 m² flat plate solar thermal collector generates over 140 kg of distillates per day under real weather conditions [6]. This finding is comparable to a regular rate of distillate output of 19.7 kg/m² of membranes or 6.3 kg/m² of solar thermal collectors. The overall thermal efficiency of the system varies from 0 (early morning and late afternoon) to about 0.5 (peak solar radiation). The results showed that DCMD operation under concurrent and countercurrent flow results in two

distinctive profiles in water flux, temperature polarization effect, and thermal efficiency along the channel length. A modern solar thermal polygeneration (STP) system for the development of cooling, healthy water, and hot domestic water for the United Arab Emirates (UAE) was developed and evaluated [7].

Three separate solar collectors were evaluated for STP performance: flat plate collectors (FPCs), evacuated tube collectors (ETCs), and parabolic compound collectors (CPCs). The device was designed and dynamically simulated using TRNSYS. Economic analyses were conducted for all three collector configurations with an inflation rate of 10% and reduction of 5%. The lowest payback period was 6.75 years, and it was achieved by the STP with an ETC field with a gross area of 216 m². The STP system offers cumulative savings of USD 520,000. Economic and environmental benefits are provided by the steady system performance of the absorption chiller (35 kW), membrane distiller (80 L/day), and heat recovery system (1.2 m³/h) throughout the year. In terms of global warming potential, 109 tons of carbon dioxide (CO₂) emission will be avoided every year.

The use of solar energy in small- and medium-capacity thermal desalination systems with low maintenance requirements in terms of the projected cost of water supply was studied [8]. The findings revealed that the costs associated with the solar supply are highly dependent on the actual utilization of thermal energy by the desalination system at different locations. Therefore, the system was simulated (and dimensioned) for a specific distillate production of 1 m³/day at operation temperatures between 70 °C and 95 °C. The cost reduction of thermal energy storage (TES) highly depends on the cost of the system (EUR 100/m³ used from a range of EUR 50/m³ to EUR 200/m³). However, for financial constraints presented (solar field costs of EUR 150/m³ and TES costs of EUR 100/m³) in Abu Dhabi (UAE), Almeria (SP), and Cairo (EGY), the cost reduction of using TES is less significant. Laboratory experiments in remote areas of solar-powered stand-alone MD systems were conducted [9]. In addition, the Fraunhofer Institute for Solar Energy Systems designed a solar thermal MD system with a capacity range of 100–500 L/day and larger systems with a capacity up to 10 m³/day. Simulation computations were conducted for the system design and the development of an adapted control strategy for two different pilot plants. The design capacity for the Aqaba system was up to 1000 L/day in December, and that for the Gran Canaria system was up to 1600 L/day in February. Long-term performance tests in different countries demonstrated that a durable operation is possible even with very low maintenance.

To optimize flow by adjusting the flow rate, mean temperature, and initial salt concentrations, DCMD and response surface methodology (RSM) models were applied [10]. Model predictions on four different membranes were evaluated in comparison with

experimental results obtained using the R^2 coefficient of determination. The AGMD method used in desalination was developed and optimized [11]. Regression models were developed to estimate the output index and the basic performance index; these models consider energy use as a function of different variables. For the performance index, the optimal solution was a cooling inlet temperature of 13.9 °C, a feed inlet temperature of 59 °C, and a feed flow rate of 205 L/h. A maximum specific performance index of 188.703 kg/kWh was obtained experimentally under these AGMD operating conditions. This index value corresponds to a specific energy consumption of 5.3 kWh/m³.

Air gap membrane distillation module was evaluated to ascertain the effect of process parameters on distillate flux and thermal efficiency and to achieve a distillate flow rate of 1.5–3 kg/h [12]. Factorial design was conducted for the experiments. In addition, success metrics and response surface regression (RSM) were used to develop an analytical regression model for the operational parameters of the AGMD framework. They were tested via variance analysis, and the RSM methodology model was analyzed using ANOVA.

Regression analysis demonstrated compliance with the experimental knowledge fitted with a second-order polynomial model with coefficient of determination (R^2) values of 0.996 and 0.941 for distillate flux and specific performance ratio, respectively. For a desired distillate flux of 15 kg/h m², the difference between the hot- and cold-side temperatures of MD has to be between 40 °C and 45 °C, and the flow rate needs to be adjusted from 6 L/min to 7 L/min, depending on the season of operation. In addition, the assessed in accordance with the software TRNSYS. The dynamic transient device simulation (TRNSYS) method was reported to model large cassette MD modules to assess the co-production performance of a novel solar AGMD system that was designed for the simultaneous delivery of pure water and hot water to urban households in the UAE [13]. A solar combined membrane distillation (SCMD) system was experimentally tested for the simultaneous production 20 L/day of pure water and 250 L/day of hot water for a single household without any auxiliary heating device. Distillate productivity was decreased by only 6%, and there was a twofold increase in the domestic hot water in the SCMD system.

Testing of commercial scale was performed to study the efficiency of two multichannel spiral-wound AGMD systems for water desalination [14]. The only difference between the two systems was the membrane surface area (7.2 and 24 m²) and thus the channel length (from 1.5 m to 5 m, respectively). The results showed that 3.72 m was the optimum channel length needed to simultaneously maximize productivity and thermal efficiency; it produced a permeate flux of 2.44 L/h m² and specific thermal energy consumption (STEC) of 141.5 kWh/m³. However, the optimum values of the three main operating parameters that maximize the flux

heat efficiency (80 °C evaporator inlet temperature, 20 °C condenser inlet temperature, and 560.6 L/h feed flow rate) can decrease productivity. Experiments were conducted on full-scale MD modules spiral-wound with a 5–14 m² membrane area [15].

Flat plate collectors (FPCs) and a spiral-wound MD module were tested. All results showed a strong influence of the feed flow rate on the module performance due to the changing bulk temperature difference and hydrodynamics. The distillate flux rate was in the range of 10 to 25 kg/h with a specific energy consumption of 130–207 kWh/m³. However, the distillate output rate decreased with salt by approximately 1 kg/h of distillate per 10 g/kg of feed water salinity. Solar thermal-driven desalination plant was developed using FPCs and a spiral-wound MD module [16]. It was aimed to develop systems with a capacity ranging from 0.2 m³/day to 20 m³/day. The simulation results showed that a simple compact system with a collector area less than 6 m² and without heat storage can distill 120–160 L of water during a summer day in Freiburg, Germany. Technical simplicity, long maintenance-free operation, and high-quality potable water output are important aims that will enable the successful application of such systems.

The main objective of this work is to develop, analyze and optimize solar energy driven AGMD systems, thereby helping ensure the availability of distillate water using solar desalination. In this work, a complete test rig was installed in Port Said city, Egypt to evaluate the performance of MD module driven by solar energy using the FPC and ETC heating source. Data using the TRNSYS program has been conducted under different weather conditions throughout the year.

A closer look to the literature on AGMD system powered by solar energy, however, reveals a number of gaps and shortcomings. The main contributions of current research are as follows:

- To optimize solar-powered AGMD systems and data validation.
- To evaluate the performance of MD module driven by solar energy using the FPC and ETC heating source.
- To compare different solar energy systems integrating a multichannel spiral-wound AGMD module. To our knowledge, no prior studies have discussed the influence of several solar energy systems on AGMD performance under different weather conditions.
- To develop a technique that covers a wide range of capacities (from 0.13 L/h to 18 L/h); thus, systems can be adapted to any particular demand.
- To evaluate the benefits of the system considering the different weather conditions, and the related energy markets.

- To develop a new solar-powered AGMD configuration for higher Gain Output Ratio (GOR) and lower Specific Thermal Energy Consumption (STEC) comparing to conventional methods.

IV. 1. Methods

Description of AGMD desalination pilot plant including its capacity and units will be discussed in detail. Solar heating system including the main specifications of FPCs and ETCs are demonstrated and discussed showing the flow chart of the considered system. Changing year-round climate conditions including temperature and wind speed will be discussed in detail.

IV. 1. 1. Multi-channel spiral wound AGMD system

Air gap membrane distillation desalination pilot plant was designed, commissioned, and installed in Port Said City, Egypt (31°20'N 32°22'E). A schematic diagram of the test model and the experimental setup is shown in (Figure IV.1). Three main loops are built, namely, feed solution, heat, and cooling source loops. The permeate is collected in the distillate tank. An Aquastill multi-envelope spiral wound AGMD membrane module is used (one AGMD module with an area of 14.4 m² (Figure IV.2). The main specifications are given in Tables (IV.1) and (IV.2). In (Figure IV.2), there are two types of jackets. High-temperature water feed channels and the coolant channels. Both sides of the cooling channel function as a condenser tray, while an air space with a spacer lies between each coolant and hot water feed channel; here, the distilled water is collected at the distillate level and expelled from the module. The six membrane envelopes are spiral-wound into a cylindrical shape. The hot water feed and coolant flows are countercurrent. The hot water is supplied from the middle of the module and leaves the device, whereas the coolant flow moves in the opposite direction. Salt concentration in the sea water is 35000 ppm. Saline feed water flows from a feed pump through a filter and then into a flat plate heat exchanger. Then, it is divided into the AGMD modules using management valve systems and flow meters. Pressure sensors are used to determine whether the feed water pressure is less than the maximum allowable membrane pressure.



Figure IV.1: The experimental pilot plant.

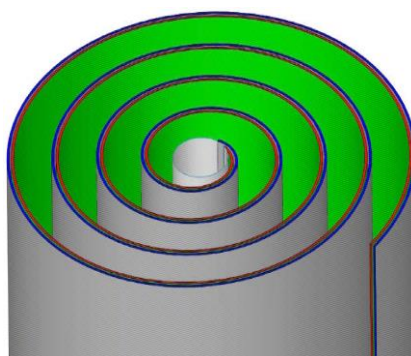


Figure IV.2: Cross section of AGMD module.

Table IV.1: AGMD module properties and specifications.

Material	Polyethylene (PE)
Total net Membrane surface area	14.4 m ²
Diameter	0.4 m
Height (width of envelope)	0.4 m
Length of envelope	3 m
Thickness of flow channel	2 mm
Air gap thickness	1 mm
Porosity of membrane sheet	85%
Tortuosity of membrane sheet	1.56
Membrane thermal conductivity	1.35 W/m K
Thickness of membrane sheet	76 micrometer
Mean pore size diameter	0.3 micrometer
Packing density	115 m ² /m ³
No. of evaporator (hot feed) channels	6
No. of condenser (coolant) channels	6
No. of distillate channels	12

Table IV.2: The spacer characteristics.

Channel thickness	2.01 mm
Spacer filament thickness	1.005 mm
Spacer angle Φ (0-90)	60 grd
length filament	4.17m

IV. 1. 2. Description of solar heating system

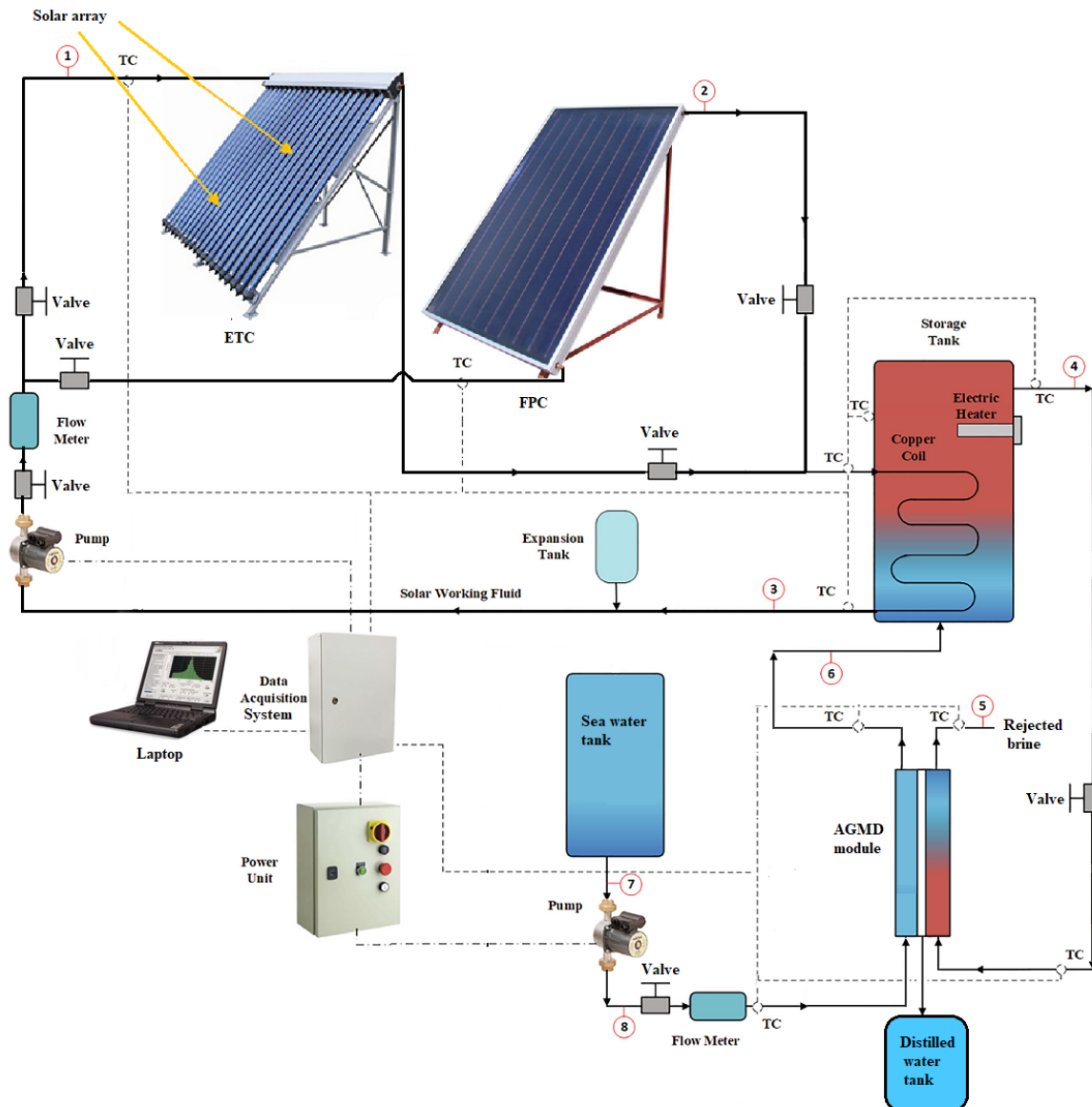
The pressurized water is heated by solar energy in the solar collector system. Then, it flows through six FPCs with total area 12 m² (6×2 m²) in the series arrangement, or through three ETCs with an area of 8 m². The main specifications of FPCs and ETCs are given in Tables 3 and 4, respectively. The water then passes through the heat exchangers to exchange the heat between the solar system and the AGMD unit. A pump is used to circulate the water in the system, as shown in (Figure IV.3).

Table IV.3: FPC specifications.

Absorber area [m ²]	2.10
Aperture area [m ²]	2.16
Dimensions [mm]	1892 x 1204 x 99
Gross area [m ²]	2.28
Maximum operating pressure [bar]	9
Stagnation temperature [°C]	189
Thermal capacity [KJ/(m ² K ²)]	10330
Incidence angle [°]	50
Instantaneous efficiency based on aperture area	0.713
Peak power [W]	1540

Table IV.4: ETC specifications.

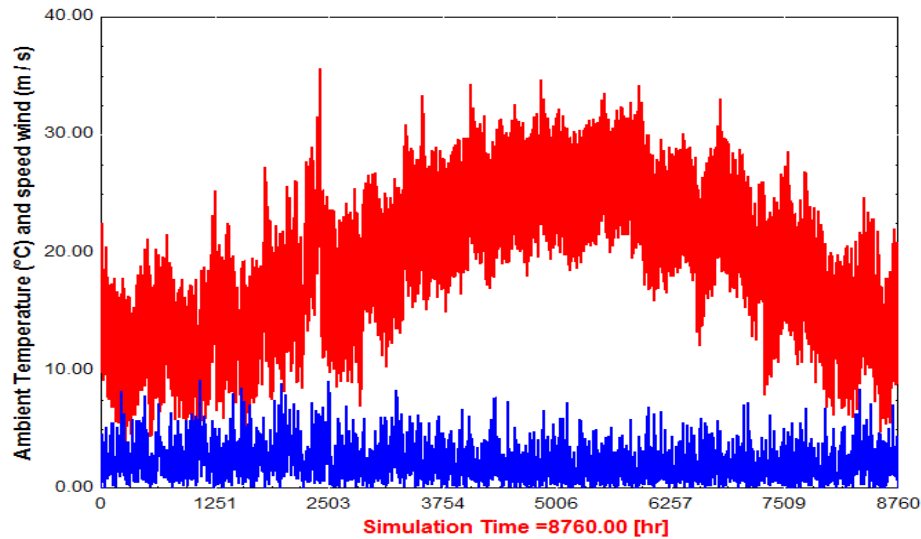
Number of evacuated tubes	30
Grid measurement (length, height) [mm]	2110×1960
Aperture area [m ²]	2.84
Efficient solar absorption area [m ²]	2.44
Capacity of fluid in copper pipe [liter]	1.82
Max working pressure [bar]	6

**Figure IV.3:** Schematic of the solar system and the flow diagram.

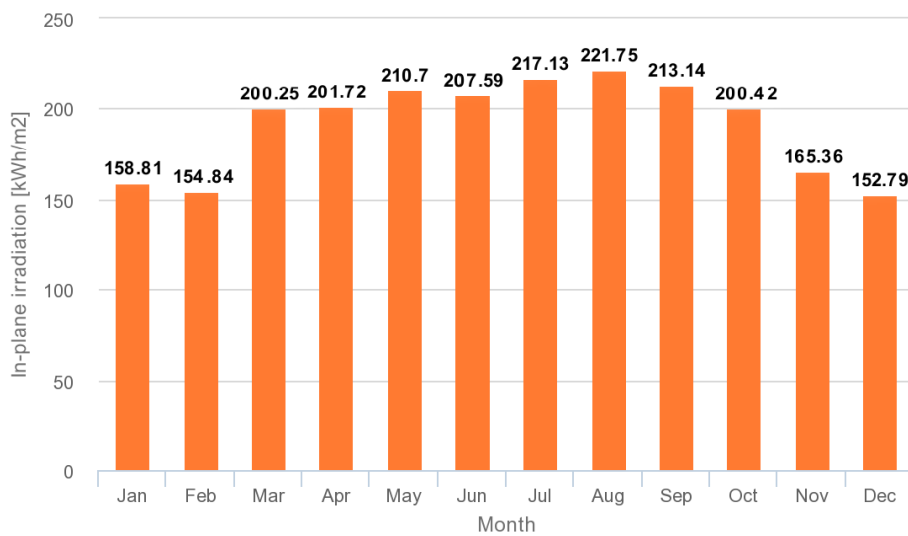
IV. 1. 3. Weather data

Figure IV.4 shows changing year-round climate conditions. In Port-Said City, Egypt, the weather is generally pleasant, warm, and moderate. We note a change in temperature during the year, which reaches up to 35.55 degrees Celsius in August, and we find that the wind speed is mild and does not exceed 9.13 m / s. For the irradiation, it varies during the months of the year and reaches up to 221.75 kWh / m² in August as shown in (Figure IV.4), since in this period of

the year the temperature is high. The experiment was performed at Port-Said Weather on 29 June. Therefore, the research simulates for a whole year and the results will occur on various days (sunny and cold) in summer and winter.



(a)



(b)

Figure IV.4: (a) Ambient air temperature, wind speed and (b) Monthly irradiation.

IV. 2. Simulation

A solar combined membrane distillation (SCMD) system was experimentally tested. Modeling of air gap membrane distillation and solar membrane distillation system were carried out.

IV. 2. 1. Modeling of AGMD module

An AGMD model is performed using Minitab and experimental data. The results from Minitab are used later to create a component in TRNSYS that behaves as an AGMD in a simplified and approximate way. The experiment is installed in Port Said University, Egypt. Therefore, the experimental data shown in (Table IV.5) is tested and analyzed with Minitab software, and a multiple regression model is obtained. Four variables are considered as independent variables: hot inlet temperature T_{hi} , cold inlet temperature T_{ci} , hot feed flowrate V_h (L/h) and cold feed flowrate V_c (L/h). The dependent variables are the permeate flow J (kg/h), hot outlet temperature T_{ho} and cold outlet temperature T_{co} .

Table IV.5: Permeate fluxes from different feed and cooling water temperatures at different flow rates.

No. of exp.	T_{ci} (°C)	T_{hi} (°C)	V_h L/h	V_c L/h	T_{co} (°C)		T_{ho} (°C)		J (kg/h)	
					Model	Deviation %	Model	Deviation %	Model	Deviation %
1	34,76	45,10	600	600	43,68	0,4	36,91	1,4	3,04	3,3
2	34,79	50,77	600	600	48,57	0,6	37,78	0,2	7,23	3,2
3	35,11	54,44	600	600	51,74	0,1	38,74	0,2	9,91	2,9
4	34,94	59,73	600	600	56,28	0,0	39,29	0,2	13,83	1,2
5	34,66	64,81	600	600	60,70	0,2	39,67	0,4	18,01	1,9
6	34,76	46,38	360	360	45,11	0,4	36,92	0,5	2,38	2,6
7	34,50	51,64	360	360	49,75	0,7	37,09	0,1	4,75	1,9
8	34,55	54,93	360	360	52,68	0,2	37,48	0,6	6,17	4,6
9	34,60	59,55	360	360	56,80	0,2	38,00	1,3	8,17	1,9
10	34,73	64,23	360	360	60,94	0,6	38,62	0,3	10,17	2,6
11	34,60	45,77	180	180	45,44	0,1	36,53	0,2	0,33	4,3
12	34,26	50,26	180	180	49,48	0,2	36,37	0,0	1,41	1,4
13	34,36	55,17	180	180	53,98	0,0	36,80	0,5	2,39	0,7
14	34,42	60,12	180	180	58,50	0,2	37,18	0,6	3,40	3,8
15	34,57	64,96	180	180	62,88	0,4	37,67	0,1	4,35	4,1
16	34,68	50,11	120	120	49,85	0,1	36,81	0,5	0,13	4,7
17	34,54	55,31	120	120	54,60	0,2	36,88	0,7	0,87	2,8
18	35,20	60,17	120	120	58,98	0,1	37,98	0,7	1,41	3,9
19	35,14	64,71	120	120	63,08	0,3	38,12	0,2	2,01	4,0
20	29,28	80,00	210	180	79,40	0,1	31,70	2,5	15,33	1,4
21	30,02	72,00	210	180	70,95	0,1	31,70	2,2	10,86	0,8
22	30,23	55,00	210	180	53,85	0,1	31,41	0,7	6,02	3,9

The minimum and maximum values of the model are:

Table IV.6: Range of data.

Data	T_{hi} (°C)	T_{ci} (°C)	J (L/h)
Min	40	30	0.13
Max	80	35	18.01

The relationship between J and Thi is usually exponential [17], but as can be seen in literature [12], in the range of 50-80 °C of Thi it is mainly linear. The model created in Minitab fitted the data into a quadratic equation with the general form. The regression quadratic model with coded parameters can be expressed as [18]:

$$J = \alpha_0 + \alpha_1 T_{hi} + \alpha_2 T_{ci} + \alpha_3 V_c + \alpha_4 V_h + \alpha_{12} T_{hi} T_{ci} + \alpha_{13} T_{hi} V_c + \alpha_{14} T_{hi} V_h + \alpha_{23} T_{ci} V_c + \alpha_{24} T_{ci} V_h + \alpha_{34} T_{ci} V_h + \alpha_{34} V_h V_c + \alpha_{11} T_{hi}^2 + \alpha_{22} T_{ci}^2 + \alpha_{33} V_c^2 + \alpha_{44} V_h^2 \quad (1)$$

α_0 : is the starting point for the central composite design of orthogonal type with four variables.

Minitab optimized the equation to the best fit; removing terms that do not help to explain additional variation in permeate flow J .

The final regression equations for J , T_{cout} and T_{Hout} are determined in terms of actual operating parameters as follows:

Table IV.7: Operational conditions of tested AGMD module.

Operational parameter	Specification
Feed flow rate, L/min	2, 6 and 10
Hot water operation temperature, °C	40–80
Coldwater operation temperature, °C	30–35
Salinity of hot flow, g/kg	40–60
Salinity of cold flow, g/kg	35

These relationships work for the data range shown in Table 8. The R-squared is high and close to one in each case, and the p-value of each variable in the model is statistically significant (lower than 0.05). Even though 99.74, 97.16 and 99.97 % of the variation in J , $Thout$, $Tcout$ can be explained by the regression model respectively. Therefore, the model can be explained more than 97.16% of the data and the p-value is lower than 0.01. The results are as follows:

Table IV.8: Minitab results summary.

Equations	R2	p-value	Independent variable that contributes the most
$J = 377.35 - 0.1874 * V_h + 0.1452 * V_c - 21.56 * T_{ci} - 0.0178 * T_{hi} + 0.00001 * V_c * V_c + 0.3068 * T_{ci} * T_{ci} + 0.001262 * V_h * T_{hi}$	99.74 %	0.008	Tci, Thi, Vh and Vc
$T_{ho} = -9.69 - 0.0087 * V_c + 1.3005 * T_{ci} + 0.0243 * T_{hi} + 0.000204 * V_c * T_{hi}$	97.16 %	0.003	Tci, Thi and Vc
$T_{co} = -37.5 + 0.0069 * V_h - 0.0122 * V_c + 1.215 * T_{ci} + 1.6879 * T_{hi} + 0.000009 * V_c * V_c - 0.000101 * V_h * T_{hi} - 0.02201 * T_{ci} * T_{hi}$	99.97 %	0.004	Tci, Thi, Vh and Vc

The basic method of measuring collector performance is to expose the operating collector to solar radiation and measure the fluid inlet and outlet temperatures and the fluid flow rate. The useful gain is [19]:

$$\dot{Q}_u = m_0 C_{pf} (T_0 - T_i) \quad (2)$$

m_0 is the solar fluid mass flow rate ($\text{kg} \cdot \text{hr}^{-1}$), C_{pf} is the specific heat capacity of solar fluid ($\text{KJ} \cdot \text{hr}^{-1}$), T_0 and T_i are the inlet and outlet temperature of the solar fluid (K).

Heat exchanger counter flow effectiveness is [17]:

$$\varepsilon = \frac{1 - \exp\left(-\frac{UA}{C_{min}}\left(1 - \frac{C_{min}}{C_{max}}\right)\right)}{1 - \left(\frac{C_{min}}{C_{max}}\right) \exp\left(-\frac{UA}{C_{min}}\left(1 - \frac{C_{min}}{C_{max}}\right)\right)} \quad (3)$$

UA is the overall loss coefficient between the heater and its surroundings during operation ($\text{kg} \cdot \text{hr}^{-1}$), C_{max} is the maximum capacity rate ($\text{KJ} \cdot \text{hr}^{-1} \cdot \text{K}$), C_{min} is the minimum capacity rate ($\text{KJ} \cdot \text{hr}^{-1} \cdot \text{K}$).

Required heating rate including efficiency effects in the auxiliary heaters is [17]:

$$Q_{aux} = Q_{loss} + Q_{fluid} \quad (4)$$

With:

$$Q_{loss} = UA(\bar{T} - T_{env}) + (1 - \eta_{htr})Q_{max} \quad \text{and}$$

$$Q_{fluid} = \dot{m}_0 C_{pf}(T_{set} - T_i)$$

Q_{aux} is the required heating rate including efficiency effects ($\text{kg}\cdot\text{hr}^{-1}$), Q_{fluid} is the rate of heat addition to fluid stream ($\text{kg}\cdot\text{hr}^{-1}$), Q_{loss} is the rate of thermal losses from the heater to environment ($\text{kg}\cdot\text{hr}^{-1}$). Q_{max} is the maximum heating rate of the heater ($\text{kg}\cdot\text{hr}^{-1}$), η_{htr} is an efficiency of the auxiliary heater, m_0 is the outlet fluid mass flow rate ($\text{kg}\cdot\text{hr}^{-1}$), C_{pf} is the fluid specific heat ($\text{KJ}\cdot\text{hr}^{-1}$). T_i is the fluid inlet temperature (K), (\bar{T}) brackish water average temperature T_{set} set temperature of heater internal thermostat (K), T_{env} is the temperature of heater surroundings for loss calculations (K).

In MD configurations, another factor is considered for assessing the thermal performance of MD module, explicitly the GOR, that links heat consumed to generate permeate flux to the sum of thermal energy provide outwardly [19].

$$\text{GOR} = \text{mp} \times \text{Hv} / Q_e \quad (5)$$

Where Hv is Latent heat of vaporization (J/kg), mp is permeate flux (kg/s).

Hv is estimated by [20]:

$$\text{Hv} = 2501.897149 - 2.407064037 \times T + 0.001192217 \times T^2 - 0.000015863 \times T^3 \quad (6)$$

where T is the average temperature at the evaporator entrance and the exits of the condenser ($^{\circ}\text{C}$).

The thermal energy supplied was evaluated as [1]:

$$Q_e = \text{mf} \times C_p \times (T_{\text{feed,in}} - T_{\text{cooling,out}}) \quad (7)$$

where mf is the feed water flow rate (kg/h), C_p is the feed water heat capacity ($\text{kWh}/\text{kg}^{\circ}\text{C}$), $T_{\text{feed,in}}$ is the evaporator inlet temperature ($^{\circ}\text{C}$) and $T_{\text{cooling,out}}$ is the condenser outlet temperature ($^{\circ}\text{C}$).

The main objective of the MD operation is to produce a high quantity of permeate flux with the lowest possible energy. The required energy was evaluated via the specific thermal energy consumption STEC (kWhm^{-3}), defined as the external heat needed to generate quantity of permeate flux, expressed by the following relation between energy efficiency ratio Q_e and the permeate flow rate (VP) [20].

$$\text{STEC} = Q_e / V_p \quad (8)$$

The efficiency of the MD system is calculated by using equation (9) [16]. The bulk temperature of the feed is used for calculating the latent heat of evaporation.

$$\text{EE} = m_p \times H_v / Q_{in} \quad (9)$$

Where the thermal efficiency of MD unit is given by [16]:

$$Q_{in} = m_f \times C_p \times (T_{\text{feed,in}} - T_{\text{feed,out}}) \quad (10)$$

where m_f is the feed water flow rate (kg/h), C_p is the feed water heat capacity ($\text{kWh/kg}^\circ\text{C}$), $T_{\text{feed,in}}$ is the evaporator inlet temperature ($^\circ\text{C}$) and $T_{\text{feed,out}}$ is the evaporator outlet temperature ($^\circ\text{C}$).

In addition, in this study with these equations, a TRNSYS program [19] is used to predict the long-term performance of the different solar water heating systems for AGMD process. A complete test rig to evaluate the performance of membrane distillation module driven by solar energy during the flat plate and evacuated tube collectors heating process is built in Port-Said City, Egypt ($31^\circ 16' \text{N}$ $32^\circ 18' \text{E}$). Port Said is near the north coast of Egypt affected by the Mediterranean.

IV. 2. 2. Modeling of solar membrane distillation system

The model of solar thermal membrane distillation system is developed using TRNSYS program, which is a quasi-steady-state simulation program. The components are represented as preformats to be selected and interconnected in any desired manner to construct a system's model. To facilitate the selection of the system components, it is important to develop an information flow diagram. The information flow diagram for the models is shown in Table 7 as mentioned previously. The main component of the model is the AGMD unit, which is represented by a new equation in TRNSYS. Additional components to the model include TYPE109-TM2 reading and processing of meteorological data, Type 91 heat exchangers, Type

1 flat plate collectors, Type 71 evacuated tube collectors, Type 2 differential temperature controller, Type 3 single speed pump, Type 57 unit conversion and Type 65 online plotter as shown in Figures (IV.5) and (IV.6). As above, tables show the values of parameters used in the TRNSYS models.

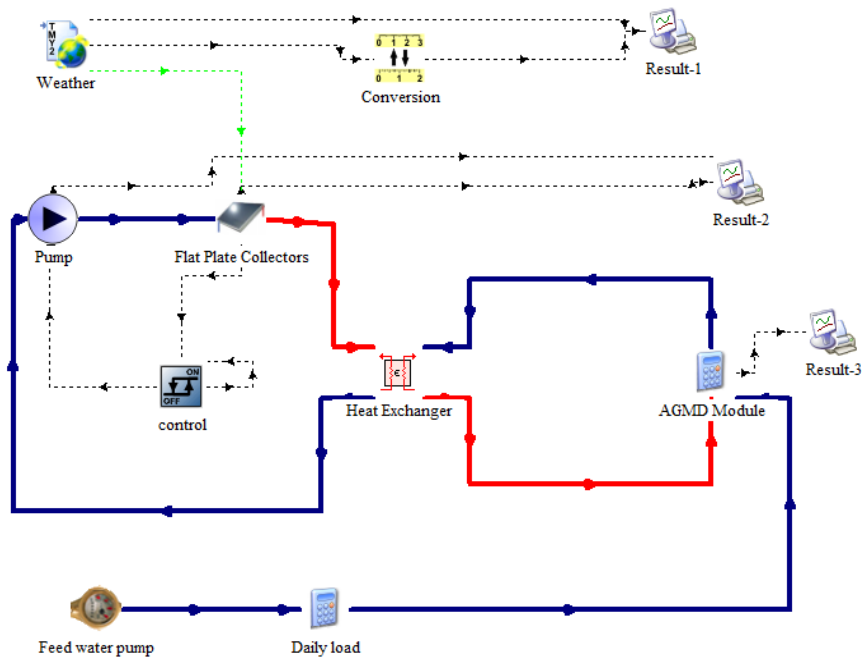


Figure IV.5: Diagram of the AGMD system using FPC in the TRNSYS simulation.

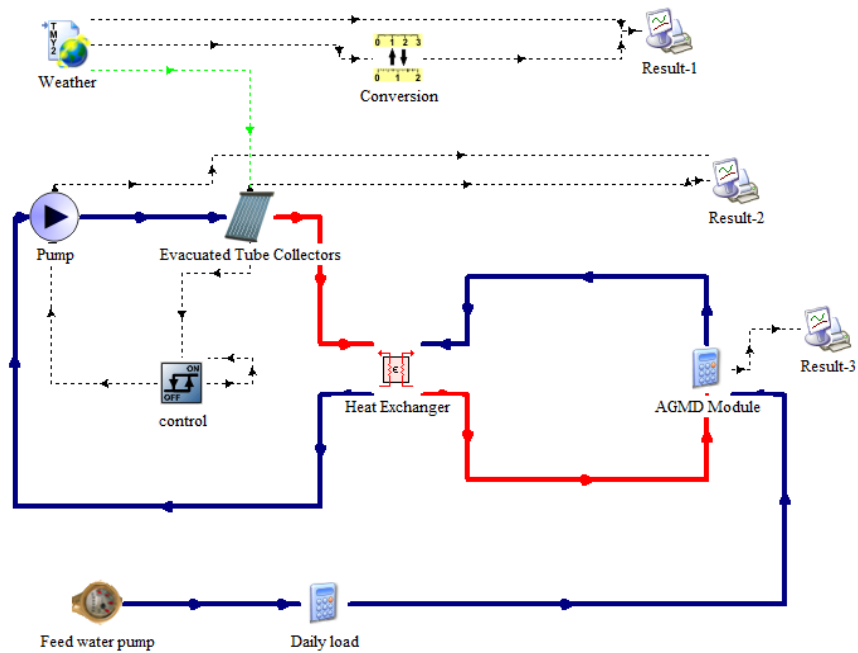


Figure IV.6: Diagram of the AGMD system using ETC in the TRNSYS simulation.

IV. 3. Conclusion

Membrane distillation is a process with several advantages regarding the integration into a solar thermally driven desalination system. In this work, an experimental study of the performance of a multi-channel spiral-wound air-gap membrane distillation module with an area 14.4 m² was evaluated at a pilot scale for water desalination to obtain production capacities reach 18 kg/h from the distillate water flow rate. Then, A complete test rig to evaluate the performance of membrane distillation module driven by solar energy during the flat plate and evacuated tube collectors heating process is built-in Port-Said City, Egypt (31°16'N 32° 18'E).

Optimized parametric conditions were used to operate the pilot-scale solar thermal driven membrane distillation system in Port-Said City and the system was simulated using the TRNSYS tool. The AGMD experimental data were tested and analyzed using a multiple regression model relating to the operating parameters of the solar AGMD system.

Empirical models developed using a multiple regression model relating the operating parameters will be useful for further simulations or applications of the technology. Besides, optimum values of the operating parameters to increase permeate flux and decrease specific heat consumption was obtained simultaneously for the AGMD module. Therefore, these types of projects that integrate renewable energy technologies with additional services are in principle attractive in terms of the associated socio-economic benefits.

Remarque:

Chapter IV includes our Articles:

- **A. Marni Sandid, M. Bassyouni, D. Nehari, Y. Elhenawy.** Experimental and simulation study of multichannel air gap membrane distillation process with two types of solar collectors. **Energy Conversion and Management** 243 (2021) 114 431
DOI: <https://doi.org/10.1016/j.enconman.2021.114431>
0196-8904/© 2021 Elsevier Ltd. All rights reserved.

References

- [1] Jury W, VauX H. The emerging global water crisis: managing scarcity and conflict between water users. *Adv Agron* 2007;95:1–76.
- [2] Yang X, Fane AG, Wang R. Membrane distillation: now and future. *Desalination* 2014;373–424. <https://doi.org/10.1002/9781118904855.ch8>.
- [3] Fath HES, Elsherbiny SM, Hassan AA, Rommel M, Wieghaus M, Koschikowski J, et al. PV and thermally driven small-scale, stand-alone solar desalination systems with very low maintenance needs. *Desalination* 2008;225(1-3):58–69. <https://doi.org/10.1016/j.desal.2006.11.029>.
- [4] Blanco Ga´lvez J, Garc´ıa-Rodr´ıguez L, Mart´ın-Mateos I. Seawater desalination by an innovative solar-powered membrane distillation system: the MEDESOL project. *Desalination* 2009;246(1–3):567–76. <https://doi.org/10.1016/j.desal.2008.12.005>.
- [5] Guill´en-Burrieza E, Blanco J, Zaragoza G, Alarco´n D-C, Palenzuela P, Ibarra M, et al. EXperimental analysis of an air gap membrane distillation solar desalination pilot system. *J Membr Sci* 2011;379(1-2):386–96. <https://doi.org/10.1016/j.memsci.2011.06.009>.
- [6] Duong HC, Xia L, Ma Z, Cooper P, Ela W, Nghiem LD. Assessing the performance of solar thermal driven membrane distillation for seawater desalination by computer simulation. *J Membr Sci* 2017;542:133–42. <https://doi.org/10.1016/j.memsci.2017.08.007>.
- [7] Mohan G, Kumar U, Pokhrel MK, Martin A. A novel solar thermal polygeneration system for sustainable production of cooling, clean water and domestic hot water in United Arab Emirates: dynamic simulation and economic evaluation. *Appl Energy* 2016;167:173–88. <https://doi.org/10.1016/j.apenergy.2015.10.116>.
- [8] Horta P, Zaragoza G, Alarco´n-Padilla DC. Assessment of the use of solar thermal collectors for desalination. *Desalin Water Treat* 2014;55(10):2856–67. <https://doi.org/10.1080/19443994.2014.947784>.
- [9] Koschikowski J, Wieghaus M, Rommel M, Ortin VS, Suarez BP, Betancort Rodr´ıguez JR. EXperimental investigations on solar driven stand-alone membrane distillation systems for remote areas. *Desalination* 2009;248(1–3):125–31. <https://doi.org/10.1016/j.desal.2008.05.047>.
- [10] Khayet M, Cojocar C, Garcia-Payo C. Application of response surface methodology and experimental design in direct contact membrane distillation. *Ind Eng Chem Res* 2007;46:5673–85.
- [11] Khayet M, Cojocar C. Air gap membrane distillation: desalination, modeling and optimization. *Desalination* 2012;287:138–45.
- [12] Elhenawy Y, Elminshawy NA, Bassyouni M, Alanezi AA, Drioli E. EXperimental and theoretical investigation of a new air gap membrane distillation module with a corrugated feed channel. *J Membr Sci* 2020;594:117461.
- [13] Uday Kumar NT, Martin A. Co-production performance evaluation of a novel solar combi system for simultaneous pure water and hot water supply in urban households of UAE. *Energies* 2017;10:481.
- [14] Ruiz-Aguirre A, Andr´es-Man˜as JA, Fern´andez-Sevilla JM, Zaragoza G. EXperimental characterization and optimization of multi-channel spiral wound air gap membrane distillation modules for seawater desalination. *Sep Purif Technol* 2018;205:212–22. <https://doi.org/10.1016/j.seppur.2018.05.044>.

- [15] Winter D, Koschikowski J, Wiegghaus M. Desalination using membrane distillation: experimental studies on full-scale spiral wound modules. *J Membr Sci* 2011;375 (1–2):104–12. <https://doi.org/10.1016/j.memsci.2011.03.030>.
- [16] Koschikowski J, Wiegghaus M, Rommel M. Solar thermal-driven desalination plants based on membrane distillation. *Desalination* 2003;156(1–3):295–304. [https://doi.org/10.1016/s0011-9164\(03\)00360-6](https://doi.org/10.1016/s0011-9164(03)00360-6).
- [17] Woldemariam DM. District Heating-Driven Membrane Distillation for Water Purification in Industrial Application. Stockholm: KTH; 2017.
- [18] Regression equation for Fit Regression Model. Minitab. (n.d.). <https://support.minitab.com/en-us/minitab/18/help-and-how-to/modeling-statistics/regression/how-to/fit-regression-model/interpret-the-results/all-statistics-and-graphs/regression-equation/#regression-equation>.
- [19] TRNSYS, Transient System Simulation, Univ. of Wisconsin Madison, WI: Solar Energy Laboratory, vol. 4, pp. 1–480.
- [20] Mabrouk AN, Elhenawy Y, Abdelkader M, Shatat M. The impact of baffle orientation on the performance of the hollow fiber membrane distillation. *Desalin Water Treat* 2017;58:35–45.



CHAPTER V: RESULTS & DISCUSSION

A. MARNI SANDID

DOCTORAL THESIS

2023



V. 1. Effects of operating parameters on the AGMD module for desalination

V. 1. 1. Models validation

The present paper studies the mass and heat transfer in the liquid boundary layer of the PVDF membrane AGMD application using the commercial CFD code ANSYS-FLUENT. The simulation results are validated with experimental data of Janajreh et al [1]. The system runs under the following operating conditions: hydrophobic PVDF membrane with a pore size of $0.15 \mu\text{m}$; the thickness of $130 \mu\text{m}$; Effective membrane area: 0.021 m^2 and 85% porosity running at Reynolds number of 10, which is equivalent to 0.01 m/s with an air gap 0.05 mm for AGMD. In addition, the warmer feed temperature is $50 \text{ }^\circ\text{C}$ and the cold permeate temperature is $27 \text{ }^\circ\text{C}$. Fig. 6 shows a comparison between the results of this simulation and the applied results from Janajreh et al [2] that it made a validation on the experimental research by Janajreh et al [1]. The results show excellent compatibility between them. The results show that the outlet cold temperatures increase to 317°K and 310°K in the membrane and bulk surfaces temperatures respectively when the outlet hot temperatures decrease to 309°K and 312°K . It can be noticed that the membrane and bulk surfaces temperatures of the AGMD module calculated by the present model has a good agreement as shown in (Figure V.1).

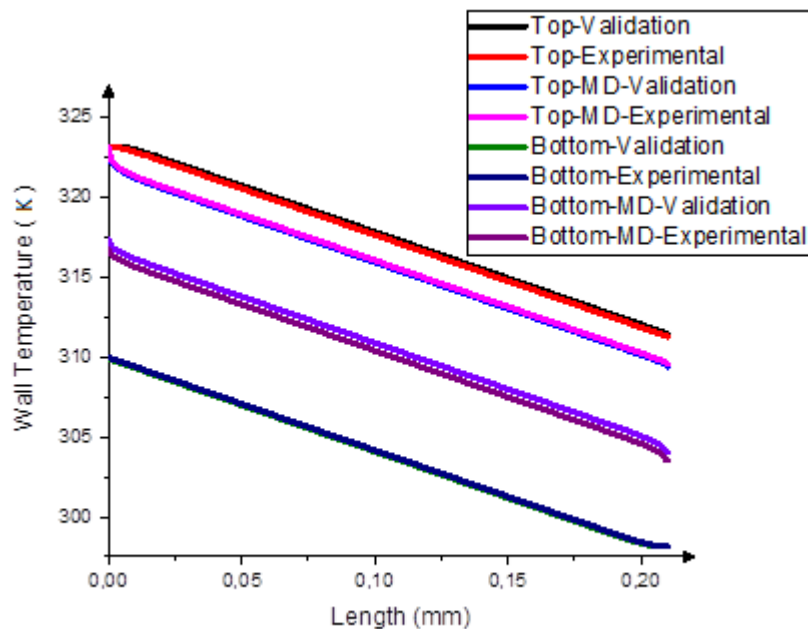


Figure V.1: Comparison between the experimental and simulation results of membrane and bulk surfaces temperatures in the AGMD module.

V. 1. 2. Temperature contours, velocity vectors, and total pressures of the AGMD module

The thermal behavior of the fluid in the AGMD module is shown in (Figure V.2). First, note that the velocity vectors coming from the inlet and heading towards the outlet on both sides of the fluid confirm the direction of flow and subsequently the counter current configuration in the AGMD module. As shown in (Figure V.2), it is clearly seen that the heat exchange happens between the hot fluid and the internal wall by convection, then by conduction through the thickness of the membrane, and finally by convection between the outer wall of the membrane and the fluid. We also note that the exchange is more important the more presides over the wall and especially at the outlets of the AGMD module.

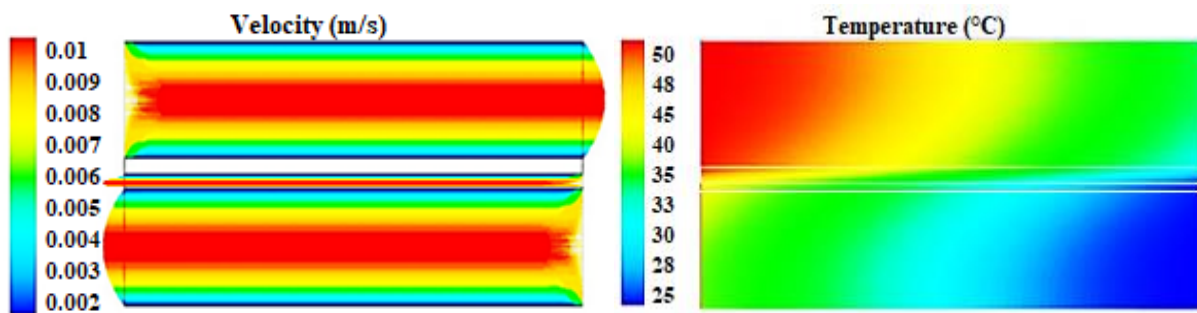


Figure V.2: Velocity vectors and Temperature contours of the AGMD module

Figure V.3 shows distributions of pressure along the membrane length permeate side of AGMD module. The total pressures reach 1748.8 Pa and 174.9 Pa at $Re=10$ and $Re=100$ respectively in permeate side. Therefore, the membrane length is more effective in the permeate side of AGMD. The vapor is condensed on a cold surface using an air gap on the permeate side of AGMD. Furthermore, the air gap separates the membrane from a condensed surface, which is the primary advantage of AGMD against all other MD applications. In the AGMD operation, the concentration of the condensed permeate in AGMD isn't never in direct contact with the membrane surface, hence there isn't risk of membrane wetness on the permeate side.

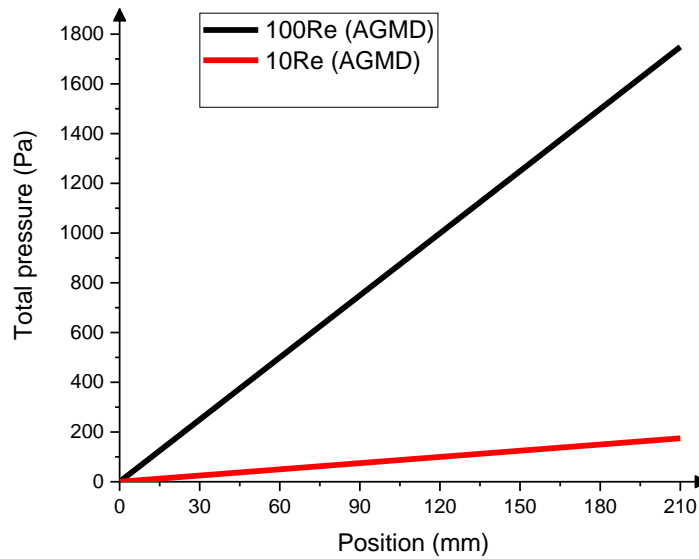


Figure V.3: Distribution of pressure along the membrane length permeate side of AGMD module.

V. 1. 3. Effect of operating temperatures

In order to study the influence of inlet feed temperature on mass flux, the feed temperature varies from 50 °C to 90 °C. The system is run under the following operating conditions: hydrophobic PVDF membrane with a pore size of 0.15 μm , the thickness of 130 μm , Effective membrane area: 0.021 m^2 and 85% porosity running at velocity of 10 with an air gap 0.05 mm. Figure V. 4 shows the result of the simulation at selected inlet cold temperature of 15, 25 and 35 °C. It can be seen that increasing the feed temperature increases the system flux significantly. Increasing the feed temperature increases the vapor production and the driving force to permeation (the trans-membrane temperature difference, and consequently the difference at partial pressures along membrane surfaces) which enhance permeation across the membrane. The percentage increase in flux when the feed temperature is increased from 50 °C to 90 °C is 89 % at the cold temperature of 35 °C, 85 % at 25 °C and 83 % at 15 °C. Thus, percentagewise, higher cold temperature gives more percentage increase in mass flux.

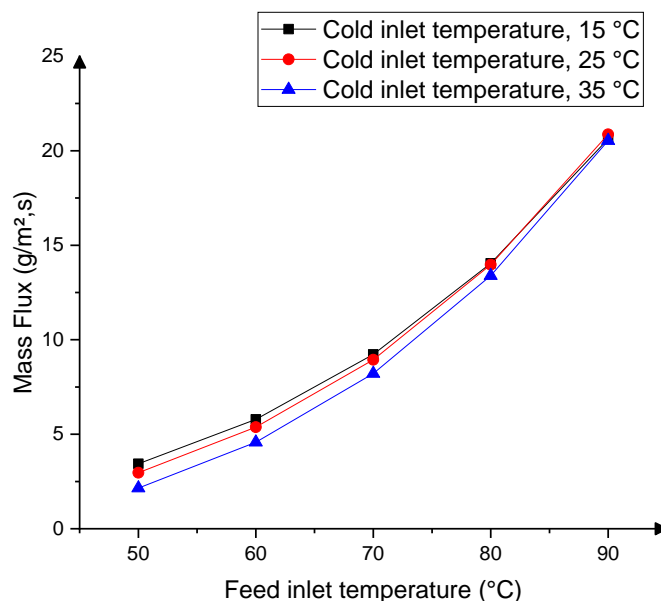


Figure V.4: Effect of feed inlet temperature on mass flux.

The effect of cold inlet temperature observes at selected different feed inlet temperatures of 50, 70, and 90 °C. The simulation is performed under the same conditions as above (hydrophobic PVDF membrane with a pore size of 0.15 μm , the thickness of 130 μm , Effective membrane area: 0.021 m² and 85% porosity running at velocity of 0.1 with an air gap 0.05 mm). It observes that for a given feed temperature, by decreasing the cold temperature, mass flux increases as shown in (Figure V.5). Decreasing the cold temperature increases the difference of partial pressure that assist the permeation process across the membrane. Percentagewise, reducing the cold temperature from 35 °C to 5 °C results in mass flux increase of 2 % at feed temperature of 90 °C. , 10 % at feed temperature of 70 °C, and 41 % at feed temperature of 50 °C.

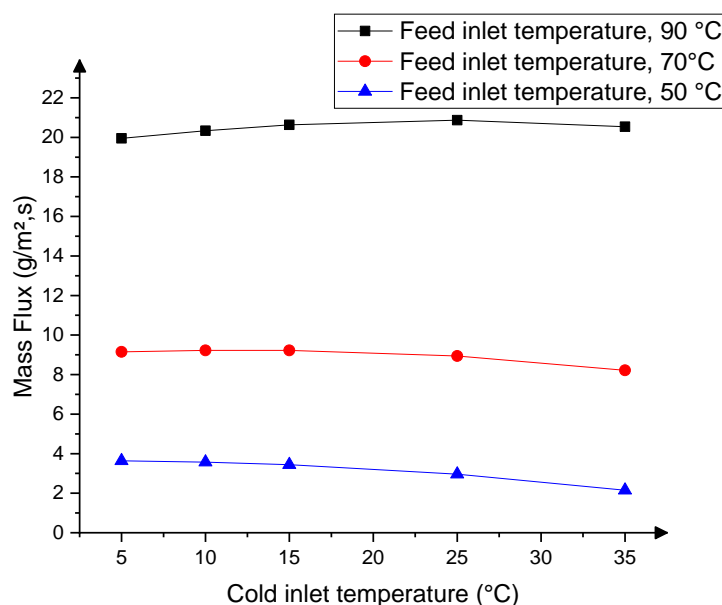


Figure V.5: Effect of cold inlet temperature on mass flux.

V. 1. 4. Effect of operating flow rates

In order to investigate the effect of Reynolds number (Re) in the feed side on the mass flux; the simulation is conducted with variable feed flow rates while keeping all other parameters constant. The feed flow rate varies from 0.01 m/s to 0.1 m/s (10 Re to 100 Re). The operating conditions for the simulation are; hydrophobic PVDF membrane with a pore size of 0.15 μm , the thickness of 130 μm , Effective membrane area: 0.021 m², 85% porosity, and an air gap 0.05 mm with permeate temperature 25 °C and cold flow rate 0.1 m/s. Figure V.6 shows the variation of mass flux with feed flow rate for selected feed temperature of 50, 70, and 90°C. The trend shows that increasing the feed flow rate increases the mass flux substantially. Feed flow rate is very effective variable to increase the system flux at different feed temperatures. It is worth mentioning that the exponential nature of flux increase can better be observed at 90 °C as compared to other feed temperatures of 50 °C and 70 °C .Over the entire range of feed flow rate, (0.01 to 0.1 m/s) 48 % increase in mass flux is obtained at feed temperature of 90 °C, 43 % is obtained at 70 °C and 35 % is obtained at 50 °C.

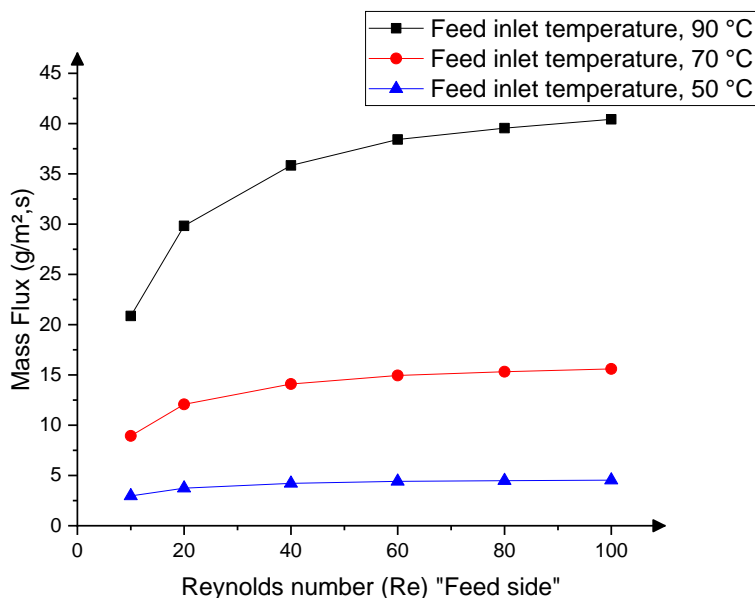


Figure V.6: Effect of Reynolds number (Feed side) on mass flux.

In order to examine the effect of Re in the cold side; the cold flow rate varies from 0.01 m/s to 0.1 m/s (10Re to 100Re) while keeping all other parameters constant. The operating conditions for the simulation are; hydrophobic PVDF membrane with a pore size of 0.15 μm , the thickness of 130 μm , Effective membrane area: 0.021 m^2 , 85% porosity and an air gap 0.05 mm with permeate temperature 25 $^{\circ}\text{C}$ and feed flow rate 0.01 m/s.

Figure V.7 shows the variation of mass flux with cold flow rate for selected feed temperature of 50, 70, and 90 $^{\circ}\text{C}$. The trends show that increasing the cold flow rate increases the mass flux marginally. Cold flow rate seems more effective at high feed temperature as compared to low feed temperature. Over the entire range of the tested cold flow rate (0.01 to 0.1 m/s), only 15 % increase in flux is obtained at 90 $^{\circ}\text{C}$, 6.4 % increase in flux at 70 $^{\circ}\text{C}$ and 6.1 % is obtained at 50 $^{\circ}\text{C}$.

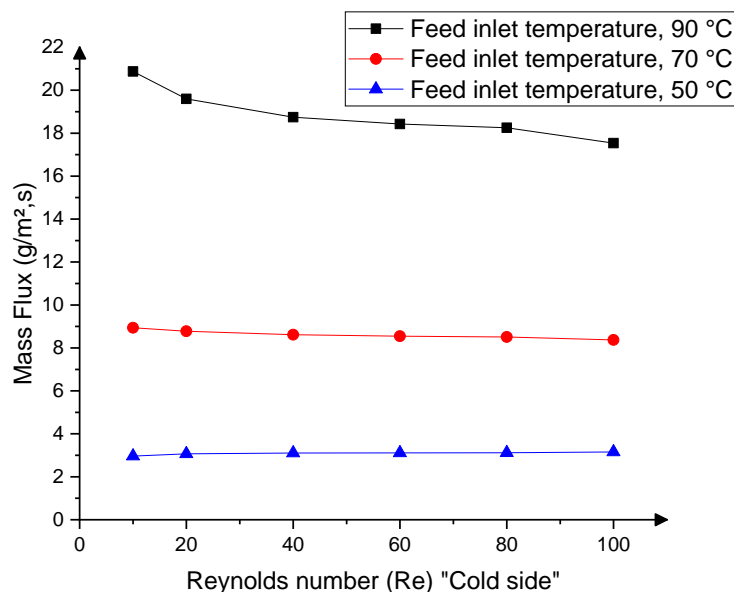


Figure V.7: Effect of Reynolds number (Cold side) on mass flux.

V. 1. 5. Effects of different thermal properties on various materials of MD

All Thermal properties of different materials (Polyvinylidene fluoride (PVDF) polymers, copolymers and blends) is shown as above in (Table V.1):

Table V.1: Thermal properties of different materials of MD [3].

Number	Materials of MD	Specific heat (J/kg K)	Density (kg/m ³)	Thermal diffusivity (*10 ⁻⁶ m ² /s)	Thermal conductivity (W/m K)
1	PVDF	1325	1775	0.1115	0.2622
2	PVDF/P(VDF-TrFE) (70/30)	1172	1938	0.0797	0.1810
3	PVDF/P(VDF-TrFE) (50/50)	1049	2067	0.1473	0.3193
4	P(VDF-TrFE) (80/20)	1092	1657	0.0934	0.1690
5	P(VDF-TrFE) (70/30)	1159	1786	0.943	0.1952
6	P(VDF-TrFE) (50/50)	1066	1936	0.1029	0.2123

Figure V.8 shows the efficiency, mass flux, and TPC on different Materials of MD. The feed inlet temperature is 70 °C while keeping all other parameters constant. The operating conditions for the simulation are; hydrophobic PVDF membrane with a pore size of 0.15 μm , the thickness of 130 μm , Effective membrane area: 0.021 m^2 , an air gap 0.05 mm and 85% porosity with cold temperature 25 °C and feed flow rate 0.01 m/s. It can be seen that the copolymer P(VDF-TrFE) (80/20) is better than the other materials. In addition, the mass flux, efficiency and TPC reach 12.99 ($\text{g}/\text{m}^2\text{s}$), 44.74 % and 45.06 respectively. As shown in (Table V.1) and (Figure V.8), if the density and thermal conductivity are lower, the efficiency, mass flux, and TPC of MD are higher and more effective for seawater desalination.

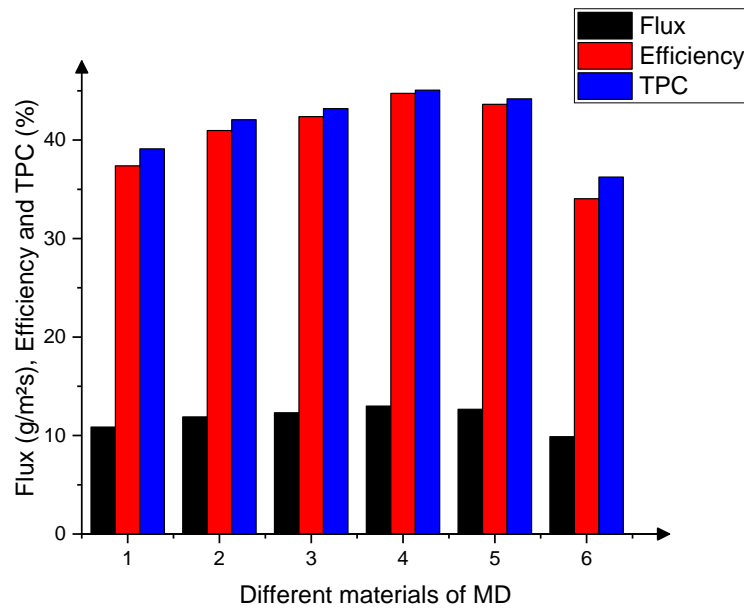


Figure V.8: Efficiency, mass flux, and TPC on different materials of MD.

V. 1. 6. Effects of different areas and flow regimes

Table V.2 shows the comparison of different membrane parameters (area and flow rates) using different flow regimes (laminar and turbulent). The used material of MD is the hydrophobic copolymer P(VDF-TrFE) (80/20) while keeping all other parameters constant (the pore size of 0.15 μm , the thickness of 130 μm and 85% porosity with feed inlet temperature is 70 °C and cold temperature 25 °C).

Table V.2: Comparison of different membrane parameters using different flow regimes.

Membrane area (m ²)	0.021	1.05	2.1	2.1	3.15
Feed and permeate flow rates (m/s)	0.01	0.1	0.05	0.1	1
Flow regimes	Laminar	Laminar	Laminar	Turbulent	Turbulent
Flux average (g/m ² s)	12.99	64.5	118.95	129	193.5

The variations on the different membrane parameters are very effective as shown in (Table V.2). The mass flux reaches 118.95 (g/m²s) using the laminar flow regime while it reaches 193.5 (g/m²s) using the turbulent flow regime, respectively. Therefore, the model turbulent is better than the laminar flow regime. In addition, increasing the feed flow rate and the area of MD is increased the mass flux and efficiency.

V. 2. Simulation and controlling and optimization study of the solar AGMD system small scale

V. 2. 1. Model validation

Based on the experimental characteristics of AGMD module, the simulation results have been validated with experimental data obtained from a pilot-scale solar thermal membrane distillation system that installed in UAE [4]. This part aimed at checking the validity of the input data and output results to obtain correct and reliable results in the same conditions used in the maximum radiation from October on solar collectors in UAE.

In (Figure V.9), a single cassette air-gap membrane distillation (AGMD) module is characterized to identify the effect of process parameters on distillate flux. Figure V.9 shows a comparison between the results of this simulation and the applied results from Kumar's article et al [4]. The results showed excellent compatibility between them, and this is shown by the distillation flow rate value. Therefore, favorable conditions were determined and validated to obtain a distillate flow rate of 4.5 kg/h.

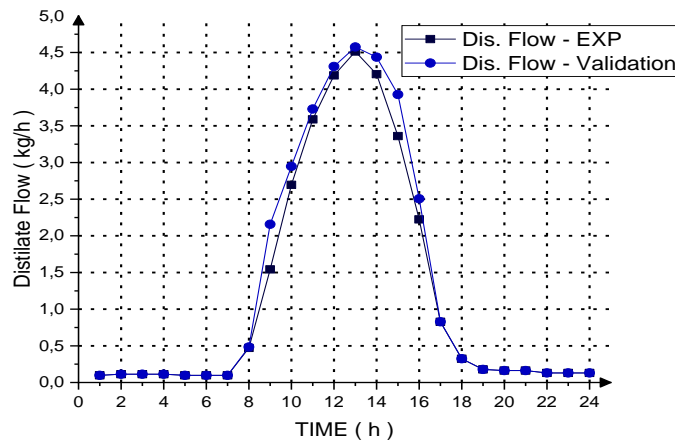


Figure V.9: Comparison of distillate flow between the simulation and the experimental data [4].

Figure V.10 shows the comparison of the inlet hot feed side temperature of the AGMD module between the given experiment results [4] and the simulated results obtained from the model used. It can be noticed that the inlet hot feed side temperature of the AGMD module predicted by the present model has a good agreement with the experiment. The outlet temperature of the thermal system of an AGMD module reaches 84 °C in the maximum radiation from October on solar collectors in UAE. Based on this result as shown in figure 8,

the present study aims at simulating the solar-based solar thermal membrane distillation system considered as a field trial installation in UAE.

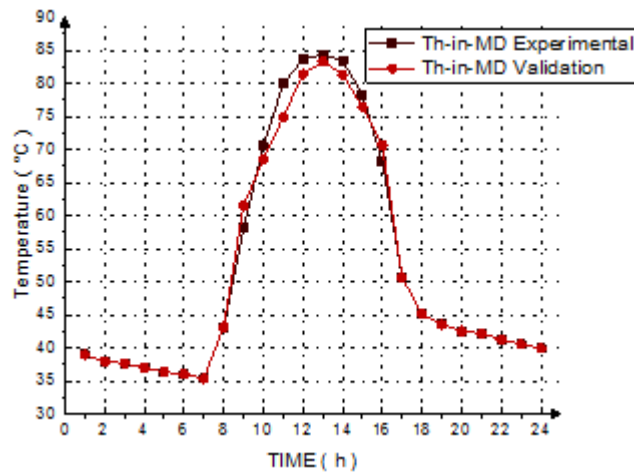


Figure V.10: Comparison of temperature outlet of the thermal system between the simulation and the experimental data [4].

V. 2. 2. Temperatures inlet of AGMD and Distillate Flows without auxiliary heaters

The change in feed inlet temperature of AGMD module profiles without using an auxiliary heater for day 11th of December, March, August, and October is illustrated in (Figure V.11). The results show that the temperature decreases in December that reach 52 °C, but it increases in August when the temperature is high and reaches 87 °C, as it reaches 72 and 81 °C respectively in March and October. This change is due to the change in ambient temperature and radiation in the daytime and, their difference from month to month.

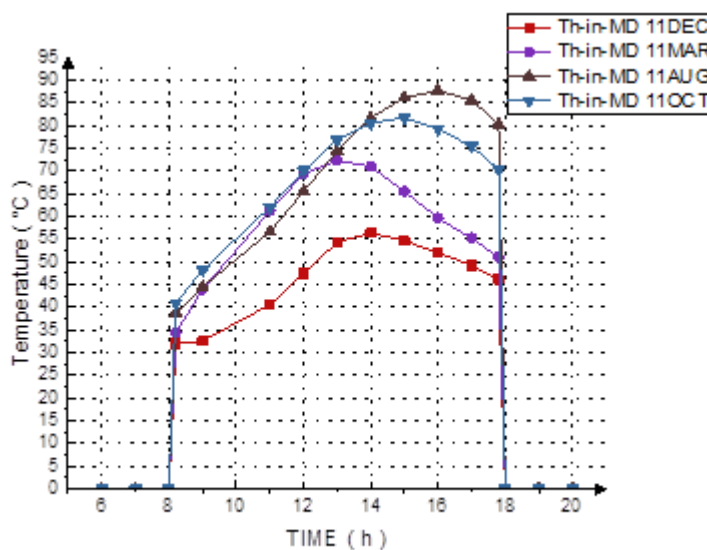


Figure V.11: Feed AGMD inlet temperatures without auxiliary heaters (°C).

Figure V.12 illustrates the amount of distilled water obtained from AGMD in different climatic conditions throughout the year. We note that the productivity of distilled water is decreased in December and reaches 1.6 kg/hr and increases in August, which reaches 5.5 kg/hour, where it is 3.4 and 4.6 in March and October respectively. Consequently, the changes in temperature and climatic conditions as clarified in (Figure V.11) effect the distilled water flow in different months on the same day 11th of four months selected. The temperature is related to the flow of distilled water. Therefore, when the temperature decreases, the flow of distilled water also decreases and vice versa.

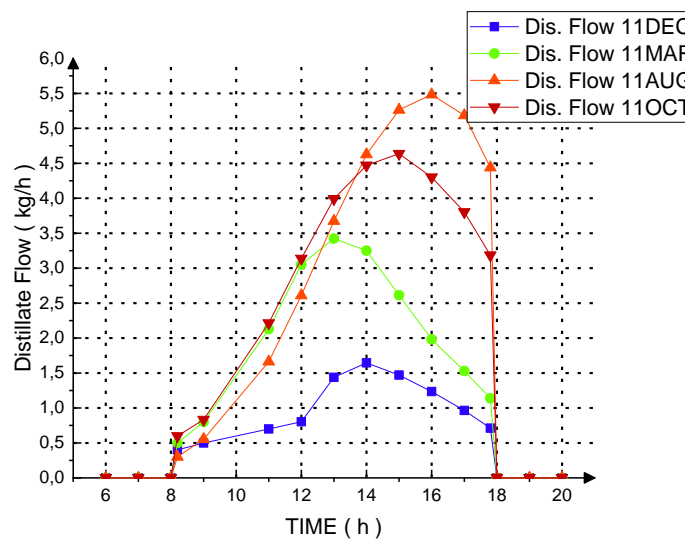


Figure V.12: Distillate flows of AGMD module without auxiliary heaters (Kg/h).

V. 2. 3. Temperatures inlet of AGMD and Distillate Flows with auxiliary heaters

In (Figure V.13), there are feed inlet temperatures changes of the AGMD module in different climatic conditions by adding an electrical heater to this used system. Therefore, we notice that inlet temperatures of AGMD reach 85-87 C° and stay stable in each day: (11/12, 11/03, 11/08, and 11/10) and in different climatic conditions throughout the year in Ain-Temouchent as well. The auxiliary heater compensates for the necessary heat for the AGMD unit. Thus, this system is appropriate to keep the temperatures stable at the same temperature 87 degrees Celsius for different seasonal weather conditions in Ain-Temouchent.

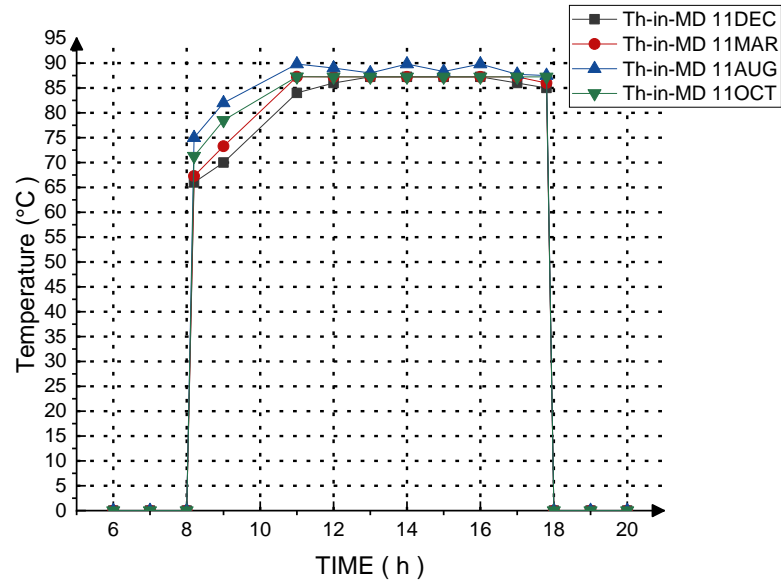


Figure V.13: Feed AGMD inlet temperatures with auxiliary heaters (°C).

Figure V.14 illustrates the variations of the distilled water flow produced by the AGMD module by adding an auxiliary heater at different climatic conditions for four months. In this case, we note that distilled water flow from the distillation membrane reaches 5.5 kg /h and stays stable on different days throughout the year. This also explains why the stability of heat occurs when adding an auxiliary heater to this system and this greatly helps in the flow of distilled water that reaches the same flow 5.5 kg /hour in different climatic conditions throughout the year in the weather of Ain-Temouchent.

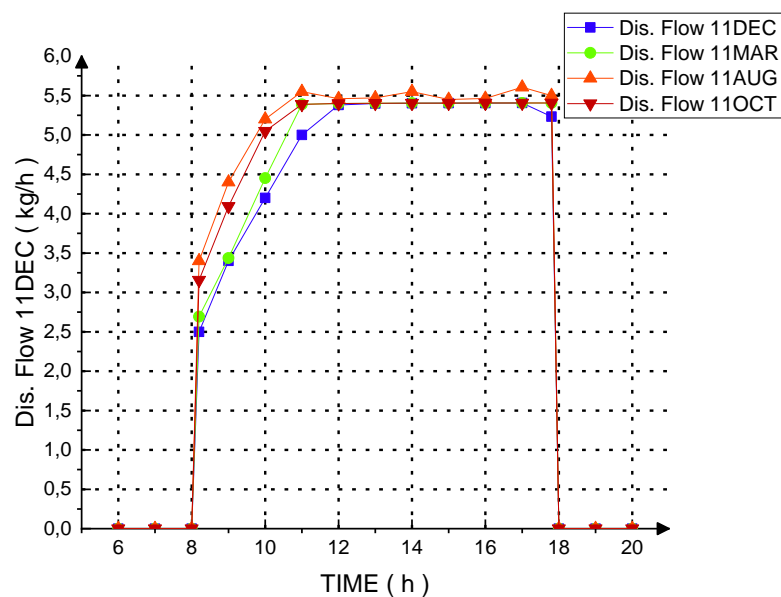


Figure V.14: Distillate flows of AGMD module with auxiliary heaters (Kg/h).

V. 2. 4. Auxiliary heating rate and power to load of the photovoltaic (PV) system

Adding an auxiliary heater consumes additional electrical energy to this system and that is due to interruptions and climate changes in Ain-Temouchent throughout the year as shown in (Figure V.15). We note on December 11, the electricity power of the auxiliary heater reaches 1.5 kW, unlike on August 11, when the required energy reaches only 0.28 kW because the temperature in this month increases as shown in (Figure V.11). In addition to that, the electric power in March and October reaches between 0.1-1.4 and 0.4-1.4 KW respectively. Thus, when the more temperature decreases, the more electric power is required to reach the desired value. However, the auxiliary heater is useful to producing more distilled water with a stable flow throughout the year in the weather of Ain-Temouchent, but it consumes additional electrical energy that affects and increases the cost of this water desalination system.

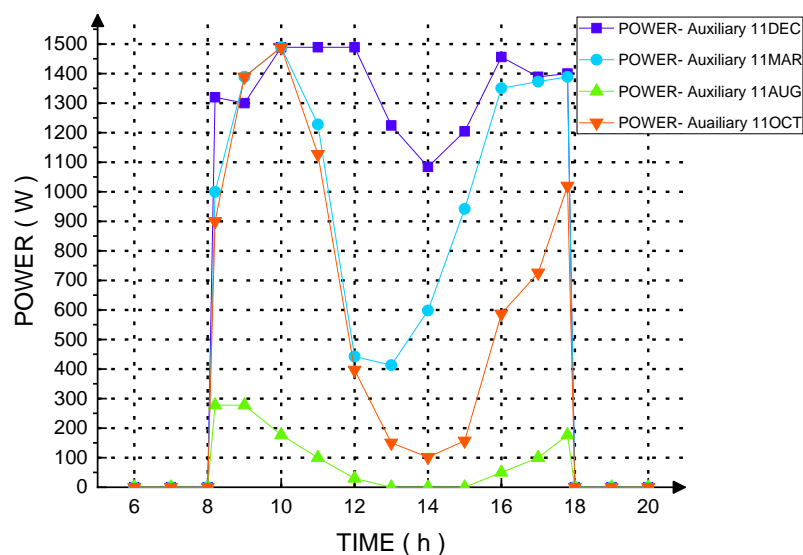


Figure V.15: Power to load of the auxiliary heaters of the thermal system for AGMD.

To save costs, a photovoltaic system uses based on renewable energy (solar energy). Therefore, the energy needed calculates for the auxiliary heater and replaces by 10 photovoltaic panels, each one has an area of 1.6 m² using three of the energy storage batteries (12V, 100Ah) with 1.5 kilowatts via TRNSYS program. Accordingly, the purpose of this study is the use of solar panels in the photovoltaic system to produce the necessary electrical energy. Therefore, we note in (Figure V.16) that the electric power of the auxiliary heater is the same energy that comes out of the photovoltaic system. Consequently, the electrical energy of the auxiliary

heater replaces by using the PV system panels in various intermittent climatic conditions (11/12, 11/03, 11/08, and 11/10) as shown in (Figure V.16).

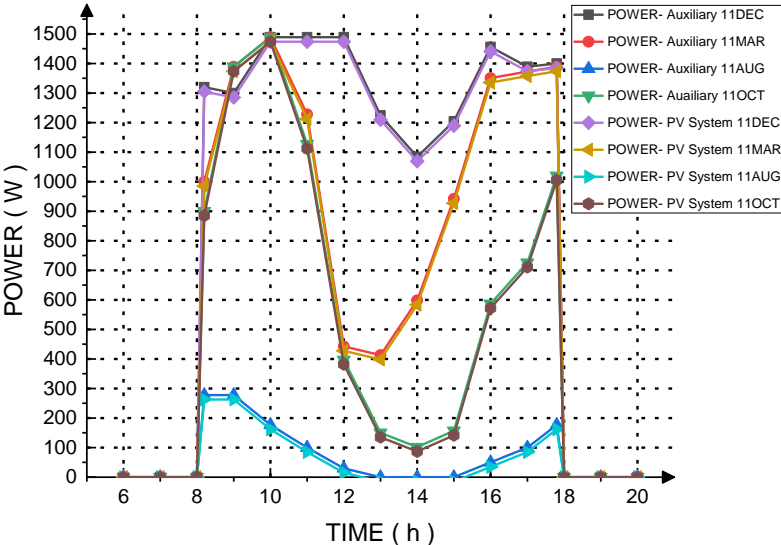


Figure V.16: Power to load of the photovoltaic system for the auxiliary heaters for AGMD.

V. 3. Development and optimization study of the solar AGMD system small scale

V. 3. 1. Model validation

The aim of this section is the validity of input data and output results under the same operating conditions for the AGMD module in order to obtain correct and accurate results. Figure V.17 shows the comparison between the experimental results and the simulated results obtained from the model used. Then, it presents the effect of inlet feed temperature on permeate flux, the feed temperature varies from 40 °C to 90 °C. The system runs under the following operating conditions: hydrophobic PTFE membrane with a pore size of 0.2 μm , the thickness of 280 μm , total membrane area: 0.2 m^2 , permeate flow rate of 3.65 L/min, and feed flow rate of 4.65 L/min with feed salinity of 2 g/L.

As shown in Figures (V.17), (V18) and (V19), it can be noticed that the hot and cold feed outlet temperatures and permeate flux of the AGMD module calculated by the present model have good compatibility of no more than 5% in this experiment. This good compatibility using the TRNSYS program on the experimental AGMD system installed in the UAE [4] makes it suitable for use in various climatic changes like Ain Temouchent weather in Algeria, which is characterized by a good solar climate. The results show that increasing the feed inlet temperature increases the system flux significantly. Increasing the feed inlet temperature increases the vapor production and the driving force to permeation (the transmembrane temperature difference, and consequently the difference in partial pressures across membrane surfaces) which enhance permeation across the membrane. The percentage increase in flux when the feed temperature is increased from 40 °C to 90 °C is 56 % at permeate temperature of 25 °C, 41 % at 15 °C, and 30 % at 5 °C as shown in fig.6. Thus, percentagewise, higher cold permeate temperature gives more percentage increase in flux.

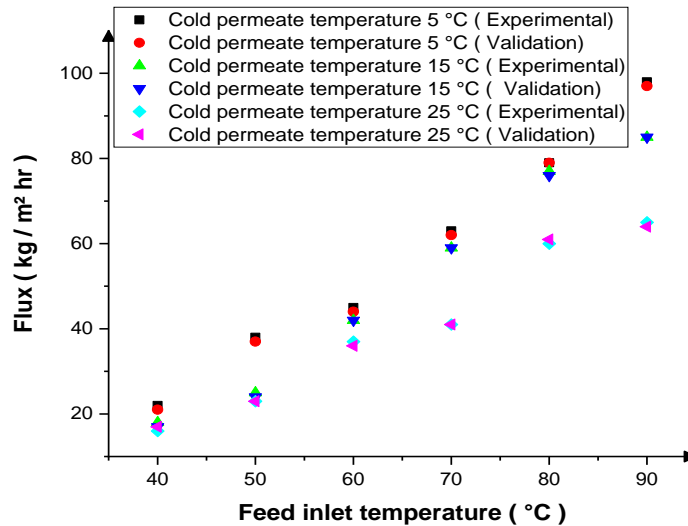


Figure V.17: Effect of feed inlet temperature on flux.

Figure V.18 shows the comparison of the inlet hot feed side temperature of the AGMD module between the given experiment results [4] and the simulated results obtained from the model used. It can be noticed that the inlet hot feed side temperature of the AGMD module predicted by the present model has a good agreement with the experiment. The outlet temperature of the thermal system of an AGMD module reaches 84 °C in the maximum radiation from October on solar collectors in UAE. Based on this result as shown in figure 7, the present study aims at simulating the solar-based solar thermal membrane distillation system considered as a field trial installation in UAE.

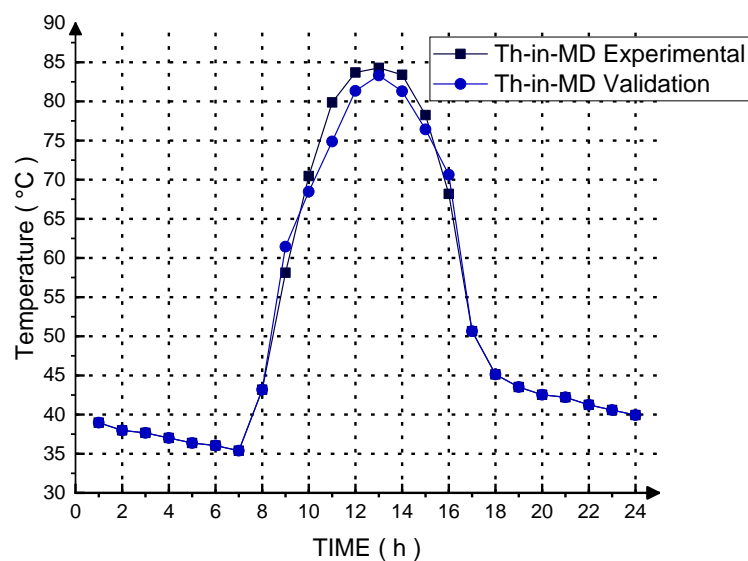


Figure V.18: Comparison of temperature outlet of the thermal system between the simulation and the experimental data [4].

In (Figure V.19), a single cassette air-gap membrane distillation (AGMD) module is studied to identify the effect of process parameters on distillate flux. Figure V.19 shows a comparison between the results of this simulation and the applied results from Kumar's article et al [4]. The results show excellent compatibility between them. This agreement using the experimental parameters of the article by Kumar et al. [4] confirms the validity of this system studied in this paper. This is shown by the distillation flow rate value. Therefore, favorable conditions were determined and validated to obtain a distillate flow rate of 4.5 kg/h.

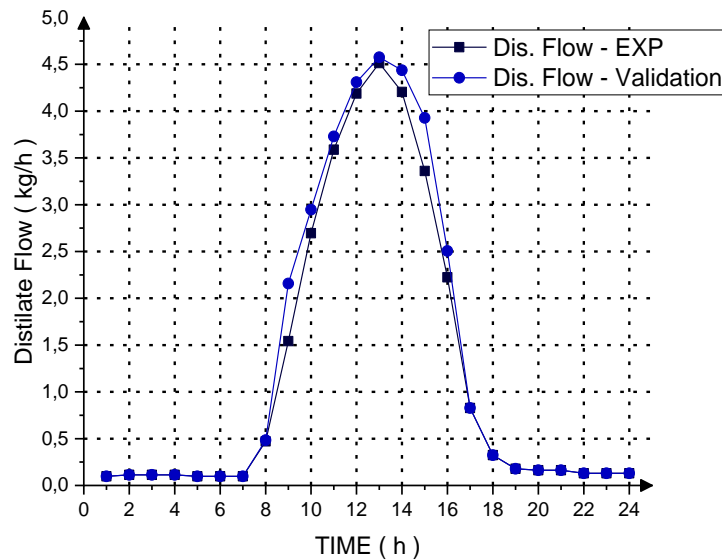


Figure V.19: Comparison of distillate flow between the simulation and the experimental data[4].

Based on the experimental characteristics of the AGMD module, the simulation results are validated with experimental data obtained from the pilot solar thermal membrane distillation system mounted in UAE [4].

V. 3. 2. Weather data

This model has been studied in Ain-Temouchent weather, (Figure V.20) shows changing climate conditions throughout the year. The weather in Ain-Temouchent state is pleasant, warm, and moderate in general. At an average temperature of 25.7 degrees Celsius, August is the hottest month of the year. At 10.8°C on average, January is the coldest month of the year. Therefore, in (Figure V.20), we notice a change in temperature throughout the year, which reaches up to 40 degrees Celsius in August, and we note that the wind is moderate and does not exceed the velocity of 15 m/s. For the irradiation, it changes during the months of the year and reaches up to 220 KWh/m² in August and July as shown in (Figure V.21), because the

temperature is high in this period of the year. This study has been simulating for a full year and the results will appear on different days in Ain-Temouchent weather affected by the Mediterranean Sea.

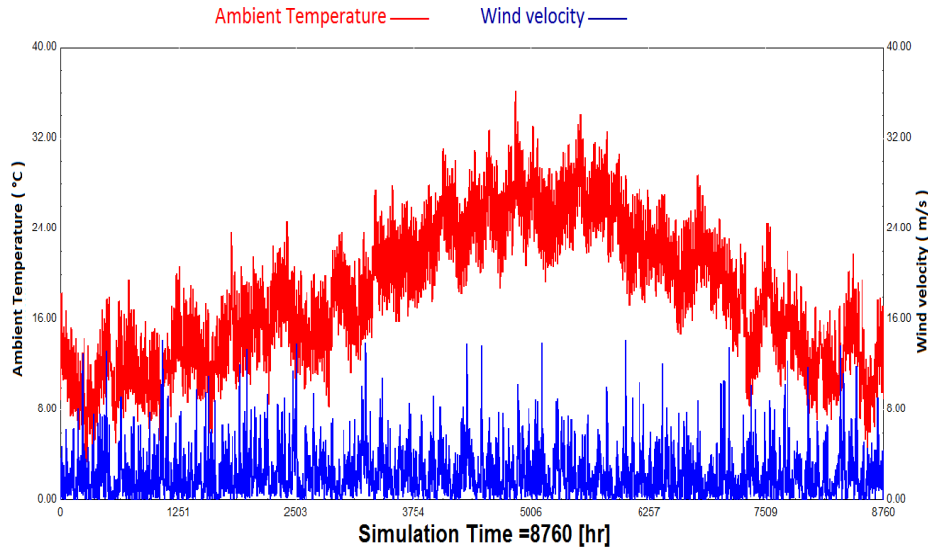


Figure V.20: Ambient temperature and wind velocity throughout the year in Ain-Temouchent weather.

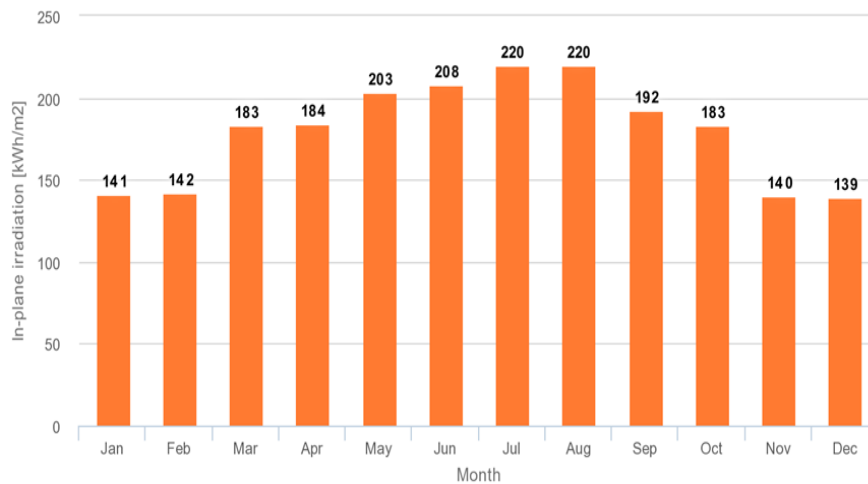


Figure V.21: Irradiation throughout the year in Ain-Temouchent weather.

V. 3. 3. Thermal capacity and permeate flux

Figure V.22 shows the outlet temperatures for five flat plate collectors that have a total area of 12.75 m^2 considered for both experiments and the simulation model. It is found that the change in feed inlet temperature of AGMD module profiles for the first day of January, April, August, and November is illustrated in (Figure V.22). The temperature decreases in January and reaches $78 \text{ }^\circ\text{C}$, but it increases in August when the temperature is high and reaches $95 \text{ }^\circ\text{C}$, as it reaches 84 and $82 \text{ }^\circ\text{C}$ respectively in April and November. This change is due to the change in

ambient temperature and radiation in the daytime and their difference from month to month. Therefore, plots show a remarkable influence of the hot feed temperatures during the days of winter and summer seasons by the percentage reaches 18 %.

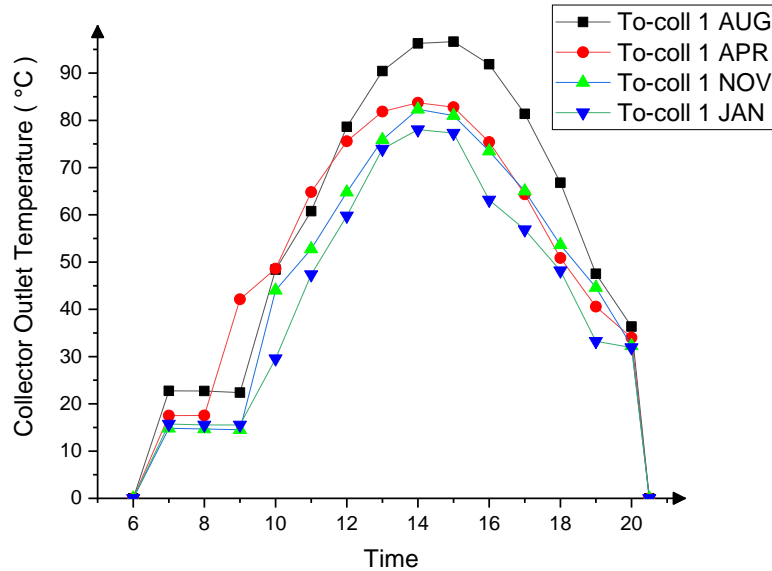


Figure V.22: Distribution of collector outlet temperature along the day during 4 seasons.

Figure V.23 shows the inlet feed temperatures of AGMD coming from the exchanger heaters and using the flat plate collectors. The system runs under the following operating conditions: hydrophobic PTFE membrane with a pore size of $0.2 \mu\text{m}$, the thickness of $280 \mu\text{m}$, total membrane area: 0.2 m^2 , and permeate flow rate of 3.65 L/min , the feed flow rate of 4.65 L/min with feed salinity of 2 g/L . The inlet feed temperatures reach $70 \text{ }^\circ\text{C}$ and $74 \text{ }^\circ\text{C}$ in January and November, as it reaches $75 \text{ }^\circ\text{C}$ and $85 \text{ }^\circ\text{C}$ in April and August respectively. Therefore, it can be seen that the percentage increases in the high temperature during the days of winter and summer seasons by the percentage 17.8 %.

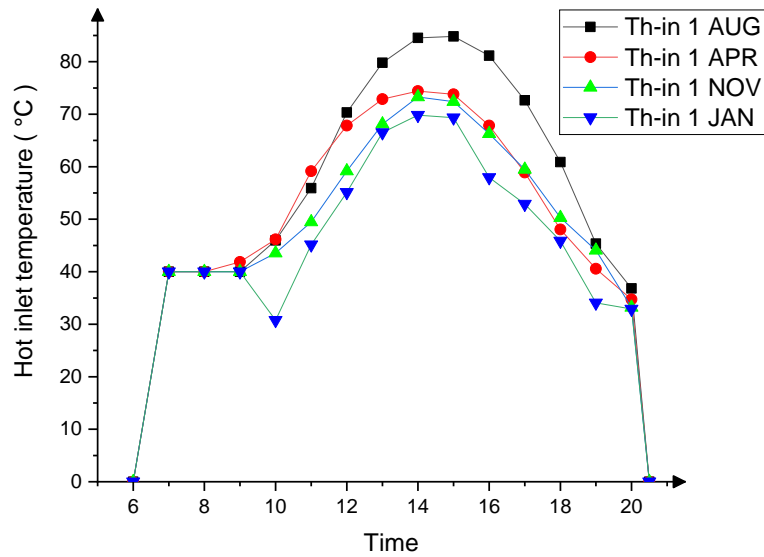


Figure V.23: Distribution feed inlet temperature of AGMD.

Figure V.24 shows the variation of permeate flux variation with keeping all other parameters constant as above. Clearly, the trends show that the permeate flux increases with various intermittent climatic conditions. Therefore, the inlet hot temperature is very effective to increase the permeate flux at different times as shown in (Figure V.24). It is worth mentioning that the exponential nature of flux increase can better be observed in summer as compared to other times. Over the entire range of permeate flux (3 to 5 L/h) and throughout the year, the percentage increases in flux and reaches 40 % between winter and summer.

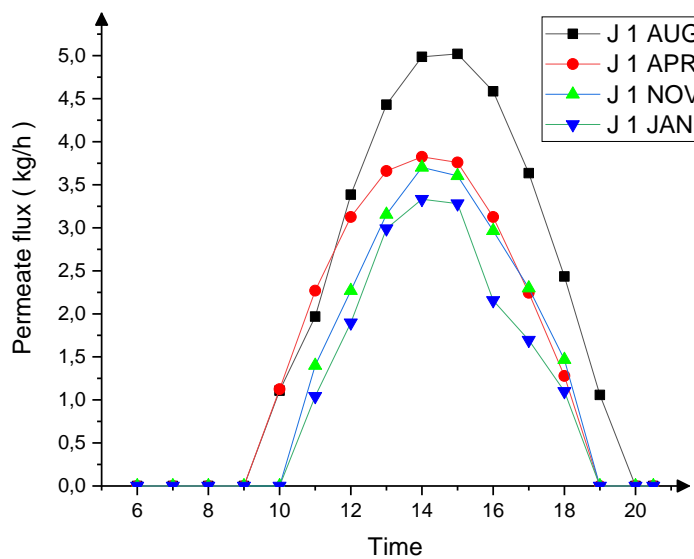


Figure V.24: Permeate flux of AGMD.

V. 3. 4. Power to load of the Photovoltaic (PV) System

To save costs, a photovoltaic system uses based on renewable energy (solar energy). Therefore, the energy needed calculates for the pumps and replaces by two photovoltaic panels, each one has an area of 1.6 m² using an energy storage battery (12V, 100Ah) via TRNSYS and PVGIS help programs. Accordingly, the purpose of this study is the use of solar panels in the photovoltaic system to produce the necessary electrical energy. Therefore, we note in (Figure V.25) that the electric power of the pumps that reaches 0.2 kilowatts is the same energy that comes out of the photovoltaic system. Consequently, the electrical energy of the pumps is replaced by using the PV system panels in various intermittent climatic conditions as shown in (Figure V.25).

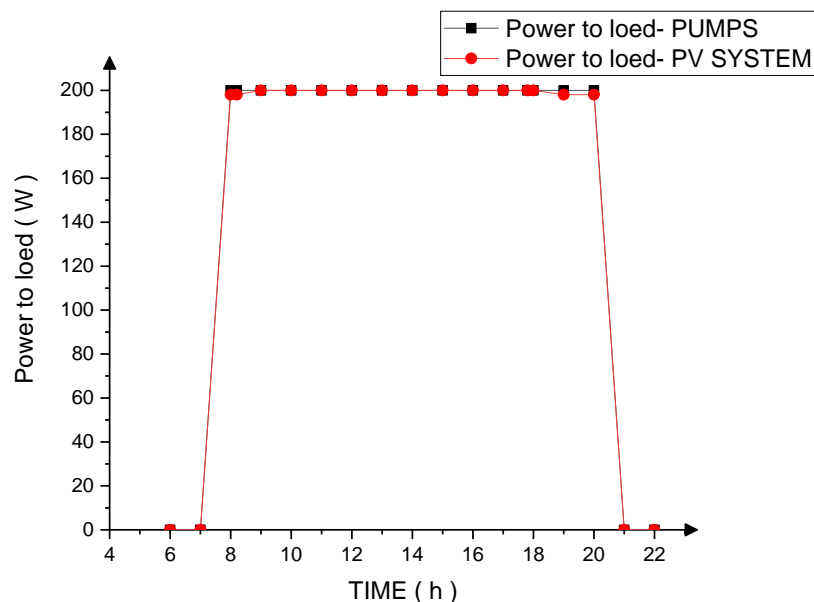


Figure V.25: Power to load of the PV System and pumps for the AGMD system.

V. 3. 5. The flat plate thermal solar collector efficiency

Figure V.26 shows the four efficiencies for the evolution of the entire year. The results show that the efficiencies increase from 0.65 to 0.74 during summer, as they reach 0.59, 0.63, and 0.64 respectively in January, November, and April. Therefore, the changing climate conditions throughout the year are very effective in increasing the flat plate thermal solar collector efficiencies. Percentagewise, the efficiencies increase from 18.4 % to 66.6 % throughout the entire year.

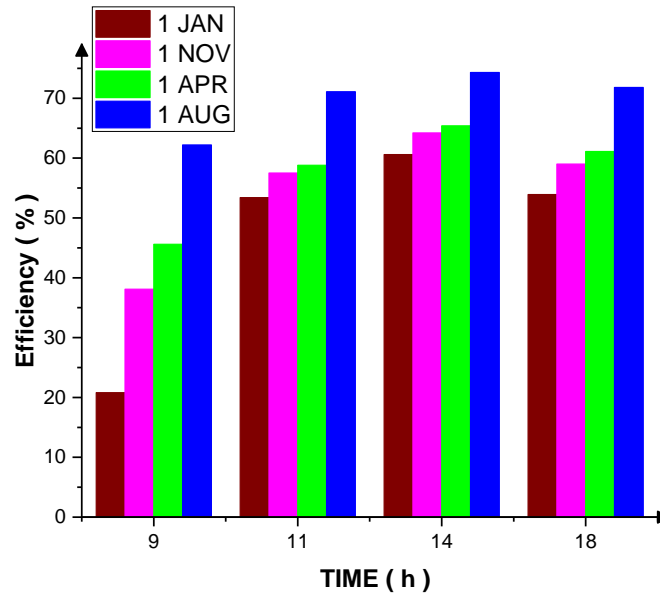


Figure V.26: The flat plate thermal solar collector efficiency during 4 days.

V. 3. 6. The thermal energy efficiency of the AGMD system

Figure V.27 shows the effect of the thermal energy efficiency of the AGMD module on different days of the year. The changing climate conditions are varied from winter to summer while keeping all other parameters constant as mentioned in (Table V.3). As shown in (Figure V.27) and by percentage, the energy efficiency increases by 67.2 % between winter and summer. Over the entire range of time (throughout the year) 40.6 % increase in the energy efficiency is obtained at 9h, 34.7 % is obtained at 11h, 13.2 % is obtained at 14h and 39.7 % is obtained at 18h. Therefore, increasing the temperatures with the changing climate conditions every day from the year increases the thermal energy efficiency of the AGMD module. Thus, it increases the difference in partial pressure that assists the permeation process across the membrane.

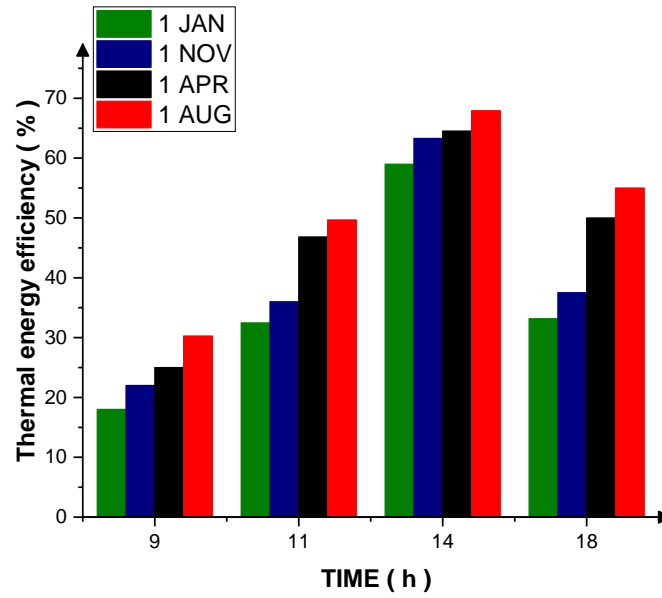


Figure V.27: The thermal energy efficiency of the AGMD module during 4 days.

V. 4. Experimental, simulation and economical Study of the solar AGMD system large scale

V. 4. 1. Model validation

Based on the experimental characteristics of the AGMD module, the simulation results are validated with experimental data obtained from the pilot solar thermal membrane distillation system mounted in Port Said, Egypt. The aim of this section was to test the validity of input data and output results under the same operating conditions for the AGMD module in order to obtain correct and accurate results. Figure V.28 shows the comparison between the experiment results and the simulated results obtained from the model used. Then, it presents the effect of inlet feed temperature on permeate flux at the hot and cold feed flow rate of 210 and 180 L/h respectively. The feed hot inlet temperature in the AGMD module is varied from 55 °C to 80 °C.

The system is run under the following operating conditions: hydrophobic PE membrane with pore size of 0.3 μm , thickness: 76 μm , total membrane area: 14.4 m^2 . As shown in Figures (V.28) and (V.29), It can be noticed that the hot and cold feed outlet temperatures and permeate flux of the AGMD module calculated by the present model has a good compatibility of no more than 5% in this experiment. The results show that increasing the feed inlet temperature increases the system flux significantly. Increasing the feed inlet temperature increases the vapor production and the driving force to permeation (the transmembrane temperature difference, and consequently the difference in partial pressures across membrane surfaces) which enhance permeation across the membrane.

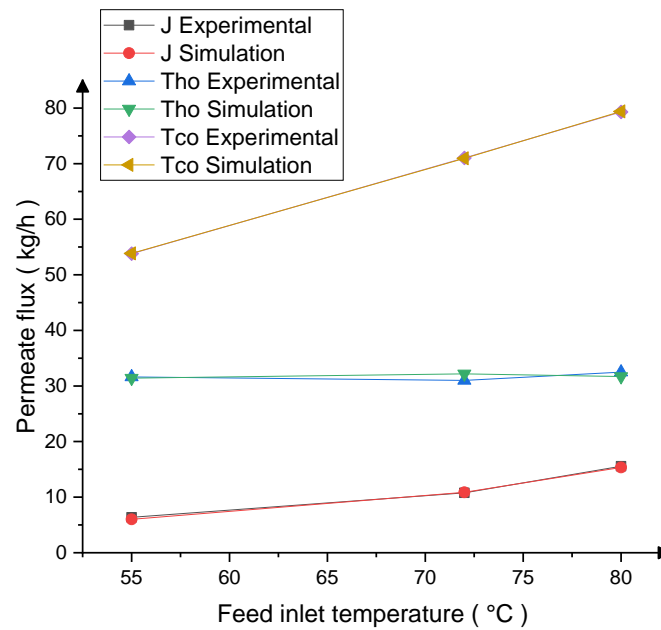


Figure V.28: The simulation and the experimental data of the permeate flux, hot and Cold feed outlet temperatures of the AGMD module with ($V_h=210$ L/h, $V_c=180$ L/h).

In order to examine the effect of feed flow rate on the AGMD flux; an experiment is conducted with variable feed flow rates while keeping all other parameters constant. It can be noticed that the distillate water flow of the AGMD module calculated by the present model has a good agreement with the experiment. The feed flow rate is selected at 120, 360 and 600 L/h in both of hot and cold feed inlet temperature. Figure V.29 shows the variation of distillate water flow with feed flow rate for selected feed hot inlet temperature in the AGMD module from 50 to 65 °C. The trend shows that increasing the feed flow rate increases the permeate flux substantially. Feed flow rate is very effective variable to increase the permeate flux at different feed temperatures. It is worth mentioning that the exponential nature of flux increase can better be observed at 600 L/h as compared to other feed flows of 120 and 360 L/h. Over the entire range of feed hot inlet temperature (50 to 65 °C) 45.5 % increase in flux is obtained at feed flow of 120 L/h, 52.6 % is obtained at 360 L/h and 61.3 % is obtained at 600 L/h.

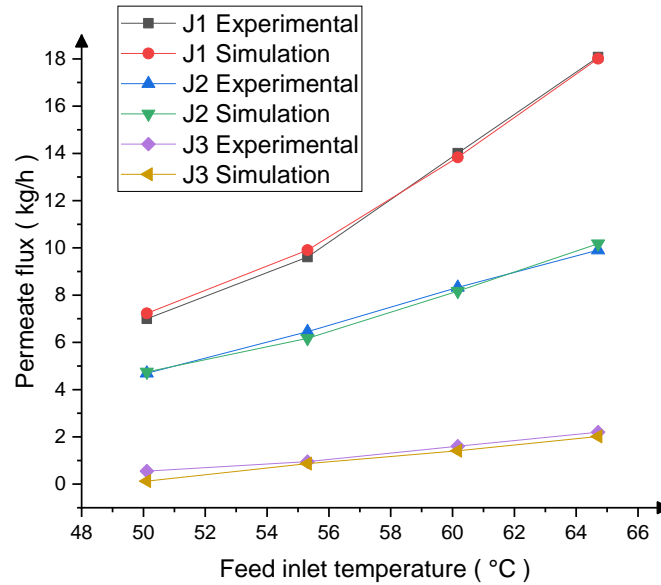


Figure V.29: The simulation and the experimental data of the permeate flux with (J1: $V_h=V_c= 600$ L/h, J2: $V_h=V_c= 360$ L/h and J3: $V_h=V_c= 120$ L/h).

V. 4. 2. Thermal capacity and permeate flux

Figure V.30 shows the outlet temperatures for flat plate and evacuated tube collectors, they have an area of 12 and 8 m² respectively. It is found that the outlet temperature increases and reaches 76 and 91 °C in winter and summer (29th June and December). Then, the result shows that ETC seems more effective as compared to FPC in each season. Therefore, plots show a remarkable influence of hot feed temperature during the day in winter and summer seasons by the percentage reaches 16.5-23.4 %.

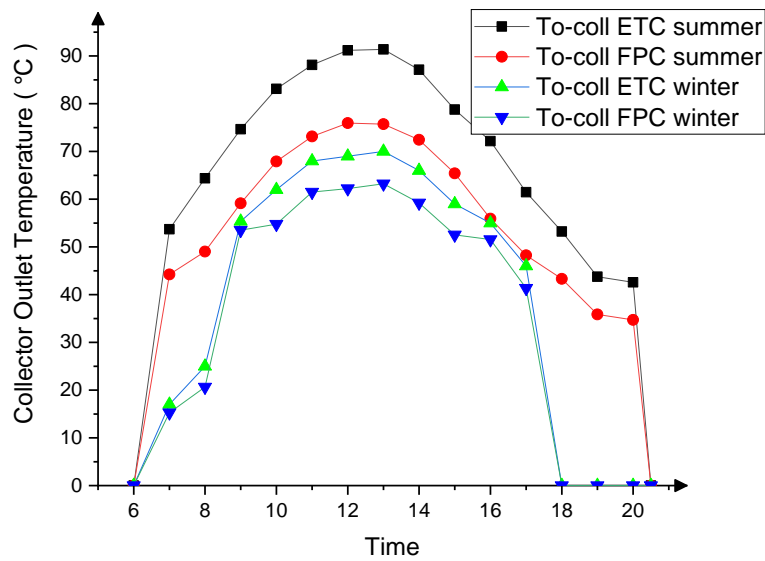


Figure V.30: Distribution of collector outlet temperature along the day during summer and winter season.

Figure V.31 shows the inlet feed temperatures of AGMD coming from the exchanger heaters and using the flat plate and evacuated tube collectors. The system runs under the following operating conditions: hydrophobic PE membrane with a pore size of $0.3 \mu\text{m}$, feed flow rate of 10 L/min with feed salinity of 38.5 g/kg . The inlet feed temperatures reach $56 \text{ }^\circ\text{C}$ in winter and $65.6 \text{ }^\circ\text{C}$ in summer. Therefore, it can be seen that the percentage increase in the high temperature when using ETC bigger than using FPC with 8 to 10.7 %.

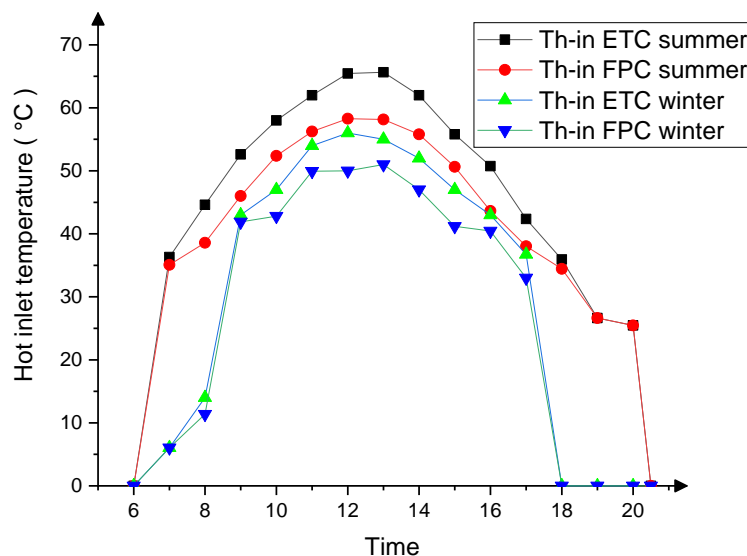


Figure V.31: Distribution feed inlet temperature of AGMD using FPC and ETC.

Figure V.32 shows the variation of permeate flux variation with keeping all other parameters constant as above. Clearly, the trends show that the permeate flux increases with time. Therefore, using ETC is very effective to increase the permeate flux than FPC at different times. It is worth mentioning that the exponential nature of flux increase can better be observed in summer as compared to other times in winter. Over the entire range of permeate flux (8.2 to 18.11 Kg/h) and between using ETC and FPC, 18.81 % increases in flux in winter and 30.44 % in summer.

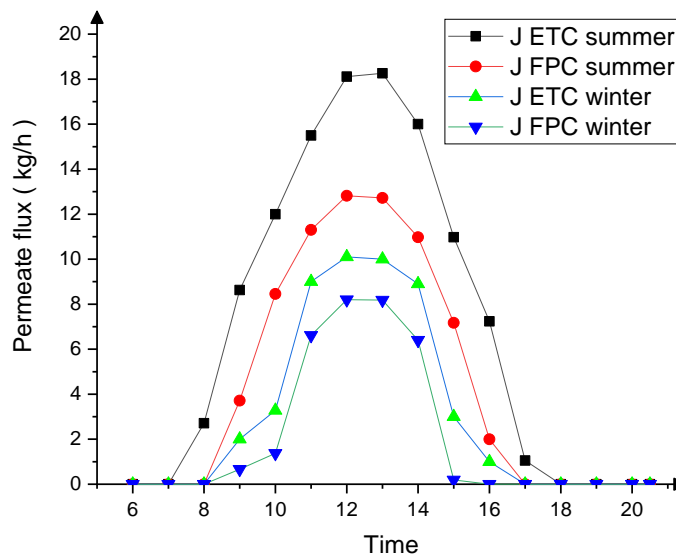


Figure V.32: Permeate flux of AGMD.

V. 4. 3. The Gain output ratio and the specific thermal energy consumption of the AGMD system

Figure V.33 shows the effect of the average feed water temperature and flow rate on the GOR and STEC for the AGMD module. In this figure, the coolant flow rate (V_c) was kept equal to the feed flow rate (V_f). The water flow rate varies from 2 to 10 L/min at each average feed water temperature 43, 46, 49, and 52 °C. The feed water temperature varies from 50, 55, and 60 to 65 °C. As shown in (Figure V.33), the GOR increases from 0.5 to 4.4 as flow rates, hot and average feed water temperatures increase, while the STEC decreases from 346.55 to 158.83 kWh/m³ with increasing, and this is very effective variables to increase the GOR of the AGMD system. This appears more at the high feed water temperatures and flow rates. By percentage, increasing the average feed temperature from 43 to 52 °C and flow rate from 2 to 10 L/min resulted in GOR increase from 12.9 % to 59 % while resulted in STEC decrease from 10.5 % to 25 %.

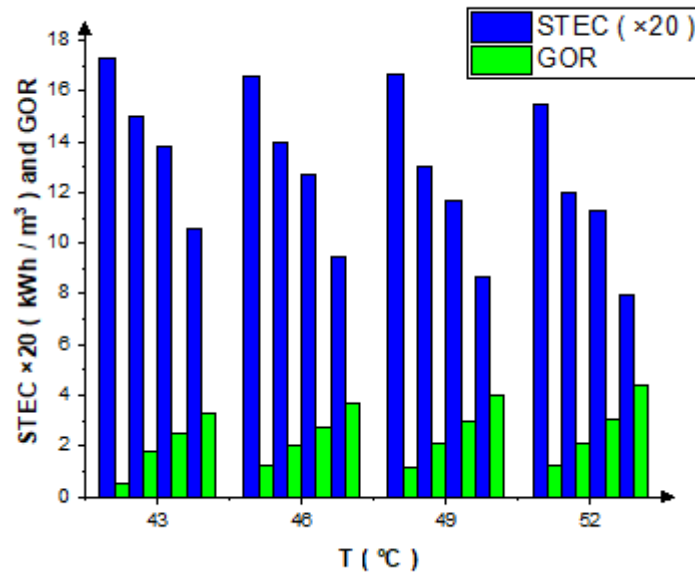


Figure V.33: Average temperatures on STEC (kWh/m^3) and GOR of the AGMD system ($V_f = V_c = 2, 3, 6$ and 10 L/min).

Results of the comparison study between the performance of the current proposed system and the results of several surveyed studies are listed in (Table V.3). In comparison to the other published data, the current study achieved a remarkable improvement as STEC has been reduced to $158 \text{ kWh per } 1 \text{ m}^3$. This can be attributed to the modified system configuration to reduce the amount of heat source required to raise the temperature. Superior enhancement in the GOR has been obtained in the present membrane desalination system using solar collectors compared to other surveyed systems. This can be ascribed to the low thermal energy needed to raise the feed temperature.

Table V.3: Comparison between the present study and previous studies.

	Present study	Literature					
		[5]	[6]	[7]	[8]	[9]	[10]
Feed water flow rate (L/h)	600	200	250-400	-	500	600	180
Inlet feed temperature to the evaporator	52	85	-	60-80	85	80	70
STEC (kWh/m^3)	158.83	200	200-300	200-300	600	269.8	1080
GOR	4.4	4	0.3-0.9	0.4-0.7	-	2.21	0.41

V. 4. 4. The thermal energy efficiency of the AGMD system

Figure V.34 shows the effect of the average feed temperatures on the thermal energy efficiency at different flow rates of the AGMD module. The flow rate is varied from 2 to 10 L/min while keeping all other parameters constant as mentioned in (Figure V.33). As show in (Figure V.34), the energy efficiency increases of 72% at the average feed temperature 52 °C and the flow rate 10 L/min. The results showed the energy efficiency at the high feed temperatures is 17.2 to 86.9 % higher than the low feed temperatures. Over the entire range of average feed temperature (43 to 52 °C) 86.9 % increase in energy efficiency is obtained at the feed flow rate of 2 L/min, 35.8 % is obtained at 3 L/min, 17.2 % is obtained at 6 L/min and 22.3 % is obtained at 10 L/min. Therefore, increasing the feed temperature and flow rate increases the difference in partial pressure that assists the permeation process across the membrane.

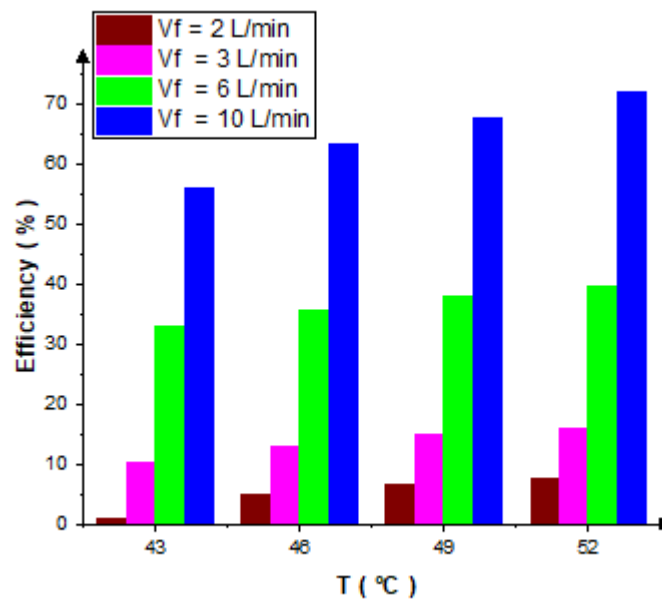


Figure V.34: Average temperatures on the thermal energy efficiency of the AGMD system (Vf = Vc = 2, 3, 6 and 10 L/min).

V. 4. 5. Mitigation potential of CO2 emissions

Fossil fuel power stations seriously contribute to the problem of global CO2 emissions. This severe environmental problem requires urgent attention and, therefore, can be relatively tackled by expanding the use of renewable sources of energy including solar energy as a clean energy source to reduce the CO2 emission [11]. An additional benefit of implementing the CPV technology, besides sustainability, is its cleanness. Moreover, AGMD systems, which utilize FPC and ETC for water heating for desalination, offer a new sustainable trend for decreasing

the reliance on grid electricity and, subsequently, highly participating in reducing carbon oxides emission levels. The reduction of CO₂ release level utilizing the proposed AGMD system is estimated as the following formula [12]:

$$m_t = m_e \times dE \times t_{life} \quad (11)$$

where m_t is the reduction in the emission level of CO₂ (g) over its life cycle, m_e is the average emission of CO₂ (904 g/kWh) issued from a coal fuel-driven power station [13], dE (kWh/ day) is the total energy saving per day of the proposed AGMD system, and t_{life} (day) is the economic lifespan of the AGMD system, counted as 20 years [14].

Figure V.35 shows the accumulated solar intensity, the reduction in CO₂ emissions, and, therefore, the freshwater productivity for various solar collector configurations on each day. This figure illustrates that the accumulated daily irradiance values for the two test days of June 28th and June 29th, were 11,951 W/day and 12,000 W/day, respectively, during the experiments with FPC and ETC. Clearly, the daily accumulated production of fresh water is highly increased by use the ETC system. The peak of freshwater productivity achieved for this set of experiments at ETC system is 78.87 kg/day. Moreover, the reduction in CO₂ emissions per day due to the utilization of the FPC system is 12.73 kg. These figures demonstrate the proportionality of the cut down in CO₂ with the solar collector configuration, which is referred to as the increase in the freshwater productivity with the ETC, as previously discussed. In the case of an ETC system, the daily accumulated cut down of carbon dioxide CO₂ as a result of employing the proposed AGMD system reached a value of 19.93 kg.

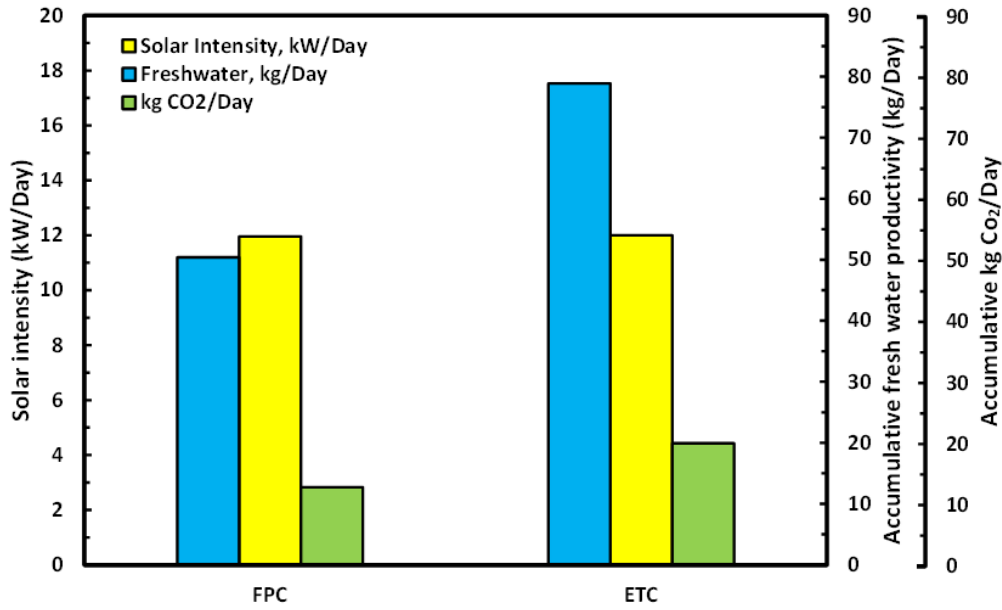


Figure V.35: The daily accumulated solar intensity: accumulated daily potable water productivity and saving of CO₂ against the solar collector configurations.

V. 4. 6. Economic analysis

The total cost of producing potable water from the SMD system is mainly affected by both operational and capital expenditures. In this study, economic assessment is conducted using Leveled Cost Of Water (LCOW) for assessing the cost-efficiency of water generated by the SMD system. LCOW deals with costs of determining the price per m³ of water production over the considered lifetime period [15]. The detailed LCOW formulas used in the current work are given in Eqs. (12) to (16), taking into account the leveled cost of the investment LC_{inv} (\$), the maintenance and operation expenditures LCO and M (\$), and the running cost (rc) of the powered components of system. The cost breakdown of the solar system using FPC and ETC with SMD system are illustrated in Tables (V.4), (V.5) and (V.6) respectively. The cost of purifying 1 m³ of water LCOW (US\$/m³) can be expressed as in Eq. (12) [16]:

$$LCOW = \frac{LC_{inv} \times CRF + LCO_{\&M} + rc - ASV}{V_P} \quad (12)$$

The capital recovery factor referred as CRF represented in Eq. (13) [16].

$$CRF = \frac{i \times (1+i)^n}{(1+i)^n - 1} \quad (13)$$

Where i is the annual interest rate.

The result of the Salvage Value (half of the reusable components) and Sinking Fund Factor (SFF) gives the Annual Salvage Value (ASV), which is formed as [17]:

$$ASV = SFF \times LC_{inv} \quad (14)$$

Sinking Fund Factor (SFF) represented as:

$$SFF = \frac{i}{(1+i)^n - 1} \quad (15)$$

Table V.4: Cost breakdown of FPC case.

Investment costs	Unitary cost (US\$)	Quantity	Costs (US\$)
FPC cost (Ccol)	100 /m ²	12 m ²	1,200
Solar Pump	50		50
Heat storage tank [18]	800 /m ³	0.3 m ³	240
Hydraulics/piping	30% · Ccol [19]		360
Installation costs	5% of total component cost [20]		92.5
Total			1,942.5

Table V.5: Cost breakdown of ETC case.

Investment costs	Unitary cost (US\$)	Quantity	Costs (US\$)
ETC cost (Ccol)	110 /m ²	8 m ²	880
Solar Pump	50		50
Heat storage tank [18]	800 /m ³	0.3 m ³	240
Hydraulics/piping	30% Ccol [19]		264
Installation costs	5% of total component cost [20]		71.7
Total			1,505.7

Table V.6: Cost breakdown of MD system.

Components	(MD) (US\$)
AGMD module	1000
Membrane 36 \$/m ² [18]	529.2
Galvanized steel, stand and constructions	50
Water pump	50
Piping, valves and tanks	100

The water production by the proposed SMD system during the year is estimated to be 18390 kg, 28789 kg when used FPC and ETC solar system, respectively. The initial investment cost of MD system is 1729.2 US\$, solar FPC and ETC system is 1,942.5 US\$, 1,505.5 US\$, respectively. The economic life of the SMD system considered as 20 years and the annual rate of interest as 10% [21], while replacement of the membranes suggested to be every 5 years. The CRF of about 11.74 % was estimated by Eq. (13) and both costs of maintenance and operation are taken as 2 % of the initial capital cost [22].

The operating costs of the water pumps of the proposed SMD system during the year can be evaluated on the basis of the running cost provided by Elminshawy et al. [17]:

$$rc = 365 \times W_p \times \text{Time of day} \times \text{Cost of kWh} \quad (16)$$

where W_p is the energy consumption of circulating pumps and the cost of electricity is 0.016 US\$/ per kWh [38]. The cost of electricity of consumed power by pumps is shown in (Table V.7):

Table V.7: Running cost estimation with LCOW of SMD system.

Parameters	FPC case (US\$)	ETC case (US\$)
ASV	32.05	28.23
LC_{inv}	3,671.7	3,234.7
$LC_{O\&M}$	73.43	64.69
rc	7.00	7.88
Cost of kWh	0.016	0.016
$LCOW/ m^3$	26.08	14.73

It was estimated that the LCOW for the SMD system was 26.08 (US\$/m³), 14.73 (US\$/m³) for FPC and ETC case, respectively. A comparison is made in (Table V.8) between the present research, considering 20 years as economic life, and the work of previous studies [24]. Table V.8 shows that the combination of the SMD system with the heat source from the ETC module results in a marked decrease in the Levelled cost of water relative to other SMD systems.

Table V.8: A leveled cost comparison with others.

Reference	n (economic life of MD system), Year	Levelled cost of water (LCOW), (\$/m ³)
Current study	20	14.73
[18]	20	18.34
[24]	20	29.9
[25]	20	84.7


References

- [1] I. Janajreh, D. Suwwan, R. Hashaikeh, Assessment of direct contact membrane distillation under different configurations, velocities, and membrane properties, *Appl. Energy* 185 (2017) 58–73
- [2] I. Janajreh, K. ElKadi, R. Hashaikeh, R. Ahmed, Numerical investigation of air gap membrane distillation (AGMD): Seeking optimal performance, *Desal.* 424 (2017) 122–130
- [3] C.Y. Iguchi, W.N. dos Santos, R. Gregorio, Determination of thermal properties of pyroelectric polymers, copolymers and blends by the laser flash technique, *Polymer Testing* 26 (2007) 788–792
- [4] N.T. Uday Kumar and A. Martin, Experimental modeling of an air-gap membrane distillation module and simulation of a solar thermal integrated system for water purification. *Desal. Water Treat.*, 84 (2017) 123–134
- [5] J. Koschikowski, M. Wieghaus, and M. Rommel, Solar thermal-driven desalination plants based on membrane distillation, *Desalination* 156 (2003) 295-304.
- [6] Banat, F., Jwaied, N., Rommel, M., Koschikowski, J., & Wieghaus, M. Desalination by a “compact SMADES” autonomous solarpowered membrane distillation unit. *Desalination*, 217(2007) (1-3), 29-37.
- [7] Banat, F., Jwaied, N., Rommel, M., Koschikowski, J., & Wieghaus, M. Performance evaluation of the “large SMADES” autonomous desalination solar-driven membrane distillation plant in Aqaba, Jordan. *Desalination*, 217(2007) (1-3), 17-28.
- [8] G. Zaragoza, A. Ruiz-Aguirre, and E. Guillén-Burrieza, Efficiency in the use of solar thermal energy of small membrane desalination systems for decentralized water production, *Appl. Energy* 130 (2014) 491-499.
- [9] Ruiz-Aguirre, A., Andrés-Mañas, J. A., Fernández-Sevilla, J. M., & Zaragoza, G. (2018). Experimental characterization and optimization of multi-channel spiral wound air gap membrane distillation modules for seawater desalination. *Separation and Purification Technology*, 205, 212–222
- [10] Alawad, S. M., & Khalifa, A. E. Performance and energy evaluation of compact multistage air gap membrane distillation system: An experimental investigation. *Separation and Purification Technology*, 268, (2021), 118594
- [11] Chel A, Tiwari GN. Stand-alone photovoltaic (PV) integrated with earth to air heat exchanger (EAHE) for space heating/cooling of adobe house in New Delhi (India). *Energy Convers Manage* 2010;51(3):393–409.
- [12] Elminshawy NAS, El-Ghandour M, Elhenawy Y, Bassyouni M, El-Damhogi DG, Addas MF. Experimental investigation of a V-trough PV concentrator integrated with a buried water heat exchanger cooling system. *Sol Energy* 2019;193:706–14.
- [13] Liu Z, Yu Z, Yang T, Li S, El Mankibi M, Roccamena L, et al. Experimental investigation of a vertical earth-to-air heat exchanger system. *Energy Convers. Manag.* 2019;183:241–51.
- [14] Rafique MM, Bahaidarah HMS, Anwar MK. Enabling private sector investment in off-grid electrification for cleaner production: optimum designing and achievable rate of unit electricity. *J Cleaner Prod* 2019;206:508–23

- [15] Li Q, Beier L-J, Tan J, Brown C, Lian B, Zhong W, et al. An integrated, solar-driven membrane distillation system for water purification and energy generation. *Appl Energy* 2019;237:534–48.
- [16] Swaminathan J, Chung HW, Warsinger DM, Lienhard JHV. Energy efficiency of membrane distillation up to high salinity: evaluating critical system size and optimal membrane thickness. *Appl Energy* 2018;211:715–34.
- [17] Elminshawy NAS, Gadalla MA, Bassyouni M, El-Nahhas K, Elminshawy A, Elhenawy Y. A novel concentrated photovoltaic-driven membrane distillation hybrid system for the simultaneous production of electricity and potable water. *Renew Energ* 2020;162:802–17. <https://doi.org/10.1016/j.renene.2020.08.041>.
- [18] Li G, Lu L. Modeling and performance analysis of a fully solar-powered stand-alone sweeping gas membrane distillation desalination system for island and coastal households. *Energy Convers Manage* 2020;205:112375. <https://doi.org/10.1016/j.enconman.2019.112375>.
- [19] Report M. Performance and cost estimations of final industrial size of MEDESOL-2 technology. Spain: University of La Laguna; 2010.
- [20] Kumar NTU, Martin A. Techno-economic optimization of solar thermal integrated membrane distillation for cogeneration of heat and pure water. *Desalin Water Treat* 2017;98:16–30.
- [21] Montes MJ, Rovira A, Muñoz M, Martínez-Val JM. Performance analysis of an integrated solar combined cycle using direct steam generation in parabolic trough collectors. *Appl Energy* 2011;88(9):3228–38.
- [22] Elhenawy Y, Hafez G, Abdel-Hamid S, Elbany M. Prediction and assessment of automated lifting system performance for multi-storey parking lots powered by solar energy. *J Cleaner Prod* 2020;266:121859.
- [23] Elsakka Mohamed Mohamed, Ingham Derek B, Ma Lin, Mohamed Pourkashanian. Comparison of the computational fluid dynamics predictions of vertical axis wind turbine performance against detailed pressure measurements. *Int J Renew Energy Res* 2021;11(1):276–93.
- [24] Banat F, Jwaied N. Economic evaluation of desalination by small-scale autonomous solar-powered membrane distillation units. *Desalination* 2008;220(1-3):566–73.
- [25] Moore SE, Mirchandani SD, Karanikola V, Nenoff TM, Arnold RG, Eduardo Sáez A. Process modeling for economic optimization of a solar driven sweeping gas membrane distillation desalination system. *Desalination* 2018;437:108–20



GENERAL CONCLUSION



A. MARNI SANDID
DOCTORAL THESIS
2023

General Conclusion and perspectives

Membrane distillation is a process with several advantages regarding the integration into a solar thermally driven desalination system. In this thesis, the main studies are:

- 1) Effects of operating parameters on the AGMD module for desalination.
- 2) Development and optimization study of the solar AGMD system small scale.
- 3) Simulation and controlling and optimization study of the solar AGMD system small scale.
- 4) Experimental, simulation and economic Study of the solar AGMD system large scale.

(1) A symmetrical 2D flow systems are performed on AGMD module using non-isothermal CFD coupled thermally with the solid porous membrane.

- ✚ In the membrane surfaces temperatures, the outlet hot temperatures are more important in counter-current flow. Therefore, the thermal behavior of the fluid in AGMD module notes that the exchange is more important the more presides over the wall and especially at the outlets of the AGMD module. In the AGMD module, the concentration of the condensed permeate in AGMD isn't never in direct contact with the membrane surface, hence there isn't risk of membrane wetness on the permeate side.
- ✚ Increasing the feed temperature increases the vapor production and the driving force to permeation, which enhance permeation along the membrane surface. Decreasing the cold temperature increases the difference of partial pressure that assist the permeation process across the membrane. The variation of mass flux with feed flow rate shows that increasing the feed flow rate increases the mass flux substantially. In addition, increasing the cold flow rate increases the flux marginally.
- ✚ The copolymer P(VDF-TrFE) (80/20) is better than the other materials of MD. The flux average, efficiency and TPC reach 12.99 (g/m²s), 44.74 and 45.06 % respectively. The lower density and thermal conductivity are more effective for increasing the distilled water flow in AGMD processes. In addition, the mass flux reaches 118.95 (g/m²s) using the laminar flow regime while it reaches 193.5 (g/m²s) using the turbulent flow regime, respectively. Therefore, the variations on the different membrane parameters are very effective and the turbulent flow regime is better than the laminar flow regime.

(2) A dynamic simulation of the membrane distillation module integrated solar thermal system has been studied for controlled the distillate water at different times and in changing climatic conditions throughout the year in Ain-Temouchent weather, Algeria.

- ✚ A TRNSYS model develops solar water heating systems with flat plate collectors with an area of 12.75 m^2 , heat exchanger, storage tanks, the auxiliary heater, and 10 photovoltaic panels; each one has an area of 1.6 m^2 with three of the energy storage batteries (12V, 100Ah). Accordingly, the control system and model of the thermal system of AGMD process designs to produce distillate water depending on the solar energy only as permanent and renewable energy to save all costs, whereas the auxiliary heating consumed the highest value of 1.5 KW to augment the water temperature to $87 \text{ }^\circ\text{C}$ in the cold climatic conditions. Besides, the electric energy of the pumps uses to perform the AGMD process is 0.6 kilowatts, which is calculated and added to the photovoltaic system using TRNSYS and PVGIS programs.
- ✚ The thermal system temperatures reach the same value of $87 \text{ }^\circ\text{C}$ on different days from the year (11/12, 11/03, 11/08, and 11/10). Thus, The proposed solar AGMD system has shown favorable potential application in desalination of water can produce 5.5 kg/h of distilled water at different times and in changing climatic conditions throughout the year in Ain-Temouchent weather, Algeria.

(3) A performance study of the solar thermal driven membrane distillation system was simulated using the TRNSYS tool in Ain-Temouchent City, Algeria. A very simple AGMD system with a total collector area of 12.75 m^2 produces 3 to 5 L/h of distilled water flow throughout the entire year.

- ✚ It was observed that the effect of flow rates of feed inlet and hot temperature in AGMD is very effective to increase the permeate flux. Distillate flux was varied from 3 to 5 Kg/h in various intermittent climatic conditions. Based on the numerically characterized AGMD module, the results show that increasing the feed inlet temperature increases the system flux significantly. Increasing the feed inlet temperature increases the vapor production and the driving force to permeation (the transmembrane temperature difference, and consequently the difference in partial pressures across membrane surfaces) which enhances permeation across the membrane. Higher values are achieved with high hot feed temperature and flow rates. The energy efficiency of the AGMD module and the collector efficiency values reach 68 % and 74 % respectively. Besides, the brine

that contains the high salt concentration is completely dispensed with this process.

- ✚ To save costs, a photovoltaic system uses depending renewable energy (solar energy). Therefore, the energy needed calculates for the pumps and replaces by two photovoltaic panels, each one has an area of 1.6 m² using an energy storage battery (12V, 100Ah) via TRNSYS and PVGIS help programs. Accordingly, the purpose of this study is the use of solar panels in the photovoltaic system to produce the necessary electrical energy.

(4) A full test rig was built to evaluate the efficiency of a solar-powered MD module during the FPC and ETC heating processes in Port Said City, Egypt. A pilot-scale experimental study was conducted on the efficiency of a 14.4 m² multichannel spiral-wound AGMD module for water desalination in attaining output capacities up to 18 kg/h from the flow rate of distillate water.

- ✚ The solar-powered AGMD system's dynamic simulation findings indicated strong compliance with the experimental values. Dynamic simulation findings of the solar-powered AGMD system show good agreement with experimental results. In addition, the results showed that the permeate flow of the AGMD module with the ETC collector was 18.81%–30.44% higher than that of the AGMD module with the FPC collector, and its cost was lower by 22.48%.
- ✚ Raising the inlet temperature dramatically increased the system flow, as found by the experimentally assessed AGMD module. Furthermore, the proposed AGMD system produces 28.78 m³/year of fresh drinking water for USD 14.73/m³ while reducing carbon dioxide emissions by 7,274.45 kg/year.

Future work

- ✚ The effective study in this thesis will be useful to develop and optimize in the future both the small and large scales MD processes for desalination.
- ✚ The AGMD system using solar energy for seawater desalination will be useful for further simulations or applications of the technology.
- ✚ The equivalent of a daily distillate production rate can make the contemporary model for the AGMD process usable and suitable to be a system compatible in the future with all intermittent climatic conditions and all over the world.

Finally, these types of projects that integrate renewable energy technologies with additional services are in principle attractive in terms of the associated socio-economic benefits.

APPENDIX

Appendix A: Compositions of drinking water quality

Table 1: World Health Organization (WHO) guidelines for drinking water quality.

Parameters	WHO	Units
T	12 - 25	(°C)
pH	6.5 – 8.5	-
EC	400	µs/cm
Na ⁺	200	mg/l
Ca ²⁺	100	mg/l
Mg ²⁺	50	mg/l
K ⁺	20	mg/l
HCO ₃ ⁻	125 - 350	mg/l
Cl ⁻	250	mg/l
SO ₄ ²⁻	250	mg/l
NO ₃ ⁻	50	mg/l
TDS	500 - 1000	mg/l
TH	500	mg/l
Fe ²⁺	0.3	mg/l
Mn ²⁺	0.1 – 0.5	mg/l
Zn ²⁺	0.01 – 3	mg/l
Al ³⁺	0.2	mg/l
Pb ²⁺	0.01	mg/l
Cu ²⁺	2	mg/l
Cd ²⁺	0.003	mg/l

Appendix B: 3D Surface Plots

Based on the parameters of the Multi-channel spiral wound AGMD system in chapter VI, the 3D surface plots of T_{co} (°C), T_{ho} (°C) and J (kg/h) are:

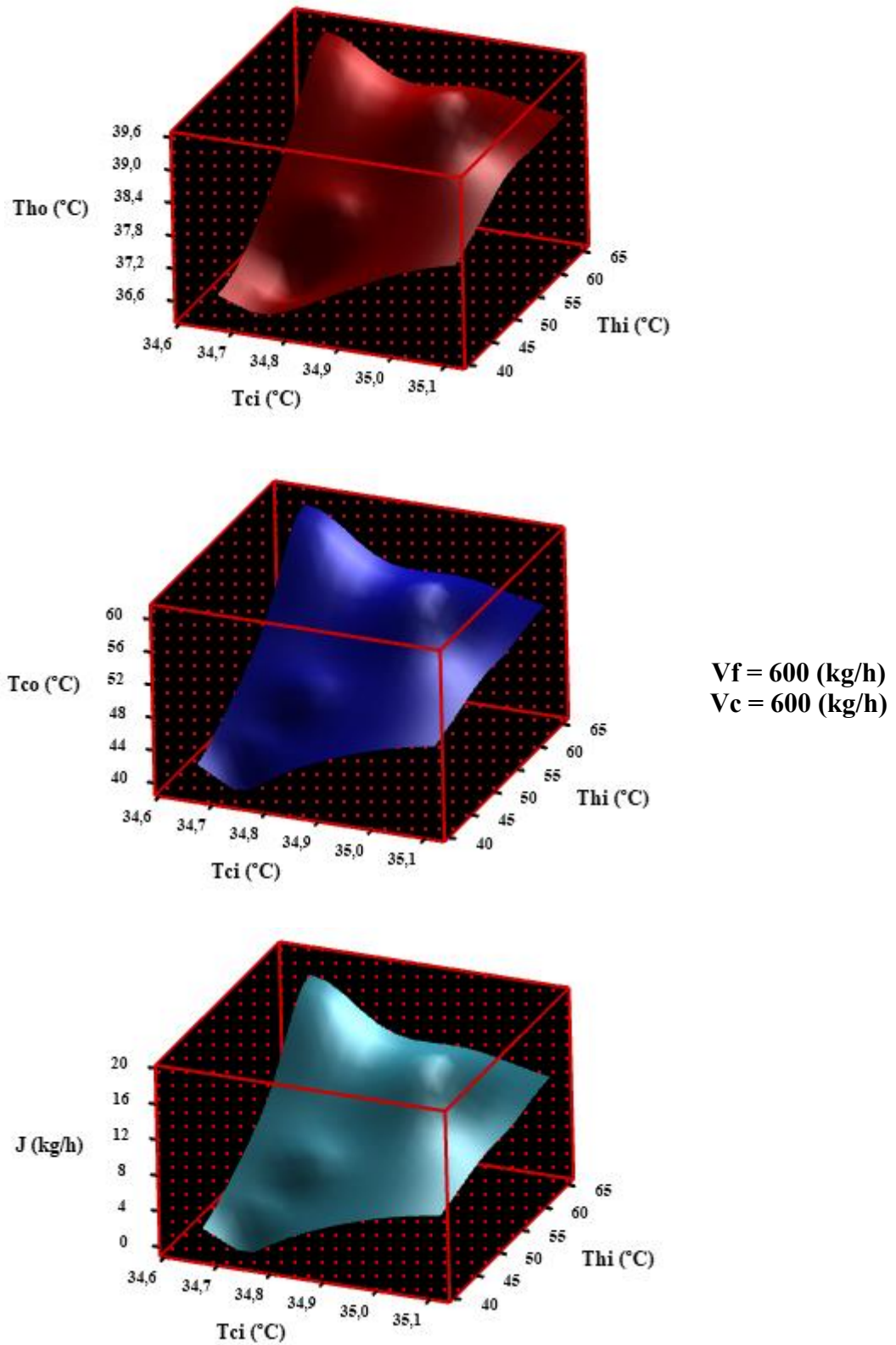
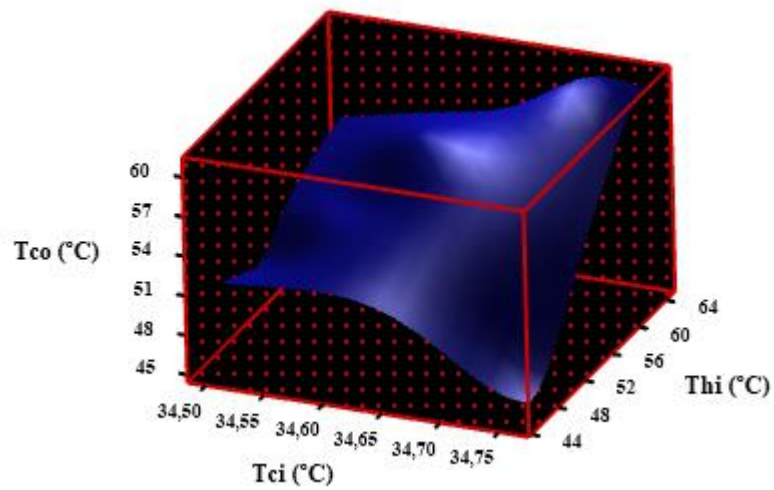
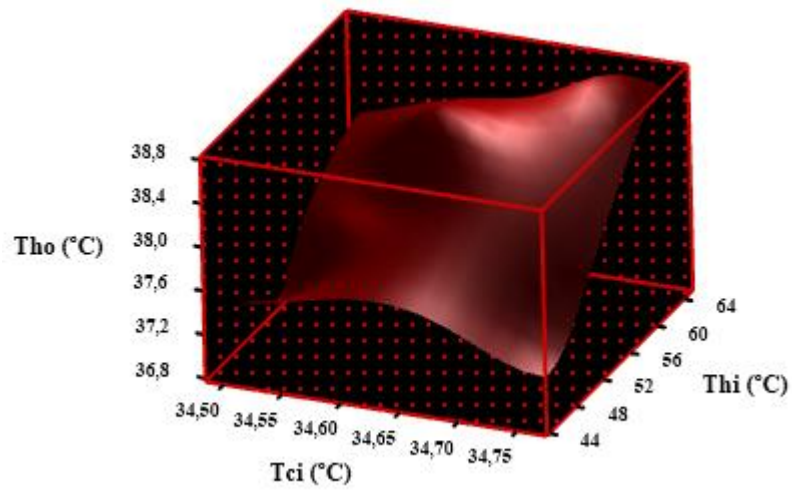


Figure 1: 3D Surface Plot of T_{ho} (°C), T_{co} (°C) and J (kg/h);

$$V_f = V_c = 600 \text{ (kg/h)}.$$



$$V_f = 360 \text{ (kg/h)}$$
$$V_c = 360 \text{ (kg/h)}$$

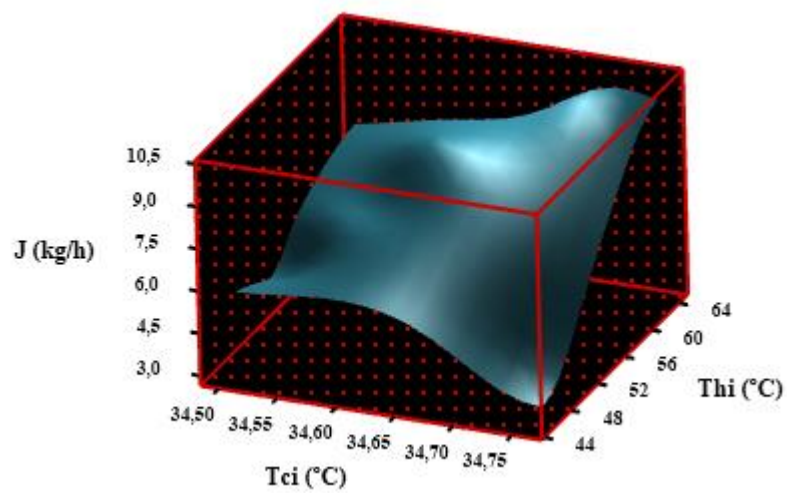


Figure 2: 3D Surface Plot of Tho (°C), Tco (°C) and J (kg/h);
 $V_f = V_c = 360 \text{ (kg/h)}$.

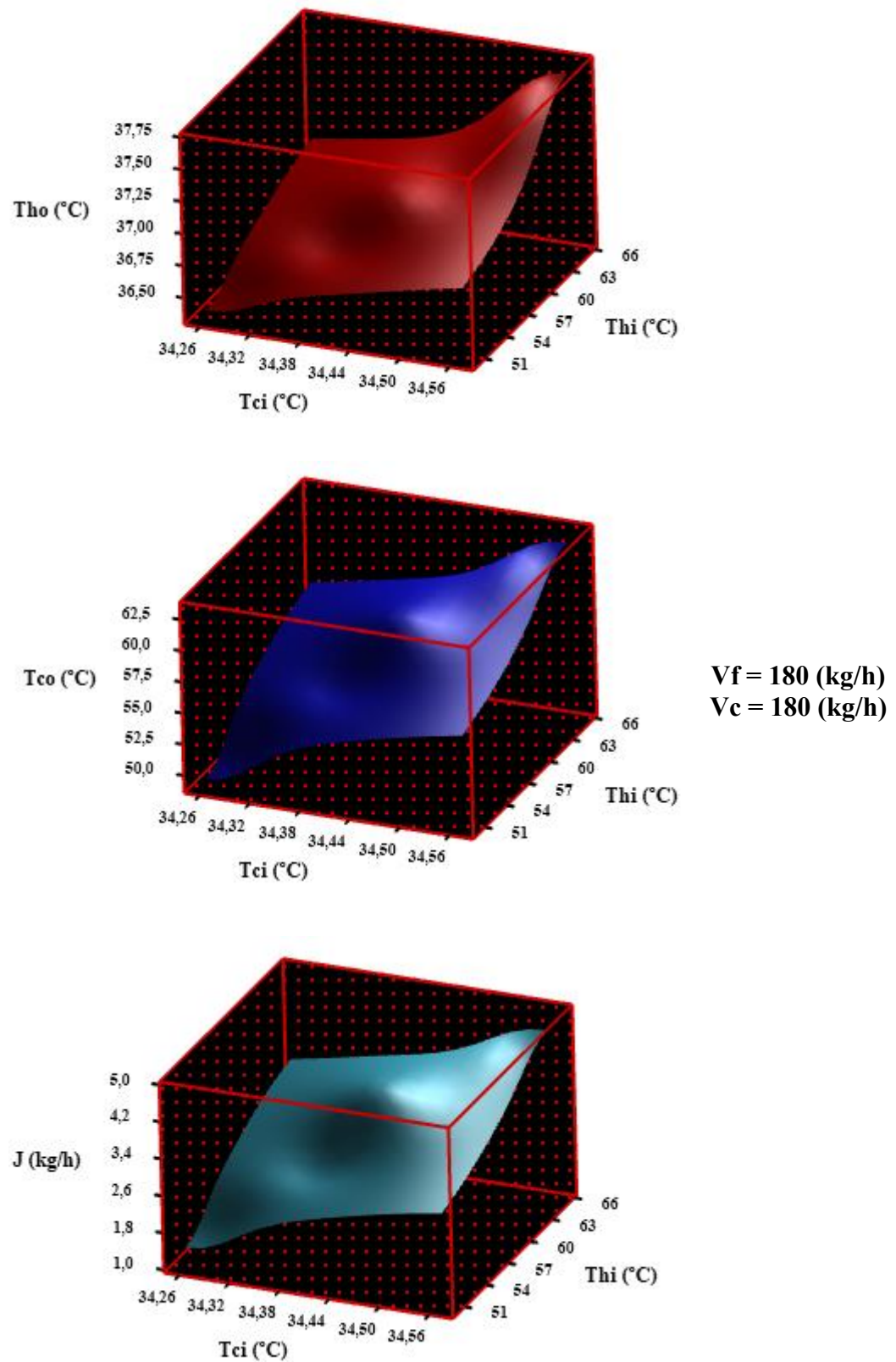


Figure 3: 3D Surface Plot of Th_o (°C), $T_{c,o}$ (°C) and J (kg/h);
 $V_f = V_c = 180$ (kg/h).

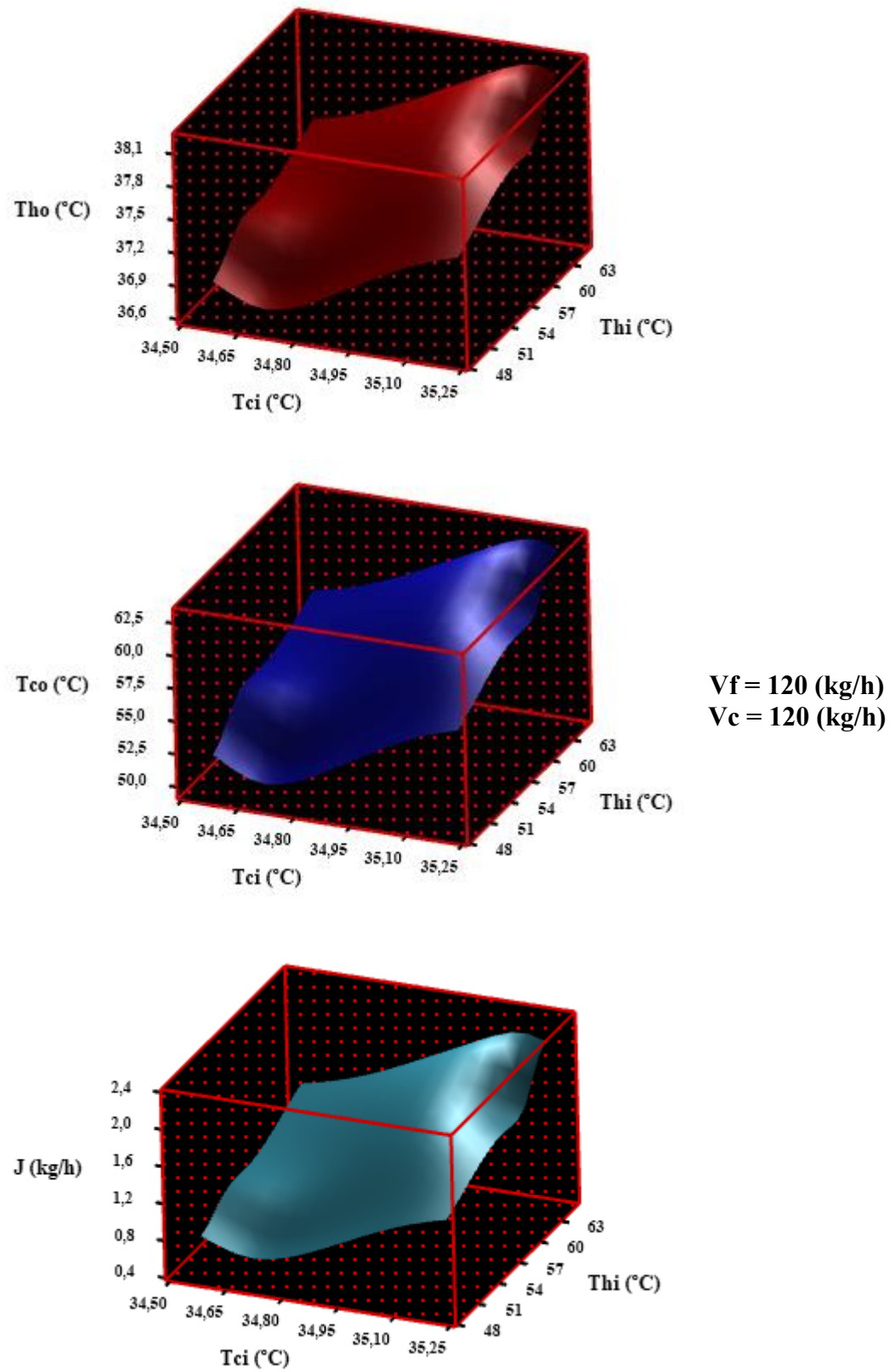


Figure 4: 3D Surface Plot of T_{ho} (°C), T_{co} (°C) and J (kg/h);
 $V_f = V_c = 120$ (kg/h).

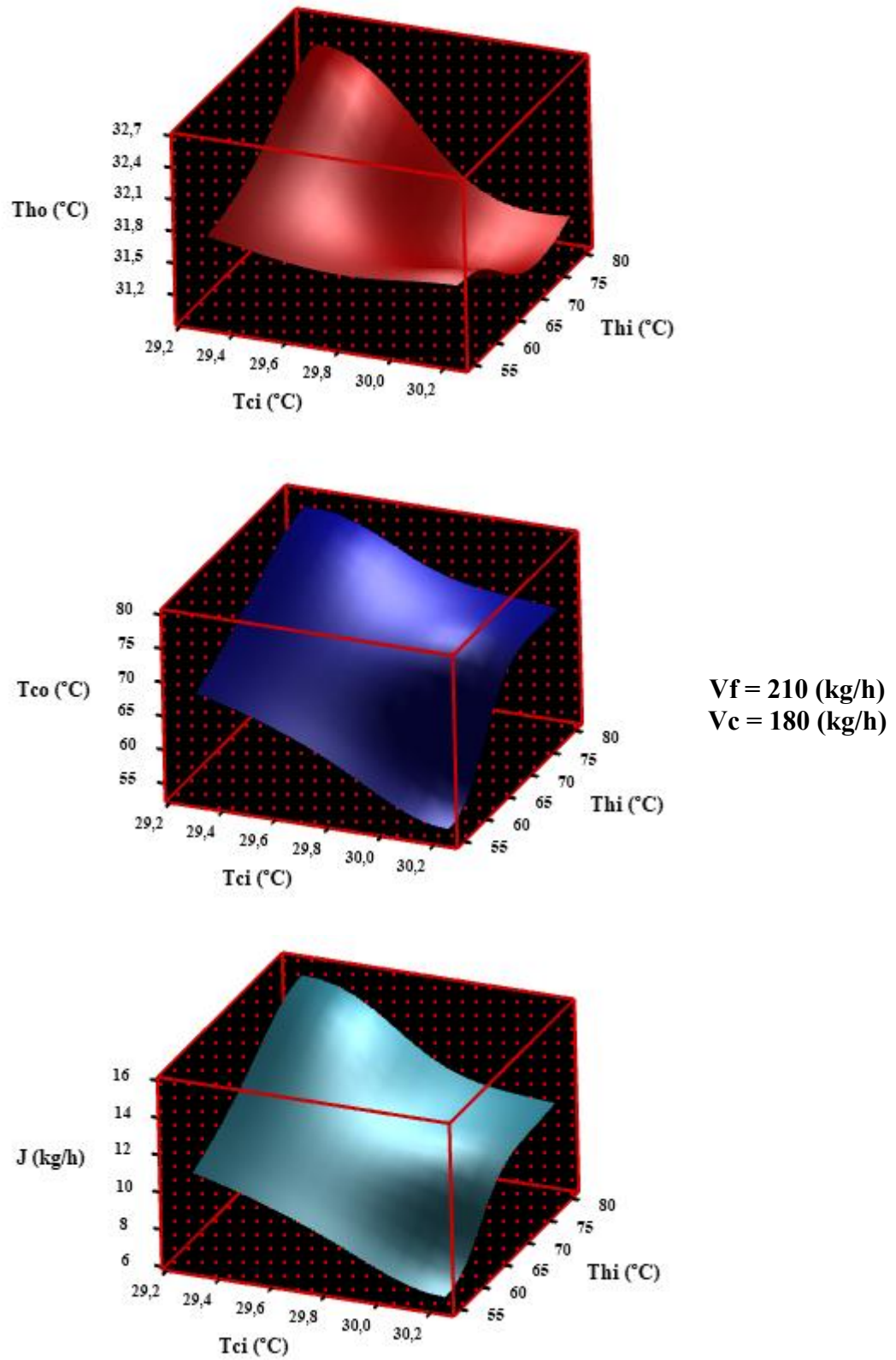


Figure 5: 3D Surface Plot of T_{ho} (°C), T_{co} (°C) and J (kg/h);
 $V_f = 210$ (kg/h) and $V_c = 180$ (kg/h).

Abstract

Solar thermal energy for membrane distillation desalination is a green and safe way for areas where water scarcity and solar irradiance are strongly correlated. In the desalination field, the membrane distillation (MD) is a new process of producing distilled water that has been developed and tested in recent years. In this thesis, the main studies include: (1) Effective study of operating parameters on the AGMD module for desalination. (2) Simulation and controlling study of the solar AGMD system small scale. (3) Development and optimization study of the solar AGMD system small scale. (4) Experimental, simulation and economic Study of the solar AGMD system large scale.

- The first study presents the effect of the operating temperatures and the flow rates on the distillate flux that can obtain from a hydrophobic membrane having the characteristics: pore size of 0.15 μm ; thickness of 130 μm ; and 85% porosity. The new approach in the present numerical modeling has allowed examining effects of the nature of materials (Polyvinylidene fluoride (PVDF) polymers, copolymers and blends) used on thermal properties. The obtained results found that, copolymer P(VDF-TrFE) (80/20) is more effective than the other materials of membrane distillation (MD). The mass flux and efficiency reach 193.5 ($\text{g}/\text{m}^2\text{s}$), and 83.29 % using turbulent flow and an effective area 3.1 m^2 , respectively.

- The second study presents the integrated single cassette AGMD module in the solar thermal desalination system which is validated and numerically simulated with the TRNSYS program. This model is studied to be ideal for obtaining a distilled water flow rate of 5.5 kg/h at different times under changing climatic conditions throughout the year in Ain-Temouchent weather, Algeria. Therefore, the energy needed is calculated for the auxiliary heater and is replaced by 10 photovoltaic panels, each one has an area of 1.6 m^2 using three of the energy storage batteries (12V, 100Ah) with 1.5 KW. It was found that when the inlet temperature of AGMD reaches 85 $^{\circ}\text{C}$, the distilled water flow from the distillation membrane reaches 5.5 kg /h and that remains stable on different days throughout the year by relying solely on solar energy.

- The third study presents a numerical study to investigate the solar AGMD system for seawater desalination. The solar MD system includes both flat plate collectors and photovoltaic panels with a total membrane area of AGMD: 0.2 m^2 . Therefore, the photovoltaic system with the energy storage batteries (12V, 100Ah) is used to power electrically the pumps and sensors. It was found that the solar AGMD system is used for the production of 3-5 L/h of distilled water flow. Besides, the brine that contains the high salt concentration is completely dispensed with this process. In addition, the energy efficiency of the AGMD module and the collector efficiency values reach 68 % and 74 % respectively.

- The fourth study presents an experimental study of the performance of a multi-channel spiral-wound AGMD module with an area 14.4 m^2 was carried out on a commercial scale. The lab-scale AGMD desalination pilot plant was driven by solar energy using the flat plate (FPC) and evacuated tube collectors (ETC) installed in Port-Said City, Egypt. The results showed that the permeate flux of AGMD with ETCs was 18.81%–30.44% higher than FPCs, and its cost was 22.48% lower. The STEC of the AGMD system ranged from 158.83 kWh/m^3 to 346.55 kWh/m^3 . The maximum GOR reaches 4.4 at 52 $^{\circ}\text{C}$, depending on the feed inlet temperature. The thermal efficiency of the air gap membrane distillation system is 72%. The proposed AGMD system produced 28.78 m^3/year of fresh drinking water at a cost of USD 14.73/ m^3 with remarkable reducing in carbon dioxide emissions by 7,274.45 kg/year.

Keywords: Solar Desalination, Air gap membrane distillation (AGMD), pilot scale analysis, solar collectors, Photovoltaic (PV) system, Temperature polarization, Thermal conductivity, Seawater, ANSYS-FLUENT, TRNSYS.